Doctoral Dissertations   Dissertations and Theses

March 2016

Rational Development of Solid Lewis Acid Catalysts for Biomass Conversion

Chun-Chih Chang
University of Massachusetts Amherst

Follow this and additional works at: https://scholarworks.umass.edu/dissertations_2

Part of the Catalysis and Reaction Engineering Commons, and the Other Materials Science and Engineering Commons

RATIONAL DEVELOPMENT OF SOLID LEWIS ACID CATALYSTS FOR BIOMASS CONVERSION

A Dissertation Presented

by

CHUN-CHIH CHANG

Submitted to the Graduate School of the
University of Massachusetts Amherst in partial fulfillment
of the requirements for the degree of

DOCTOR OF PHILOSOPHY

February 2016

Department of Chemical Engineering

RATIONAL DEVELOPMENT OF SOLID LEWIS ACID CATALYSTS FOR
BIOMASS CONVERSION

A Dissertation Presented

by

CHUN-CHIH CHANG

Approve as to style and content by:

_____
Wei Fan, Chair

_____
William Curtis Conner Jr., Member

_____
Scott M. Auerbach, Member

_____
John Collura, Interim Department Head
Department of Chemical Engineering

ACKNOWLEDGMENTS

First of all, I would like to thank Department of Chemical Engineering at the University of Massachusetts Amherst for accepting me into the program. I would like to thank my advisor, Prof. Wei Fan, who diligently advise me in research with countless conversations and set up a great model as an advisor for me to follow. I particularly appreciate his encouragement, patience, support and understanding when I have first and second baby and during my loss of father. I am grateful to have Prof. Scott Auerbach and Prof. William Connor Jr. as my committee members. The questions and suggestions from them enriched the thesis in a great extent. I would also like to thank Prof. Paul Dauenhauer for his guidance in the aromatics project.

I am thankful to have great lab members, Paul, Zhuopeng, Hong Je, Chao, Vivek, and Qi. It is always great to have discussions and fun conversations with you guys. I want to thank the undergrads who worked with me, especially Dimitri, Marco, Xuanting, and Jason for their wonderful work. I enjoyed colloborations with the Dauenhauer's lab- Andrew, Luke, and Sara. I want to thank Yu-Ting, Geoff and Chris to help me with the instruments when I was new. In addition, I want to thank Alex and Lou in Microscopy Center, Sekar and Peter in the X-ray labs, Weiguo in the NMR Center and Rinat and Stephen in the Mass Spectrometry Center. The thesis could not be finished without their efforts on proper management of the instruments.

I also appreciate the time shared with my great classmates, Paul, Szu-Chia, Thuy, Jechan, Aditya, Xu, DD, Pranav, Alex, Suhasini, Brian. Those times we spent together to work on the assignments will always be vivid memory of mine.

Last but not least, I would like to thank family. My parents, Fu-Li and Shu-Yuan always support me and provide me an environment allowing me to pursue graduate study. My wife, Yu-Hsuan, has sacrificed a lot for me and takes good care of Fifi and Alex. I really appreciate what she has done for the family. She is the one who makes these works possible.

ABSTRACT

RATIONAL DEVELOPMENT OF SOLID LEWIS CATALYSTS FOR BIOMASS

CONVERSION

FEBRUARY 2016

CHUN-CHIH CHANG, B.S., NATIONAL TAIWAN UNIVERSITY

M.S., NATIONAL TAIWAN UNIVERSITY

Ph.D., UNIVERSITY OF MASSACHUSETTS AMHERST

Directed by: Professor Wei Fan

The need for sustainable production of everyday materials in addition to declining reserves of petroleum-based feedstocks has motivated research into the production of renewable aromatic chemicals from biomass. As the third largest chemical by volume in the world produced from petroleum (catalytic reforming of naphtha) with increasing demand (6-8 % per year), there are now ongoing efforts worldwide for developing alternative routes to produce p-xylene from renewable biomass resources. We have proposed a multistep pathway to produce renewable p-xylene from lignocellulosic biomass using heterogeneous catalysts. The pathway includes formation of glucose by saccharification of cellulose, isomerization of glucose into fructose, dehydration/hydrogenolysis for production of 2,5-dimethylfuran (DMF), and final step for producing p-xylene from reacting DMF with ethylene.

Lewis acid zeolite catalysts (e.g. Sn-BEA, a tin containing molecular sieve with zeolite BEA structure) exhibited critical roles in the pathway because of its excellent catalytic activity for the conversion of glucose into fructose by intramolecular hydride transfer reaction and the production of p-xylene from DMF by cycloaddition/dehydration reactions. However, rational development of Sn-BEA is a grand challenge due to the lengthy crystallization time (up to 40 days), incorporation of Sn into the framework, and the utilization of hydrofluoric acid. In this work, a highly reproducible

seeded growth approach was invented to significantly shorten the crystallization time. It is demonstrated that the seed crystals can effectively reduce the induction time of crystallization and lower the energy barrier for induction period by bypassing the nucleation stage. Crystallization kinetic studies reveal that the highly crystalline Sn-BEA catalyst can be obtained in as short as 3 hours at 200 °C with similar catalytic activity in isomerization reaction of glucose compared to conventional Sn-BEA. The discovery is important for rational synthesis of heteroatom containing zeolite catalysts.

To avoid the utilization of toxic hydrofluoric acid, a fluoride-free method based on dry gel conversion (DGC) was developed in a caustic medium for synthesis of Sn-Beta. It is shown that the addition of seed crystals and alkali ions are indispensible for the synthesis. Furthermore, it is found that ion-exchange with ammonium ions is crucial for preservation of crystalline structure during heat treatment. Incorporation of Sn into zeolite framework is demonstrated. The activity is, however, not comparable to Sn-Beta made from fluoride medium, attributed to possibly different local Sn structure and surface property of the catalysts.

Various zeolite catalysts (ZSM-5, zeolite Y, and zeolite Beta) were tested in the tandem Diels-Alder cycloaddition/dehydration reaction of DMF and ethylene to form *p*-xylene. It is revealed that zeolite Beta shows superior catalytic performance by achieving high selectivity (90 %) at 99 % conversion of DMF and slow deactivation. The production rate of *p*-xylene exhibits a transition of kinetic control reactions from dehydration reaction to Diels-Alder cycloaddition reaction as the amount of catalyst increase, and it is universal for all catalysts examined. The results imply that the cycloaddition reaction proceeds uncatalyzed, and the maximum rate of *p*-xylene production is limited by the Diels-Alder reaction.

Zr-, Sn-, and Ti-BEA Lewis acid zeolite catalysts were employed in production of *p*-xylene from DMF and ethylene. It was found that these Lewis acid catalysts are able to catalyze the tandem reaction consisting of Diels-Alder cycloaddition and dehydration reactions to form *p*-xylene. Zr-BEA shows the best performance with improved recalcitrance to deactivation compared to Brønsted acid

zeolite catalyst (Al-BEA), reaching 90 % selectivity to *p*-xylene at 99 % conversion of DMF. Zr-BEA also features high *p*-xylene production rate due to its catalytic activity for both cycloaddition and dehydration reactions. The results provide an approach to rational develop bi-functional (Lewis+Brønsted acids) catalysts for the tandem reaction pathway to efficiently produce *p*-xylene and many other aromatics.

TABLE OF CONTENTS

LIST OF TABLES

LIST OF FIGURES

xiv

LIST OF SCHEMES

LIST OF IMAGES

CHAPTER 1

INTRODUCTION

1.1 A general picture

With the declining reserve of petroleum crude oil and increasing calls for control of green house gas emission, huge amount of research efforts have been devoted in converting non-edible and renewable biomass to transportation fuels, fuel additives, commodity chemicals and new bio-based materials.[1-4] In general, the feedstocks derived from biomass can be classified as lignocellulose, starch and tryglycerides. Among them, lignocellulose is the most abundant, does not compete with food and converts solar energy, carbon dioxide and water to carbohydrates, making it an ideal source of fuels and chemicals. Lignocellulose consists of three major polymeric components: lignin (ca. 15-20 %), hemicellulose (ca. 25-35 %) and cellulose (ca. 40-50 %).[1, 2] Lignin has three-dimensional structure consisting of phenolic biopolymers, providing rigidity of plants. Hemicellulose is formed by C_5 and C_6 sugars including D-xylose, D-galactose, D-arabinose, D-glucose and D-mannose. Cellulose is a polymer of glucose units linked by the β–glycosidic bonds.[2] In order to obtain liquid fuels and chemicals, the lignocellulose needs to be depolymerized and deoxygenated, as shown in Scheme 1.1.
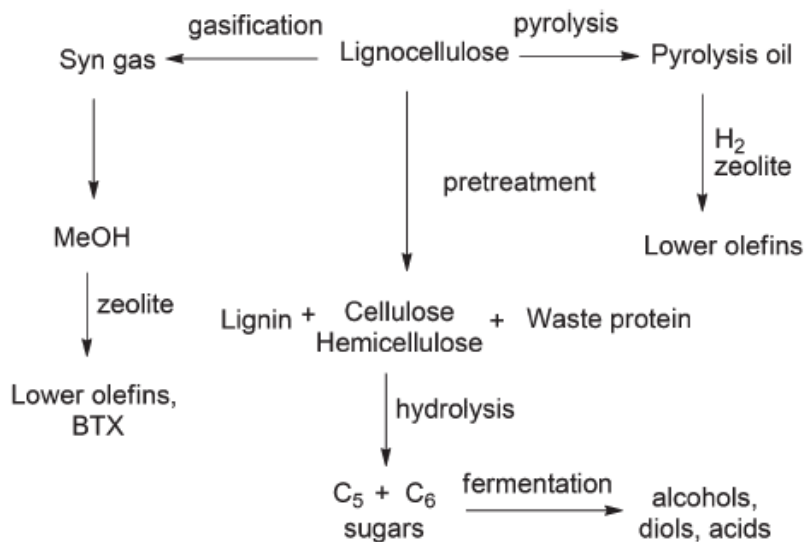
Scheme 1.1 Strategies for conversion of lignocellulose. Adapted from ref. [1].

There are two main pathways to achieve this: thermochemical and hydrolytic. In thermochemical process, pyrolysis and gasification are mainly used. Pyrolysis yields charcoal and pyrolysis oil, and the crude oil can be further refined by zeolite catalysts. Syn gas can be produced via gasification, and fuels or platform chemicals can be obtained via Fisher-Tropsch process or methanol synthesis from it. Hydrolytic process, on the other hand, usually involves catalysis by mineral acids and mixture of enzymes to break down the cellulose and hemicellulose into glucose and xylose (C_6 and C_5 monosacharrides), and the C_5 and C_6 sugars are then used as starting materials for production of biofuels or other fine chemicals by fermentation or chemical catalysis. It is worth mentioning that Dornath and Fan recently reported high glucose yield (91 %) in an efficient process combining acidulated ball milling of cellulose, impregnation of glucose and sulfonate-functionalized three-dimensionally ordered mesoporous carbon (3DOm carbon) catalyst,[5] and it shows the great potential of more effective utilization of cellulose from biomass by molecular catalysis.

In this thesis, we focus on production of commodity chemicals from biomass, particularly *p*-xylene, and the development of catalysts involved in the process. The BTX (benzene, toluene and xylenes) are currently predominantly produced from the reforming of naphtha, and they are important chemicals used as fuel additives, solvents and precursors for consumer products. For example, benzene can be used to make polystyrene and nylon, and *p*-xylene is the precursor of polyethylene terephthalate (PET). In addition, the strong demands for these end products in developing countries have increased the global consumption of BTX by 6-8 % annually.[6, 7] To achieve renewable *p*-xylene from biomass, several steps required to remove oxygenated functional groups in the biomass, as summarized in Scheme 1.2. It is proposed that, firstly, cellulose needs to be depolymerized and yield glucose, applying the procedures described above. Glucose the isomerizes to fructose over glucose isomerase[8] or Sn-Beta (interchangeable with Sn-BEA in this thesis), which is a solid Lewis acid molecular sieve which has shown similar activity compared to enzymes.[9] HMF (5-hydroxymethylfurfural), another important building block, can be obtained by dehydration of fructose over acid catalyst.[10] Further hydrogenolysis of C-O bond of HMF over CuRu or Ru/C catalyst forms

2, 5-dimethylfuran (DMF), which can be used as a transportation fuel additive.[11, 12] In the last step, DMF can react with ethylene (can be obtained via dehydration of bioethanol)[13] and undergoes [4+2] cycloaddition to form an oxa-norbornene cycloadduct followed by subsequent dehydration over acid catalysts to produce *p*-xylene.[14-18] The processes described above grant the formation of *p*-xylene from biomass-derived feedstocks, and it is important to emphasize that the efficiencies in each step could alter the market viability of the renewable *p*-xylene. From an economic analysis of *p*-xylene from HMF, the authors suggested further researches on more efficient production of HMF and discovery of superior catalysts for high selectivity/yield to *p*-xylene are keys to decrease the price of the bio-renewable *p*-xylene.[19] Thus, each catalytic step in the overall process from cellulose to *p*-xylene is worth investigating not only for scientific interests but also for realization of consumer bio-renewable plastics. The thesis in particular concerns the rational development of the solid Lewis acid zeolite, Sn-Beta catalyst, and the production of *p*-xylene from bio-derivable DMF and ethylene.
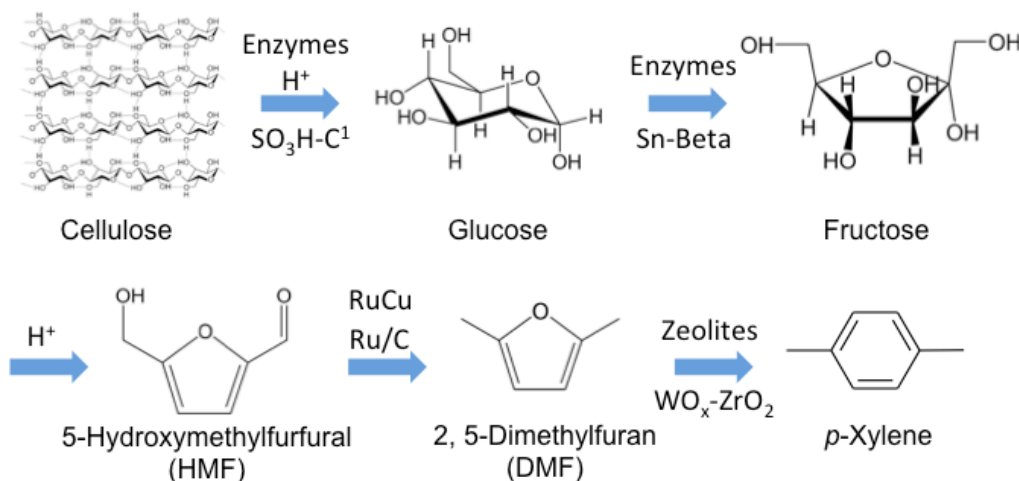
Scheme 1.2 Proposed overall process for production of renewable *p*-xylene from biomass

1.2 Lewis acid zeolites and Sn-Beta

Zeolites are natural or synthetic crystalline aluminosilicates with well-defined, ordered pore structure at molecular dimensions composed of conneted TO_4 tetrahedrals (T=Si and Al) by sharing oxygens.[20]

Elements such as P^V, Ga^{III}, B^{III}, and Zn^{II} can be used to form the tetrahedra and isotypic frameworks can be formed, and they are often called "zeotype" materials, as the definition of zeolite refers to aluminosilicates. In this thesis, the use of the word "zeolite" is not restricted to aluminosilicates but includes the concept of "zeotype". When Al is incorporated, the framework becomes negatively charged due to the oxidation state of Al (+3), and the charge is balanced by extraframework cation. These cations are exchangeable and dictate the characteristics of the formed zeolites. Thus, zeolites have been widely used in separation, adsorption, ion-exchange, and catalysis.[21] Up to date, there are more than 220 framework types according to International Zeolite Association.

Lewis acid zeolites can be formed by substituting Si by other elements such as Sn, Ti, and Zr into the framework, as shown in Scheme 1.3, using Sn-Beta as an example. Sn-Beta synthesized in fluoride medium was first reported by Corma et al.[22] It is a stannosilicate with zeolite Beta crystalline structure, and Sn is isomorphously substituted Si atom within the crystal framework, as shown in Scheme 2.1. Zeolite BEA is a large pore zeolite with 12-member ring (12-MR, 6.6 x 6.7 on <100> and 5.6 x 5.6 on [001] for *BEA)[23, 24] pore openings and constructed with three-dimensionally connected channels. A representative Different from the Brønsted acid zeolites, where the acidity
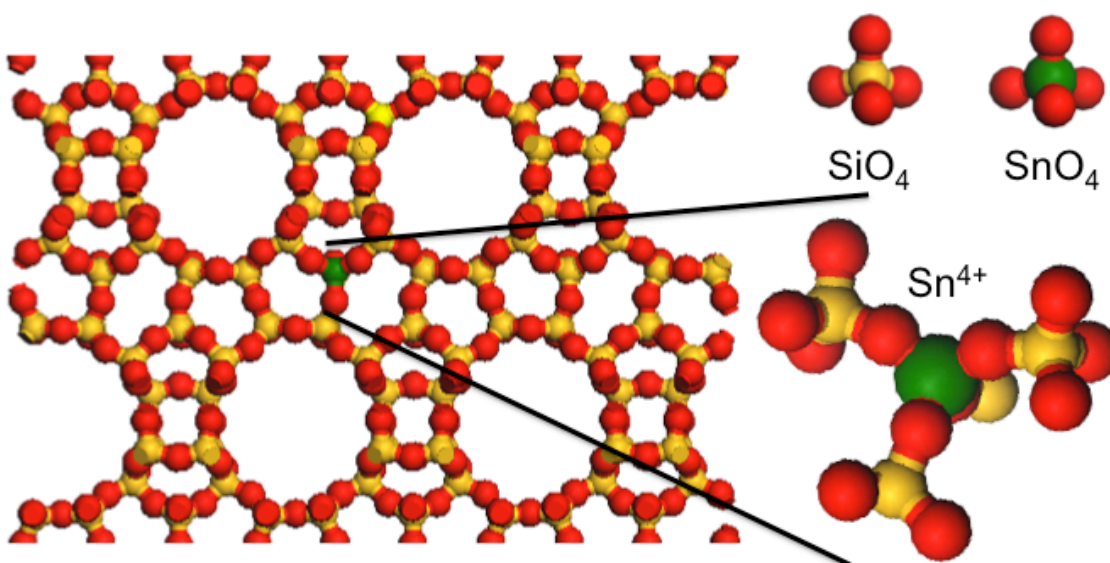
Scheme 1.3 Schematic representation of Sn-Beta structure. Yellow, green and red solid spheres represent Si, Sn and O atoms, respectively.

arising from proton (H^+) of the bridging Si-OH-Al, the Lewis acidity of the catalysts comes from the empty orbitals of the substituted elements to accept electrons. Thus, transition metals (like Ti and Zr) with incomplete *d* subshells in zeolite framework can act as Lewis acid sites to accommodate electrons; Lewis acidity of Sn as a *p*-block element may be originated from the involvement of the low-lying *d* orbitals.[25] It should be noted that Lewis acid sites could also be found in aluminosilicates and could originate from the tri-coordinated Al sites on the framework, the extraframework Al, and the charge-compensating cations.[21]

Sn-Beta has been shown promising activity for the catalytic oxidation of saturated and unsaturated ketones through the Baeyer-Villiger (BV) reaction and the reduction of carbonyl compounds with secondary alcohols through the Meerwein-Ponndorf-Verley (MPV) reaction.[26-28] More recently, Moliner et al. reported that Sn-Beta is highly active for isomerization of glucose to fructose in aqueous phase, showing activity resembling enzymic counterpart,[9] a key intermediate step for the conversion of biomass into chemicals and fuels.[29]

Sn-Beta is water-tolerant and capable of catalyzing isomerization of glucose to fructose in water. This step is considered as a crucial intermediate step not only for the production of *p*-xylene, as described earlier, but also for the formation of other building block chemicals such as 5-hydroxymethylfurfural (HMF) and levulinic acid.[10, 30] Thus, it is encouraging that the discovery of a heterogeneous inorganic catalyst in Sn-Beta for isomerization of glucose to fructose, which can reduce the operation cost of the process and make the final product more market-viable.

Aiming to utilize biomass as the feedstocks for transportation fuels and fine chemicals, monumental amount of research has been focused on the catalytic process for biomass upgrading in the past few years. Specifically, applications of water-resistant Lewis acid zeolites have been emerging topics due to the fact that the platform or starting molecules contains carbonyl functional group and the reaction requires water as a greener solvent. The hydrophobic character of these Lewis acid zeolites can be originated from its highly siliceous composition and defect-free nature due to its traditional fluoride medium synthesis. As shown later, the surface property of the zeolite can be

5

tailored by different synthetic pathways, and it could affect the adsorption properties of the reactant and thus impacts the activity of the catalysts.

1.3 Preparation of Sn-Beta

Although Sn-Beta exhibits intriguing catalytic properties, its application and commercialization has been hindered by the synthesis of the material, particularly long crystallization time and utilization of hydrofluoric acid. In the original report by Valencia and Corma, Sn-Beta is synthesized in a fluoride medium.[22] The fluoride ion functions as a mineralizer, similar to hydroxide ion in caustic medium. The mineralizing power of F^- seems to be less than that of OH^- and effective supersaturations are lower, often accompanied by higher crystallization temperature or longer crystallization time during synthesis.[31] Utilization of F^- in lower pH (near neutral pH in most cases) has shown advantages for the introduction of heteroatoms which form nonreactive precipitate in alkaline solutions, and fluoride method provides the only route to certain zeolites.[31] The long crystallization time for Sn-Beta reported in literature (Si/Sn=100, up to 40 days)[9] may be a consequence of the low degree of supersaturation of zeolite precursors in fluoride route. Seeding has been mentioned in original report, but the crystallization still requires 11-22 day.[26, 32, 33]

Typical synthesis of Sn-BEA involves the utilization of toxic hydrofluoric acid and lengthy synthesis time, leading to several environmental and practical concerns. Significant efforts have been made to improve the synthesis process of Sn-BEA, such as using less toxic chemicals[34] and shortening crystallization time by seeded growth method.[35] However, fluoride medium was still used in all syntheses. Although more benign chemicals such as ammonium fluoride (NH_4F) and sodium fluoride (NaF) can be potentially used in the synthesis, non-fluoride method is still strongly desired due to potential health risk related to chronic excessive exposure to fluorides.[36] Recently, post-synthesis approaches have been used to synthesize Sn-BEA in the absence of fluorides. For instance, Li *et al.* reported that Sn can be grafted onto dealuminated zeolite BEA by chemical vapor deposition using tin (IV) chloride vapor; Hammond *et al.* proposed a solid state ion exchange method *via* mixing tin (II) acetate with dealuminated zeolite BEA; Dijkmans *et al.* utilized a solution-based method to

6

insert Sn into dealuminated zeolite BEA.[37-39] In all post-synthesis methods, Sn was incorporated into the defects generated by the dealumination process. Condensation of various Sn sources with silanol defects resulted in the formation of tetrahedrally coordinated Sn sites. Sn concentration in the samples can be easily tailored by controlling the amount of Sn source applied in the treatment. The materials made from the post-synthesis approaches show interesting catalytic performances in Baeyer-Villiger oxidation, isomerization of triose sugar (such as dihydroxyacetone to lactates in alcohols) and glucose. However, due to the low mobility of Sn sources used in the syntheses and the lack of ability to control the type and amount of defects generated by the dealumination process, it is a challenge to completely diminish all defects in the dealuminated zeolites by the incorporation of framework Sn. This is likely one of the reasons why very different catalytic activity was observed for the Sn-BEA catalysts made by the post-synthesis methods. The benefits of the post synthesis method are controllable morphology and relatively easy preparation. It is worth mentioning that there are more variants of the post-synthesis method for preparation of Lewis acid zeolites, resulting in exciting metal containing Lewis acid zeolites with novel hierarchical/layered structures, showing exceptional activity toward bulky substrates.[40-42]

Thus, it is realized that, despite promising catalytic performance, the broad application of Sn-Beta could be limited by its lengthy and environmental-endangered synthesis, making it difficult in large-scale production. In this thesis, we demonstrated two strategies that intend to mitigate the obstacles: first, a seeded growth method was utilized to shorten the crystallization time. Second, a dry gel conversion method was developed for synthesis of Sn-Beta under a fluoride-free, caustic medium.

1.4 Production of renewable *p*-xylene from 2,5-dimethylfuran and ethylene

p-Xylene is used for the production of terephthalic acid,[43] which is used as a feedstock for polyester and polyethylene terephthalate plastics (e.g., plastic bottles)[5] and is currently produced from the separation of mixed aromatics (isomers of xylene and ethylbenzene) from the naptha fraction of petroleum. *p*-Xylene can also be selectively produced from toluene through the use of ZSM-5 catalysts[44] in combination with membrane separation.[45] New processes are currently being

implemented to produce *p*-xylene from renewable resources using a hybrid process that combines fermentation and heterogeneous catalysis.[46, 47]

p-Xylene can potentially be produced renewably starting from glucose as shown in Scheme 1.1. As the last step of this scheme, the conversion of dimethylfuran (DMF) to *p*-xylene by a two-step process (cycloaddition + dehydration) is crucial for the efficient production of high-value chemicals from biomass-derived sugars. Williams and Dauenhauer collaborated with our lab and demonstrated the chemistry using zeolite catalysts.[15] Under mild temperature (200-300 °C) and high ethylene pressure (57-62 bar), the authors demonstrated the temperature dependence of the product distribution, the higher the temperature, the higher the *p*-xylene selectivity. 51% of *p*-xylene selectivity at 95% conversion at 300 °C was achieved in a pure DMF system. Furthermore, when the reaction is carried out with heptane solvent, the selectivity of *p*-xylene can be further increased to 75 %. It was also found under the reaction conditions, the reaction is rate-controlled by the uncatalyzed Dields-Alder (DA) cycloaddition step with dehydration step catalyzed by Brønsted acids. The results is consistent with the computational work by Nikbin *et. al*. (DFT calculation in gas phase),[18] in which the authors have shown that with Brønsted acid, the reaction barrier for dehydration is greatly reduced, from 59 kcal/mol to 17 kcal/mol, while the DA reaction still renders uncatalyzed. When Lewis acid (specifically alkali ion exchanged zeolites) is modeled, the results indicates it can slightly decrease the activation energy of the DA reaction (24.7 to 16.9 kcal/mol for Li^+ exchanged zeolite) and some enhancement on the dehydration step due to stabilization of intermeidiates. The authors proposed a bifunctional catalyst featuring both Lewis (high DA rate) and Brønsted acidity (high dehydration rate) could potentially enhance the production of *p*-xylene from DMF and ethylene.

Do *et. al*. has revealed the mechanism of the reaction over zeolite Y catalyst, as shown in Scheme 3.1.[16] The desired pathway, as described previously, consists of [4+2] Diels-Alder cycloaddition of DMF and ethylene followed by a dehydration reaction to form *p*-xylene. Other byproduct includes 2, 5- hexanedione, a hydrolysis product from DMF, alkylated products (such as 4-propyltoluene) formed from an alkylation reaction of ethylene and protonated cycloadduct and oligomers (such as 1, 4-

dimethyl-2-(4-methylbenzyl)benzene) is produced from a Friedel-Craft type reaction between DMF and cycloadduct derivatives. According to the reaction network, the author suggested by removing water from the system, carefully selecting catalysts with adequate acid strengths and tuning dielectric properties of the solvents, the selectivity towards *p*-xylene can be further enhanced. Elucidation of the reaction pathways has revealed three competing side reactions to the main pathway to *p*-xylene: (1) hydrolysis of DMF to 2,5-hexanedione, (2) secondary addition of DMF to produce dimers, and (3) secondary reactions of ethylene to alkylated aromatics. From this analysis, further improvement in selectivity to *p*-xylene can be specifically defined as: (a) elimination of the hydrolysis side reaction or (b) reduction in secondary addition of either the dienophile (e.g. ethylene) or the diene (e.g. DMF).

Scheme 1.4 Simplified proposed reaction pathway of *p*-xylene formation from DMF and ethylene over zeolite Y.

Several previous studies have suggested that Lewis acid can coordinate with dienes to catalyze the Diels-Alder reaction.[48-52] DFT study on the production of *p*-xylene from DMF also suggested that

9

Lewis acid can coordinate with ethylene to catalyze the Diels Alder reaction to form cycloadduct intermediate, oxanorbornene.[18, 53] In addition, experimental and theoretical studies have also suggested that solid Lewis acid catalysts are capable of catalyzing the dehydration of cycloadduct intermediate and other alcohols.[18, 53-55]. Using Fe^{3+}-exchanged montmorillonite K10 clay as a Lewis acid catalyst for the aromatization of oxabicyclic derivatives has also been reported.[52, 56] Lewis acid zeolite catalysts, in particular Sn-BEA and Zr-BEA, have also shown superior catalytic activity for the synthesis of terephthalic acid via Diels-Alder reactions with oxidized variants of 5-hydroxymethylfurfural.[57]

In this thesis, motivated by the experimental and theoretical studies, zeolite catalysts were employed in the Diels-Alder cycloaddition-dehydration reaction pathway for producing *p*-xylene from DMF and ethylene. Brønsted and Lewis acid zeolite catalysts were studied in this reaction to understand the performance and difference of the two distinct kinds of catalysts in this catalytic system.

1.5 Thesis scope

The thesis is constructed as following: An improved synthesis strategy for Sn-Beta in traditional fluoride medium is described in Chapter 2; a development of fluoride-free synthesis for Sn-Beta is presented in Chapter 3; a catalyst-screening study for production of *p*-xylene from DMF and ethylene is examined in Chapter 4; a study of Lewis acid zeolites for production of *p*-xylene from DMF and ethylene is shown in Chapter 5. Chapter 6 will give conclusions for the accomplished work, and suggested future research directions are included in Chapter 7.

CHAPTER 2

RATIONAL SYNTHESIS OF TIN-BETA CATALYSTS FOR BIOMASS

CONVERSION IN A FLUORIDE MEDIUM

2.1 Background

Sn-Beta synthesized in fluoride medium was first reported by Corma et al.[22] It is a stannosilicate

with zeolite Beta crystalline structure, and Sn is isomorphously substituted Si atom within the crystal

framework, as shown in Scheme 2.1. Zeolite BEA is a large pore zeolite with 12-member ring (12-

MR, 6.6 x 6.7 on <100> and 5.6 x 5.6 on [001] for *BEA)[23, 24] pore openings and constructed with

three-dimensionally connected channels. It has been shown promising activity for the catalytic

oxidation of saturated and unsaturated ketones through the Baeyer-Villiger (BV) reaction and the

reduction of carbonyl compounds with secondary alcohols through the Meerwein-Ponndorf-Verley

(MPV) reaction.[26-28] More recently, Moliner et al. reported that Sn-Beta is highly active for

isomerization of glucose to fructose in aqueous phase, showing activity resembling enzymic

counterpart,[9] a key intermediate step for the conversion of biomass into chemicals and fuels.[29]

As mentioned in Chapter 1, although possessing interesting and appealing catalytic performance,

the preparation of Sn-Beta has been a challenge due to lengthy synthesis time. In this chapter, a

modified seeding approach was employed aiming to reduce the required synthesis time. The

crystallization kinetics of seeded Sn-Beta are monitored and compared to unseeded system. The effect

from the amount of seed and water in the synthesis gel were examined. It is believed that the

morphology and dispersion status of zeolite seeds in the synthesis gel can substantially affect the

crystal growth kinetics of Sn-Beta. By uniformly distributing well-crystalline zeolite beta seeds in the

synthesis gel, high-quality Sn-Beta can be synthesized in only 3 hr at 200 °C with a nearly complete

conversion (> 90 %) of the provided silica source. Moreover, further enhancement of crystallization

kinetics can be achieved by reduction of water content in the synthesis gel. Incorporation of Sn into

the zeolite framework is demonstrated by using UV-Vis spectroscopy, deuterated acetonitrile

adsorbed FT-IR, and isomerization reaction of deuterated glucose. The Sn-Beta catalyst synthesized by this approach is highly active for the isomerization of triose (C3), pentose (C5) and hexose (C6) sugars.

2.2 Experimental

2.2.1 Preparation of zeolite beta seed solution[58]

Typically, 0.1 g of sodium hydroxide ($\geq$ 98%, Aldrich) was dissolved in 11.83 g of tetraethylammonium hydroxide solution (TEAOH, 35wt%, Alfa Aesar or SACHEM). 17.85 g of Ludox HS-30 (Aldrich) was dropwise added into the above solution under stirring, and 0.365 g of aluminum isopropoxide (Aldrich) was then added into the clear solution. The composition of the solution was 25 SiO_2: 0.25 Al_2O_3: 9 TEAOH: 0.35 Na_2O: 331 H_2O. The final solution was aged for 1 day with stirring before use. The filtrate was charged into a Teflon-lined stainless steel autoclave, and heated at 120 °C for 3 day in a preheated oven. The formed zeolite nanocrystals were collected by centrifugation and washed extensively by deionized water until pH of the supernatant is less than 9. Finally, the aluminosilicate zeolite beta nanocrystals were re-dispersed into deionized water without drying, and the crystal concentration in the suspension was 0.192 g/mL. Dealumination of the crystals was achieved by treating 2.5 mL of the suspension (0.48 g of seed crystals) with 25 mL of concentrate nitric acid (69%, Fisher) in a Teflon-lined stainless steel autoclave at 80 °C for 24 hr. The dealuminated zeolite beta was collected by centrifugation and thoroughly washed by deionized water until the supernatant approached a neutral pH. The obtained products were then re-dispersed into deionized water by sonication without drying. The final crystal concentration in the suspension was 0.175 g/mL (0.163 g/g).

2.2.2 Synthesis of Sn-Beta

In a typical run, 7.70 g of tetraethylorthosilicate (TEOS, Alfa Aesar, 99 %) was added into 8.23 g of TEAOH solution (35 %), and stirred at room temperature until it became a homogeneous solution (about 1 h to 1.5 h). Then, 0.1 g of hydrated tin chloride (Alfa Aesar) dissolved in 0.64 g of

12

deionized water was added. The solution was stirred in a hood until ethanol generated from the hydrolysis of TEOS was completely evaporated. The final weight loss was 8.00 g (6.66 g of ethanol and 1.34 g of water). Then, 0.497 mL of dealuminated zeolite beta seed solution (0.175 g/mL) was added into the solution (4.1wt% with respect to the silica content) and mix by plastic spatula. Finally, 0.689 mL of hydrofluoric acid (Alfa Aesar, 49%) was added into the solution, and homogenized by using a plastic spatula for 10 min. The composition of the final gel was SiO_2: 0.54 TEAOH: 0.54 HF: 0.008 SnO_2: 7.5 H_2O. 3 g of the obtained solid-like hard gel (see Image 2.1) was then loaded into a Teflon-lined stainless steel autoclave (~50 mL). Water content of the gel was varied by drying the gel in a vacuum oven at 60-80 °C for different period of time. The autocalve was washed with 6 M KOH solution (>25 mL) prior to use to eliminated possible crystal contamination between each run for 2 day (1 day at upright position; 1 day at up-side down position) at 150 °C oven. It has been tested that the condition is able to dissolve 50 mg of as-made Sn-Beta samples. The autoclave was heated at 140-200 °C with a rotation of 2 rpm for various times. The product was filtered and thoroughly washed by deionized water, and dried in a 100 °C oven overnight. The as-made solid was calcined with a ramping rate of 1 °C/min to 550 °C for 12 hr under humidity (~ 23 Torr, introduced by bubbling air
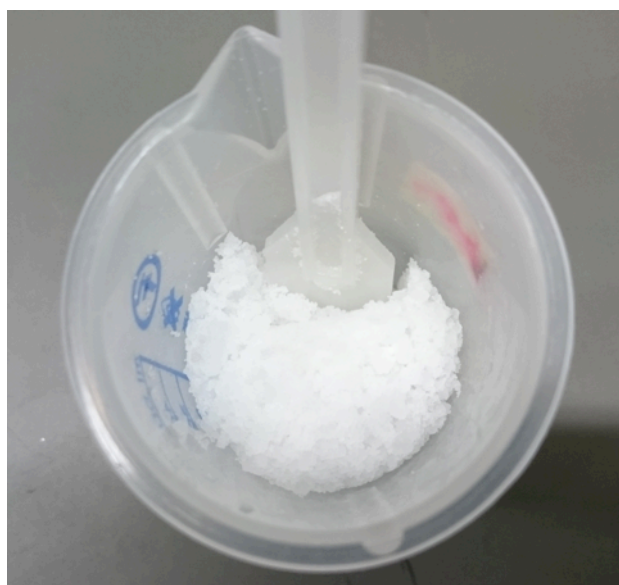
Image 2.1 The starting gel for Sn-Beta made from fluoride medium. Note the solid-like texture of the gel.

through water at room temperature) to remove the organic structure directing agent and fluoride ions.

2.2.3 Characterizations

Samples were characterized by X-ray diffraction (XRD), scanning electron microscopy (SEM), transmission electron microscopy (TEM), nitrogen sorption measurements, thermogravimetric analysis (TGA), diffuse reflectance ultraviolet-visible spectroscopy (DR UV-Vis), FT-IR spectroscopy and inductively coupled plasma mass spectroscopy (ICP-MS). XRD measurements were performed on a diffractometer (X'Pert Pro, PANalytical) using Cu Kα radiation generated at 45 kV and 40 mA from 2 theta of 4° to 40° with a step size of 0.02°. SEM was performed on a Magellan 400 (FEI) with an accelerating voltage of 3.0 kV, and the samples were coated with platinum or platinum/palladium alloy prior to observation. Nitrogen adsorption-desorption isotherms were collected on an automated gas sorption analyzer (Autosorb iQ_2, Quantachrome) at 77 K. The samples were outgassed at 300 °C for 12 h under vacuum before measurement. The thermogravimetric analysis (TGA) was performed on a thermogravimetric analyzer (SDT600, TA) with a ramping rate of 10 °C min^{-1} under air flow. DR UV-Vis measurements were done on a Cary 50 spectrometer with a diffuse reflectance attachment (Prof. Gonghu Li's lab, University of New Hampshire). Barium sulphate was used as a background material. FT-IR experiment was carried out using a Praying Mantis^{TM} DRIFT accessory (Harrick) in a high-temperature reaction cell (Harrick) allowing controls of atmosphere, temperature and adsorption of probe molecules over the zeolite samples. The samples were pretreated with helium flow at 550 °C for 1 h prior to adsorption (pyridine or deuterated acetonitrile). For FT-IR measurements of samples with adsorbed pyridine, pyridine (Alfa Aesar) vapor was carried by helium and in contact with the samples at 120 °C for 10 min. After heating up to different temperature (150, 250, 350, and 450 °C) for 1 h to desorb weakly adsorbed pyridine, the spectrum was recorded on a FT-IR spectrometer (Equinox 55, Bruker) equipped with MCT detector with a resolution of 2 cm^{-1} at 120 °C. For deuterated acetonitrile (CD_3CN, Aldrich) adsorption, it was

adsorbed on the samples at 30 °C followed by flowing helium for 30 min. CD$_3$CN was then desorbed at 100 °C for various periods of time. The spectra were acquired at 30 °C and normalized with the Si-O-Si overtones at 1800-2000 cm^{-1}. Potassium bromide (KBr, Acros) was used as background in this case. Elemental analysis was carried out in the Analytical Geochemistry Lab, Dept. of Earth Sciences in University of Minnesota using an inductively coupled plasma-optical emission spectrometer (ICP-OES, iCap 6500 dual view, Thermo Scientific) or an inductively coupled plasma-mass spectrometer (ICP-MS, XSERIES 2, Thermo Scientific) using He/H$_2$ collision-reaction mode. Y was added as internal standard.

2.2.4 Catalytic tests

All the chemicals (xylose, glucose, dihydroxyacetone dimer and methanol) used in the reactions were purchased from Sigma-Aldrich.

2.2.4.1 Isomerization of glucose

Glucose isomerization reaction was used to test the catalytic activity of the synthesized Sn-Beta catalyst. The reaction was performed according to the work of Moliner *et al.*[59] Sn-Beta was added at a 1:50 Sn: glucose molar ratio to a 10 wt% glucose solution in a 3 mL thick-walled glass reactor. The reaction vial was placed in a temperature-controlled aluminum heating block set to 90 °C with 1000 rpm stirring. After reaction for various times, the glass reactors were quenched in ice for 15 min, dried, and weighed before opening to make sure no leaking during the reaction.

2.2.4.2 Isomerization of xylose

The isomerization of xylose was performed according to the work of Choudhary *et al.*[60] Sn-Beta was added at a 1:70 Sn: glucose molar ratio to a 10 wt% xylose solution in a 3 mL thick-walled glass reactor. The reaction vial was placed in a temperature-controlled aluminum heating block set to 100

°C with 1000 rpm stirring. After reaction for various times, the glass reactors were quenched in ice for 15 minutes, dried, and weighed before opening to make sure no leaking during the reaction.

2.2.4.3 Conversion of dihydroxyacetone (DHA) to methyl lactate (ML)

Conversion of dihydroxyacetone (DHA) to methyl lactate (ML) in methanol was performed according to the work of Taarning *et al.*[61] In a typical experiment, 1.25 mmol of DHA, 4 g methanol and 80 mg Sn-Beta were added to a 3 mL thick-walled glass reactor. The reactor was placed in temperature-controlled aluminum heating block set to 70 °C with 1000 rpm stirring. After reaction for various times, the glass reactors were quenched in ice for 15 minutes, dried, and weighed before opening to make sure no leaking during the reaction.

Sample analyses

For the reactions with pentose and hexose, sample analyses were performed using liquid chromatography (Shimadzu LC-20AT). Sugars were detected with a RI detector (RID-10A), and other products were detected with a UV–Vis detector (SPD-20AV) at wavelengths of 210 and 254 nm. The column used was BIO-RAD HPX-87H sugar column. The mobile phase was 0.005 M H_2SO_4 flowing at a rate of 0.6 mL/min. The column oven was set to 30 °C. The column can efficiently separate the isomers of C6 sugar, such as glucose, fructose and mannose, but shows poor separation for xylulose (10.118 min) and lyxose (10.175 min). It was found that the response factors of xylulose and lyxose on the RI detector are similar (difference is less than 20%). The combined yield of xylulose and lyxose were, thus, calculated from the peak with a retention time from 10.1 min to 10.2 min.

DHA and ML were detected on an Agilent 6890 instrument equipped with an FID-detector and a Restek RTX-VMS capillary column (30.0 m/0.25 mm id/1.4 μm film thickness). A helium flow rate of 6.0 mL/min pressurized at 1.498 bar was used. The oven temperature program is as follows: the initial temperature is 50 ºC (hold 2 min) and then heated to 240 ºC (ramp 20 ºC/min, hold 20 min).

Conversion and yield are defined as follows:

$Conversion_{glucose} = (moles_{glucose\ reacted})/(moles_{glucose\ initial})$

$Conversion_{DHA} = (moles_{DHA\ reacted})/(moles_{DHA\ initial})$

$Conversion_{xylose} = (moles_{xylose\ reacted})/(moles_{xylose\ initial})$

$Yield_{glucose} = (moles_{glucose})/(moles_{glucose\ initial})$

$Yield_{fructose} = (moles_{fructose\ produced})/(moles_{glucose\ initial})$

$Yield_{mannose} = (moles_{mannose\ produced})/(moles_{glucose\ initial})$

$Yield_{xylulose+lyxose} = (moles_{xylulose+lyxose\ produced})/(moles_{xylose\ initial})$

$Yield_{ML} = (moles_{ML\ produced}) / (moles_{DHA\ initial})$

2.3 Results and discussions

Figure 2.1 shows the temporal XRD patterns for the Sn-Beta synthesized at 140, 170, and 200 °C using the seeded growth method, with 4 wt% seed with respect to silica in the synthesis medium. It is remarkable that only zeolite BEA phase can be observed from the spectra, indicating no impurity crystalline phase present in the sample. In general, only the diffraction peaks assigned to zeolite BEA arise as the hydrothermal time increases at each temperature (140-200 °C), and highly crystalline samples can be obtained from the synthesis protocol given long enough time. The yields of highly crystalline samples are constantly greater than 90 % on a silica basis, indicating the high efficiency of Si incorporation of the fluoride synthesis.[62] It should be noted that 140 °C is the traditional temperature for synthesis of Sn-beta.[22] Here, pure Sn-Beta can be obtained when the heat treatment temperature extends to 200 °C with increased crystallization kinetic without formation of competing phases. The spectra consist of sharp and broadened reflection peak, characteristic for intergrowth of different polymorphs, A and B.[62-64] The apparent shoulder at low angle diffraction peak (~7.5 degree) indicates the sample is likely polymorph A enriched, and the highly resolved patterns are results of

(a)

(b)
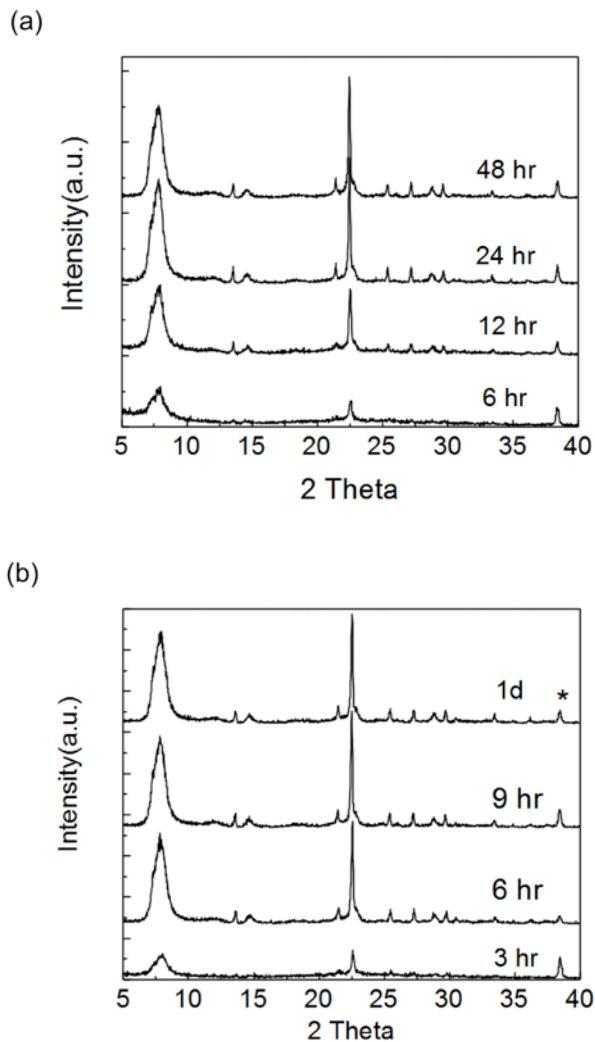
Figure 2.1 XRD patterns for Sn-Beta synthesized at (a) 140, (b) 170, and (c) 200 °C for different time with 4 % seeds. "*" represents the diffraction peak from the holder.

low extent of connectivity defect in the crystals, consistent with what Corma et al. reported for pure silica zeolite Beta.[64] The elemental analysis shows the Si/Sn=126 for the 140 °C 48 hr sample.

The data are further converted into a crystallinity versus time plot, as shown in Figure 2.2. The crystallinity is estimated using the ratio of peak height at 2-theta=22.4 degree (corresponding to (302) plane) between samples and a reference:

$$Crystallinity_t(\%) = \frac{Peak\ height_{(302),t}}{Peak\ height_{(302),ref}} \times 100 \tag{2.1}$$

(c)
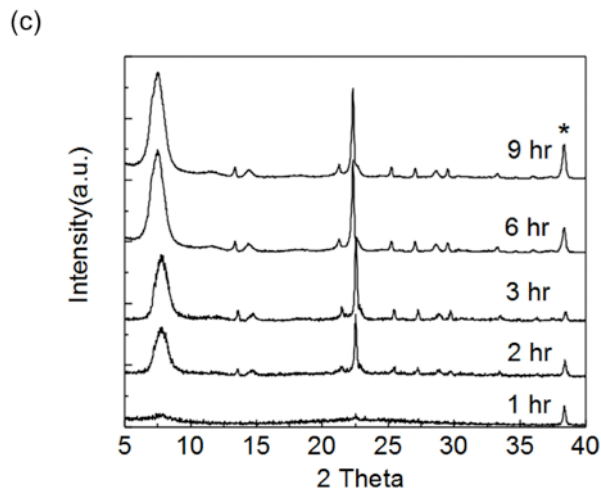
Figure 2.1 (continued) XRD patterns for Sn-Beta synthesized at (a) 140, (b) 170, and (c) 200 °C for different time with 4 % seeds. "*" represents the diffraction peak from the holder.

where t is the crystallization time, and ref is the fully crystallized sample at the hydrothermal temperature. N_2 sorption experiments were carried out for the selected reference samples (e.g., 140 °C 48 hr, 170 °C 24 hr, and 200 °C 9 hr) and all the micropore volumes of the references (Table 2.1, from t-plot) are close to 0.2 cm^3/g, which is typical for high quality zeolite beta.[27, 65, 66] The temporal crystallization shown in Figure 2.2 shows that, at 140 °C, the described seeding approach can greatly reduced the overall crystallization time from 170 hr to 24 hr to reach 90 % crystallinity, and the crystallization can be further enhanced at higher temperature, 170 °C and 200 °C. The time needed to reach 90 % crystallinity is shortened to 3 hr for 200 °C and 6 hr for 170 °C, respectively. Notably, it is clear that both the induction time and rate of overall crystal growth improved. The induction time is estimated by looking for the moment the crystals can be observed.[21] The overall crystal growth rate (conversion of stannosilicate) is estimated by the slope of linear fit from the data within 15-85 % crystallinity. At 140 °C, the induction time is reduced from 24 hr to 3 hr, and the rate of crystal growth is enhanced from 1.2 %/hr to 6 %/hr. The data indicate that the seeding process cannot only help reduce the time for induction but also improve the rate of overall crystal growth.

(a)

(b)
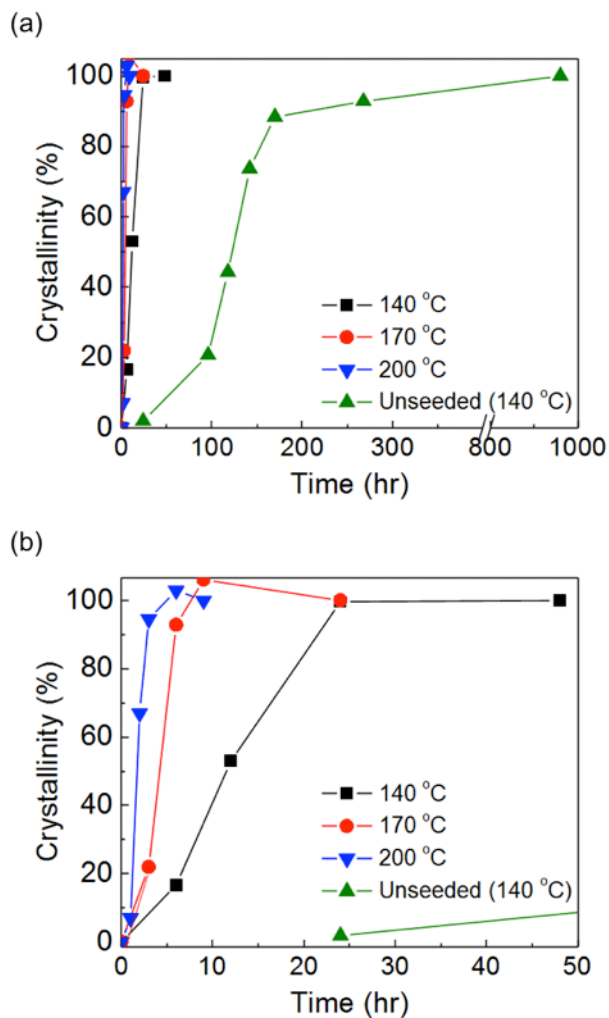
Figure 2.2 (a) Crystallization kinetics for Sn-Beta synthesized with seeds at different temperatures, 140, 170, and 200 °C. (b) is showing enlarged part for shorter crystallization time.

Table 2.1 Textural data for representative Sn-Beta synthesized in this work

Sample	BET SA (m^2/g)	V_{mic}^{a}(cm^3/g)	External SA^a (m^2/g)
140 °C 48 hr	517.4	0.202	105.1
170 °C 24 hr	504.8	0.197	102.5
200 °C 9hr	500.4	0.199	94.8
Unseeded 45d	486	0.207	66.6
^{a} from t-plot			

20
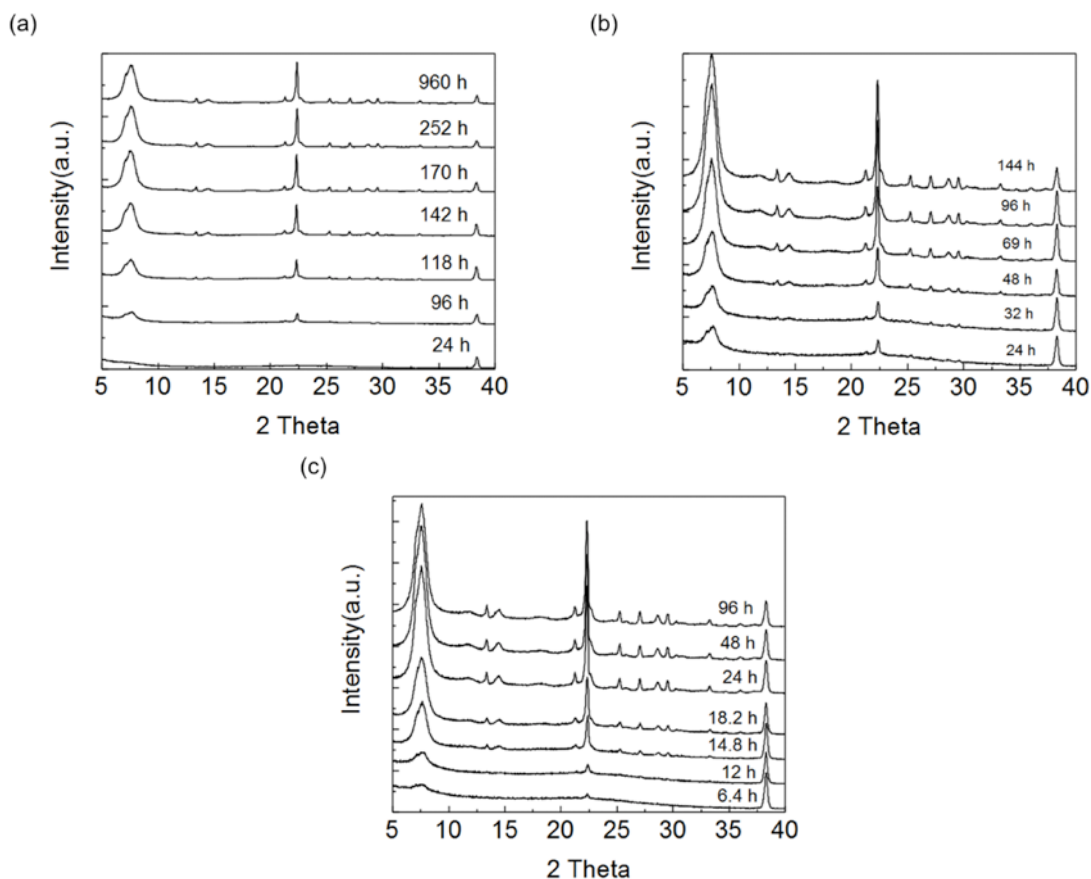
Figure 2.3 XRD patterns for Sn-Beta synthesized at (a) 140, (b) 155, and (c) 170 °C for different time without seeds.

The kinetics of crystallization were also studied for the unseeded system with same starting Si/Sn ratio in the synthesis gel. Figure 2.3 shows the temporal XRD patterns from 140 °C to 170 °C. It is clear, again, that the samples only show diffractions for zeolite beta without competing impurity zeolite phases and show similar features to the seeded Sn-Beta. It is interesting to note that, when the synthesis was carried out at 200 °C, a fully crystalline sample cannot be obtained, as shown in Figure 2.4. After 1 day crystallization, the crystal growth appears to stall and the crystallinity of the samples could not improve further up to 4 day, maintaining at about 15-20 % crystallinity when using fully crystallized sample at 170 °C as a reference. There is still no other crystalline impurity can be observed. It has been suggested that the decomposition of TEA^+ via Hofmann elimination begins at as low as 125 °C but delays at lower pH, as monitored by pressure generated within the reaction

21

vessel.[67] It is plausible that under the synthesis and hydrothermal conditions (200 °C), the TEA$^+$ ion is not stable enough to last for more than 24 hr such that further crystallization is inhibited. For the case in synthesis of Sn-Beta with addition of 4 % seed crystals, the crystallization is so fast that the crystallization completes before TEA$^+$ ion starts to degrade, even at 200 °C (Figure 2.1 and 2.2). The corresponding crystallization curves for unseeded system carried out within 140 to 170 °C is shown in Figure 2.5. With increasing crystallization temperature from 140 to 170 °C, induction time reduces, and crystal growth rate increases, similar to the seeded growth synthesis.

Assuming the processes during the induction period and crystal growth are energy activated, the apparent activation energy of induction period can be obtained according to the Arrhenius relationship. Arrhenius plots are constructed based on the temporal crystallization data and shown in Figure 2.6, and the extracted apparent activation energies are summarized in Table 2.2. As listed in Table 2.2, the apparent activation energy for induction period during Sn-Beta crystallization greatly reduced with addition of seed crystals, from 66.8 to 35.1 kJ/mol. It is likely the added seeds help the
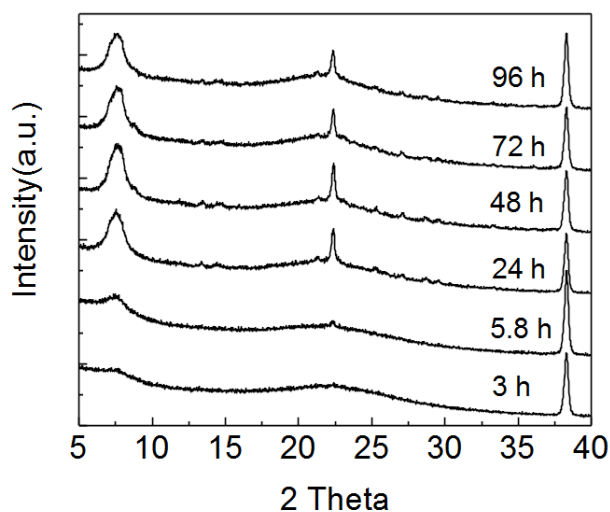
Figure 2.4 Temporal XRD patterns for Sn-Beta crystallized without seed at 200 °C.
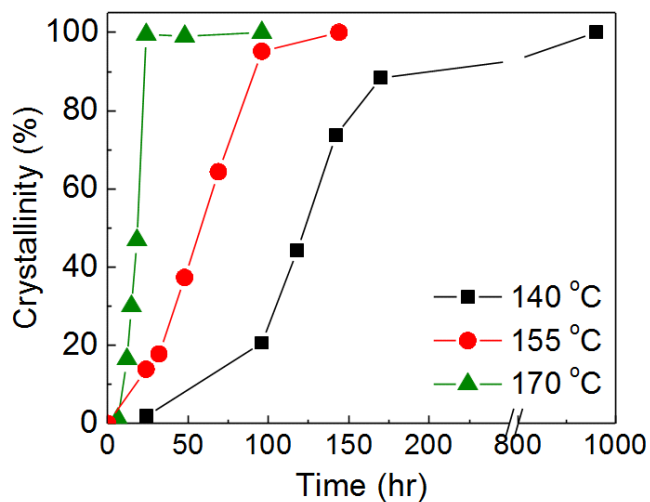
Figure 2.5 Crystallization kinetics for Sn-Beta synthesized without seeds at different temperatures, 140, 155, and 170 °C.
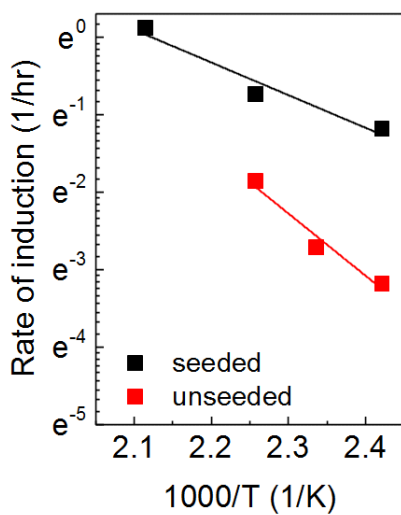
Figure 2.6 Arrhenius plots for induction period.

Table 2.2 Apparent activation energies extracted from the Arrhenius plots (Figure 2.6)

Sample	Induction period (kJ/mol)
Seeded	35.1
Unseeded	66.8

23

crystallization bypass the nucleation process (which involves relaxation of synthesis gel, formation of stable nuclei, and growth of nuclei to observable size), efficiently reduced the energy barrier during the induction stage of crystal growth.[21, 31] For the crystal growth rate, it should be noted that using the crystallinity curve to estimate the rate of crystal growth is not straightforward, as the crystallinity (or, more precisely in this case, the conversion of the precursors) not only depends on the rate of crystal growth but also depends on the status of the nuclei (size and amount).[21] It is generally observed that seeding does not influence the crystal growth rate, i.e., the rate of crystal growth remains similar with and without seeds.[21, 68, 69] The difference in the absolute rate of precursor conversion shown here
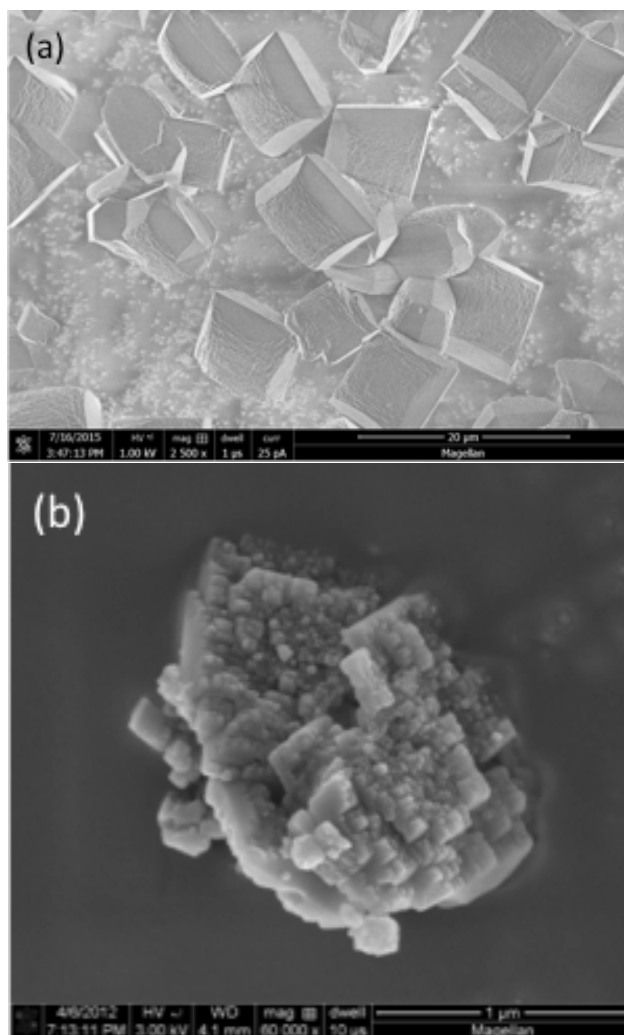
Figure 2.7 Representative SEM micrographs of (a) unseeded (155 °C, 6 day) and (b) seeded Sn-Beta (140 °C, 52 hr).

might be a result of different numbers of nuclei present in the system, as the crystal size is largely different (Figure 2.7). This shall be revisited in the future by measuring linear growth rate of the crystals to clarify the roles and functions of the seeds in this system using microscopy techniques, while the indiscernible morphology and intergrowth of the crystals during the course of the crystallization may be difficult to observe.

Figure 2.8 shows SEM images of a series of unseeded samples crystallizing at 140 °C, illustrating the macroscopic change in morphology along the crystallization. At the beginning (~0% crystallinity, Fig. 2.8(a)), only amorphous phase can be observed and those reactive precursors composed of nanometer scale domains. As the crystallization proceeds, once there is a nuclei formed in the gel, the precursors would be consumed and form crystals, and the unreacted amorphous phase can be observed on the crystal surface for further growth (Fig. 2.8(b)). The surface of the crystal thus usually is rough and blurred due to the amorphous phase. Once the crystallization is complete, the surface of the crystal would be more distinct and shows the edges and facets of the crystals (Fig. 2.8 (c)).

The effect from the amount of seeding was also studied with samples crystallized at 140 °C with 1, 4, and 10 wt% seed with respect to silica source in the synthesis gel. As shown in Figure 2.9, again, the XRD patterns shows only reflections for zeolite Beta, no crystalline impurities can be observed after prolonged heating. From the crystallinity plot (Figure 2.10), the conversion of the amorphous stannosilicate gel is enhanced with increasing amount of seeds. SEM images for Sn-Beta synthesized at 140 °C for 2 day with different amount of seeds (1, 4, and 10 wt % with respect to silica) are shown in Figure 2.11. Typical truncated bipyrimidal morphology for zeolite Beta was obtained in each case, with crystal size ranges from 500 to 1000 nm. Figure 2.12 depicts the particle size distribution as a function of amount of seed crystals, obtained by measuring the crystal size from SEM images with at least 20 crystals. The crystal size reduces from 1.2 μm for 1 wt % seed sample to about 500 nm for 10 wt % seed sample, revealing the impact of seeding on final crystal size. Since the size and shape (spherical) of the seed crystals, the amount of seeds, and yields are known, with the assumption one

seed turns into one final crystal, one can make a prediction of the size of the final product (as a tetragonal with dimension of L x L x 0.25L) by using the following equation:

$$L = \sqrt[3]{\left(\frac{V_{seed}}{C_{seed}}\right) + V_{seed}} \qquad (2.2)$$

where V_{seed} is the volume of the seed and C_{seed} is the weight percentage of seeds relative to silica. Final product size predicted from Eq. 2.2 and the experimental value yielded from SEM have been summarized in Table 2.3. From the comparison between experiments and calculation, it is plausible
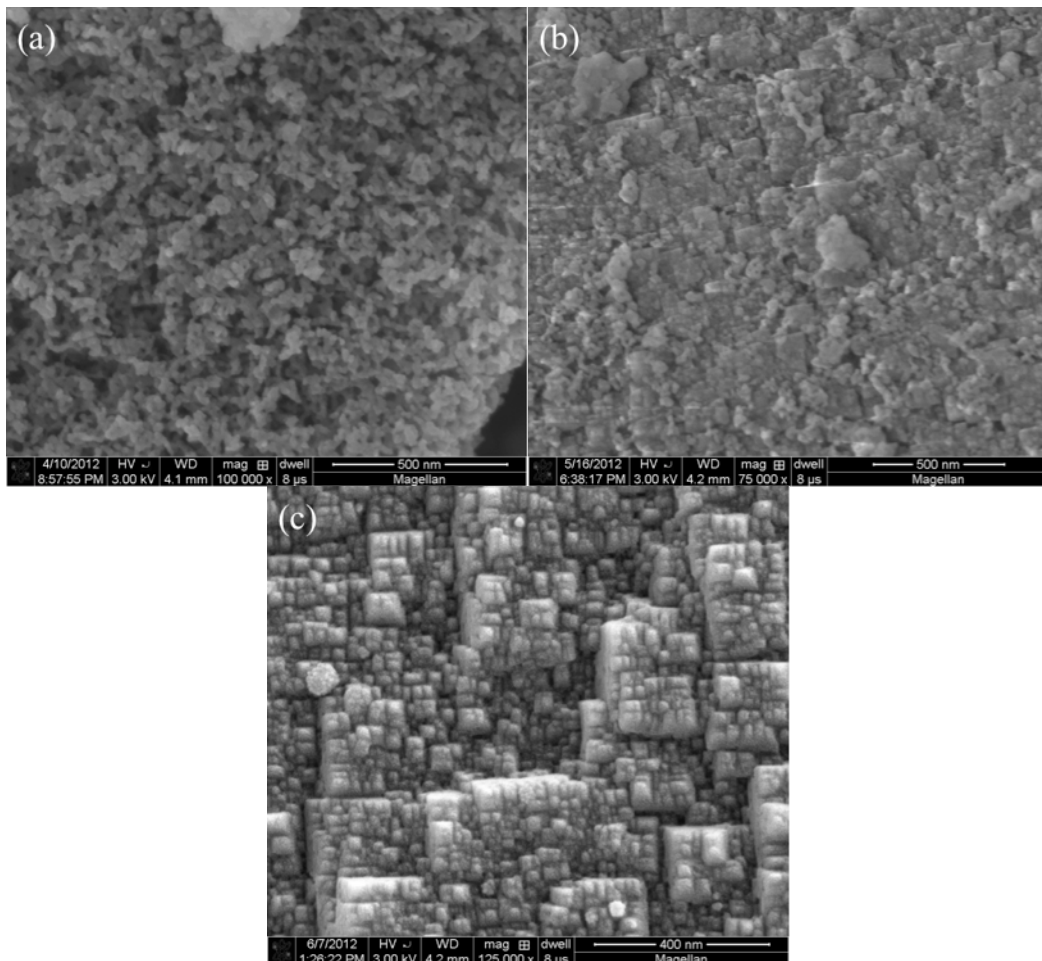
Figure 2.8 SEM micrographs of Sn-Beta with crystallnity of (a) 0, (b) 50-60, and (c) 100 %, which show only the amorphous phase exists at the early stage, and then it is consumed during the crystallization and closely in contact with crystals until fully converted to crystalline phase.

(a)

(b)
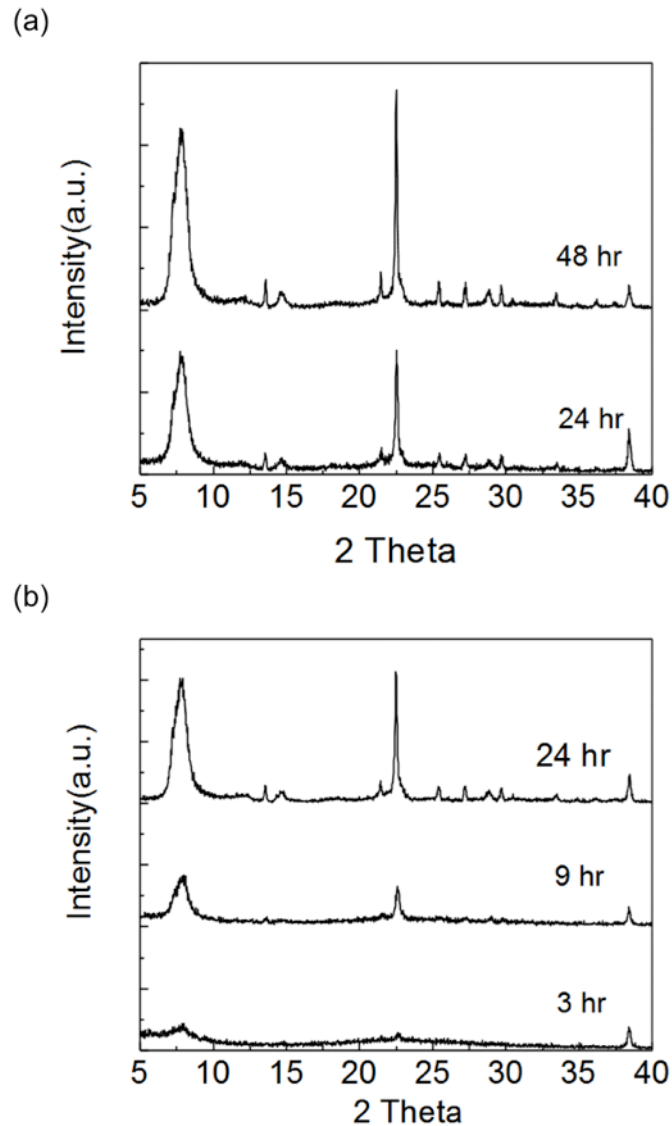
Figure 2.9 XRD patterns of seeded Sn-Beta synthesized at 140 °C with (a) 1 and (b) 10 wt % seeds. The holder gives the diffraction peak at 2-theta=38.5°.

that one seed crystal can turn into one final crystals. The SEM observation is consistent with the statement. As shown in Figure 2.13, it can be seen that the seeds in contact with the final crystals, and part of the seed is submerged in the large crystals, providing a piece of evidence of the role of the seed during the synthesis. In general, the basic function of the seed crystals is to provide surface area for desired crystalline phase to grow, and the seeds could remain inert, be dissolved, act as pure seed, or promote secondary nucleation.[31] In this case, the seed crystals seem to be intact and provide the surface area for Sn-Beta to crystallize. Secondary nucleation does not seem to happen in a large

27
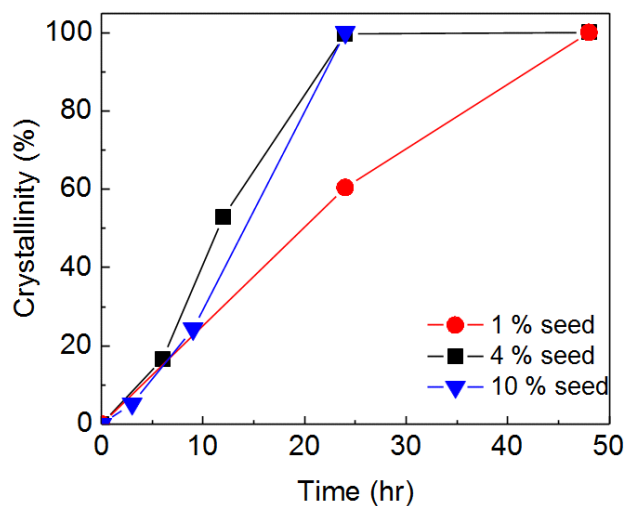
Figure 2.10 Crystallization kinetics for Sn-Beta synthesized at 140 °C with 1, 4, and 10 wt %.
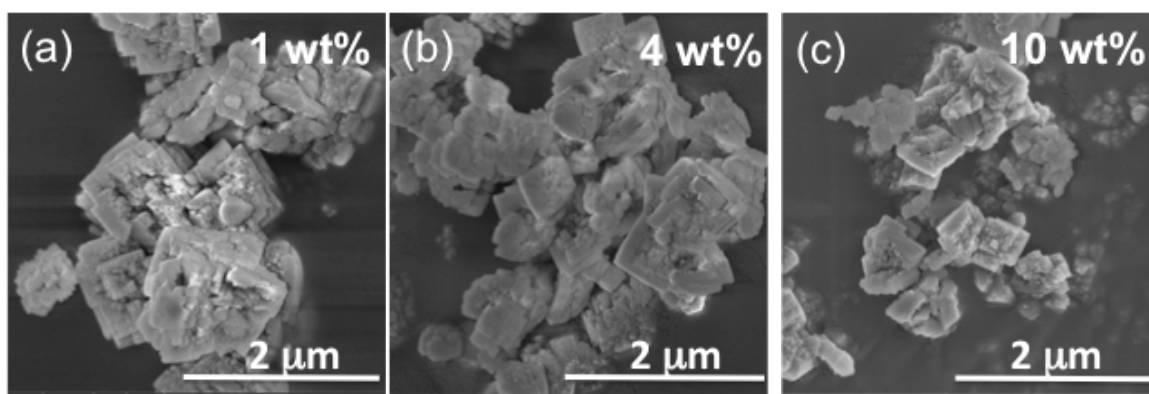
Figure 2.11 SEM mircrographs for the Sn-Beta synthesized at 140 °C for 2 day with (a) 1, (b) 4, and (c) 10 wt %.

extent, from the particle size distributions (bimodal distribution could be expected) and the crystal size calculations. It is likely that the added seeds consume the ingredient flux from the synthesis medium, and the nutrients content in the gel becomes lower and lower, such that secondary nucleation is not observed before the nuclei formed. It also indicates the addition of seeds does not induced nucleation in the current system.
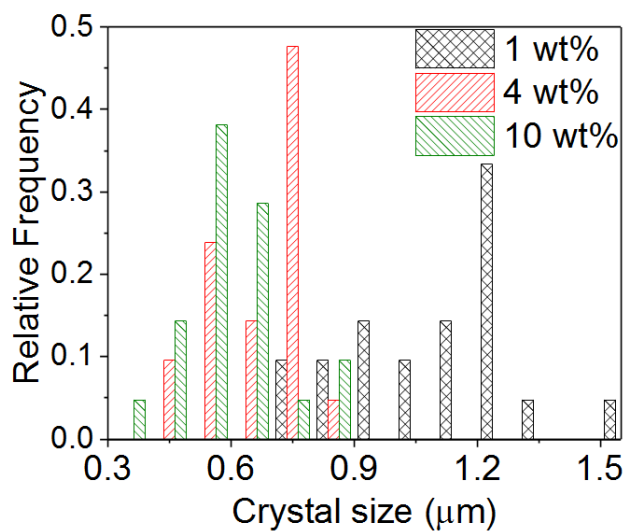
Figure 2.12 Crystal size distribution obtained from SEM as a function of different amount of seeds in the synthesis.

Table 2.3 Particle size for different amount of seeds from SEM and calculation

	Unseeded	1 wt%	4 wt%	10 wt%
Particle size[a] (μm)	12	1.11±0.074	0.66±0.043	0.56±0.043
Calculated size (μm)	-	1.19	0.76	0.57

[a]From SEM
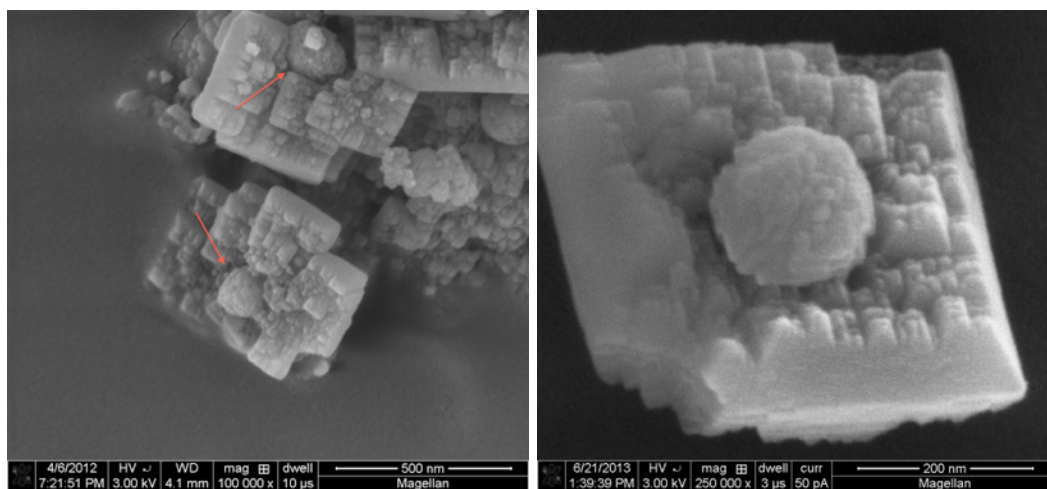
Figure 2.13 Representative SEM images for Sn-Beta made from seeded growth method. Left: 140 °C 52 hr; right: 170 °C 12 hr. Arrows indicate the seeds in contact with the crystals.

Based on above crystallization studies, a macroscopic crystallization scheme is proposed, as shown in Scheme 2.1 to discern the effect of seeding and the nature of the synthesis gel. In the unseeded case, the induction time for the stable nuclei formation is long, in the order of days. Once the nuclei form, the amorphous phase in contact with the nuclei start to transform into crystalline phase, resulting in large crystals (~ 5-10 μm) (Scheme 2.1A). As in the seeded growth case, the onset of crystallization is in the order of hours, greatly reduced the induction time. At the same time, adding seeds provide the surface for the nutrient flux to deposit, thus greatly reduced the overall crystallization time and small crystals can be formed (Scheme 2.1B and C). It is also reasonable to expect particle size control using this concept in the current system.

During the exploration, there were certain samples show faster crystallization kinetics, and it was found that those samples tend to contain less synthesis gel in the autoclave. Two hypotheses were introduced to explain the result, one is that the small amount of the gel helps the heat transfer within the sample and thus increase the kinetic; the other assumption is that, due to the small mass of the gel, the water content in the gel has changed under vapor-liquid phase equilibrium at crystallization temperature, and the dense gel reaches higher supersaturation and thus enhances the kinetics. To examine the hypotheses, several H_2O/Si ratios of Sn-Beta were prepared. The samples were prepared by placing the 4 wt% seeded synthesis mixture (H_2O/Si=7.5) into a vacuum (-30 in. Hg) oven at 60-80 °C for different periods of time, and 3 g of the precursor was charged into Teflon lined autoclaves. The autoclaves were then placed in a preheated convection oven at 200 °C under rotation (2 rpm) for 1 hr. Figure 2.14 shows the XRD patterns for the series of the samples. The spectra reveal the reflection peaks only corresponding to zeolite Beta phase, and kinetic of crystallization is greatly affected by water content. With reducing water content from H_2O/Si=7.5 to 2, the crystal growth increases, indicating the crystallization rate of Sn-Beta can be further improved; while further evacuating water (H_2O/Si=1.35 and 0.41) from the precursor results in samples with low degree of crystallinity. The data suggest that water plays a vital role during the crystallization of Sn-Beta zeolite. With the reduction of water, the concentration of the stannosilicate species in the gel

30
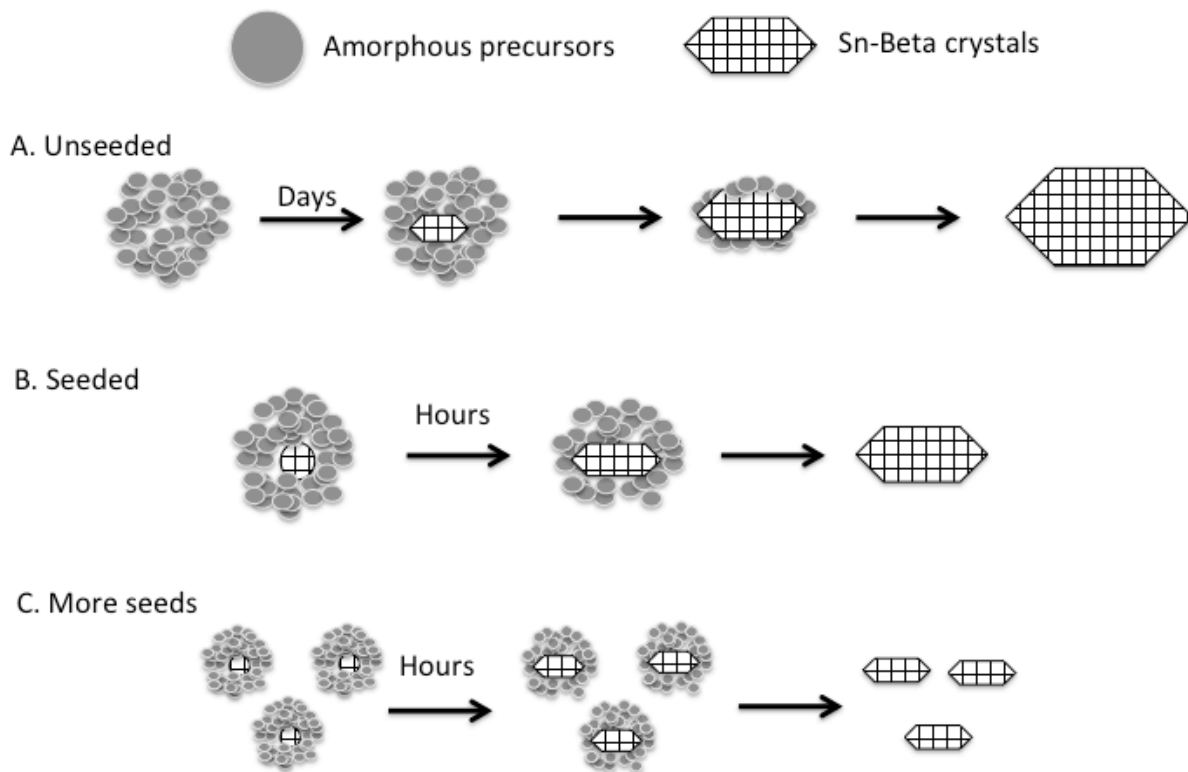
Scheme 2.1 Illustration of the effect of seeding on crystallization in Sn-Beta system based on experimental findings.
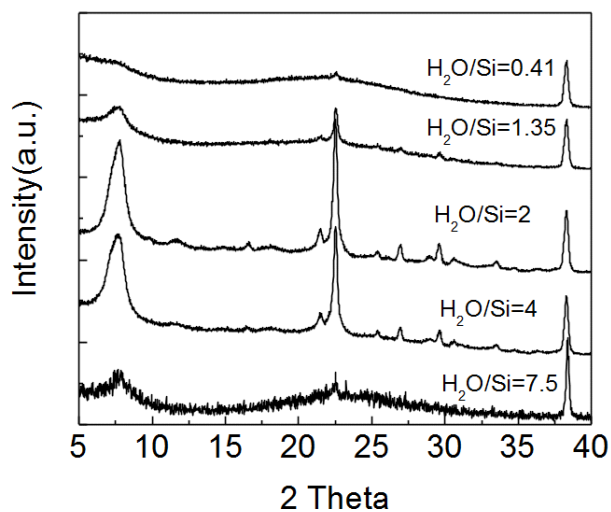
Figure 2.14 XRD patterns for Sn-Beta samples with different H_2O/Si ratios. The precursor gels (3 g in a 50 mL autoclave) were heated at 200 °C for 1 hr.

increases and enhances the crystal growth kinetics. However, with low water amount in the gel, the transport of the ingredient and T-O-T bond breaking (by hydrolysis) might be hindered. It has been proposed that T-O-T bond forming and breaking are the basic actions for zeolite crystal growth:[31]

$$T - O - T + H_2O \leftrightarrow T - OH + T - OH \hspace{3cm} (2.3)$$

It should be noted that, under basic conditions, the bond breaking and remaking can be catalyzed by hydroxyl ions (OH⁻). Thus, it is plausible that if higher pH is employed in this system (using ammonium fluoride (NH_4F) as fluoride source instead of hydrofluoric acid (HF)), the crystallization rate may be further improved. Recently, the solvent free routes for zeolite formation were reported, implying that solvent is not necessary in the synthesis.[70, 71] Inspecting the details in the reports and combine the discussions here, very little amount of water should be needed in the synthesis, and the formation of crystals would be kinetic consequences depending on the composition of the gel systems.

An implication from the H_2O/Si study is that the ratio between the amount of the precursor and the volume of the autoclave is also an important factor regarding to crystallization of Sn-Beta. Considering the water containing in the synthesis mixture is to be heated to high temperature, 140-200 °C in this case, the water vapor in the autoclave would be in vapor-liquid equilibrium with the water in the gel phase. The vapor pressure might not be as high as pure water case due to the presence of solute, but loss of water from the synthesis gel is inevitable. With low amount of water (H_2O/Si=7.5) to start, loss of water could result in significant change in water content in the synthesis precursor during heating particularly if the amount of the precursor is small, and faster crystallization rate can be observed. Kang et al. proposed a steam assisted crystallization (SAC) method in fluoride medium, which uses saturated steam generating in the autoclave (not in direct contact) to crystallize a very dense zeolite precursor phase, shortening the crystallization time by forming Sn-Beta in 5 hr (Si/Sn=125, 180 °C), while featuring low micropore volume (~0.16 cm^3/g).[34] The authors then examined the water amount placed at the bottom of the autoclave in the following report and found that the composition change of the synthesis gel due to the condensation of water, resulting in

amorphous phase when large amount of water in the autoclave (180 °C, 6 hr), which is consistent with our results.[72]

The Sn environment is characterized for the sample crystallized at 140 °C for 2 days. DR-UV-Vis spectroscopy, depicted in Figure 2.15, reveals a sharp adsorption band at ~200 nm, characteristic for tetrahedrally coordinated Sn in zeolite framework featuring the ligand (O^{2-}) to metal (Sn^{4+}) charge transfer.[40, 73, 74] The absence of broad adsorption band at 245-325 nm (assigned to extraframework Sn and Sn in SnO_2) indicates most of Sn is incorporated into the framework. Temperature-programmed desorption (TPD) pyridine FT-IR was employed to study the acidity of the sample, and the results are shown in Figure 2.16. The IR spectra of adsorbed pyridine in the range of pyridine ring-stretching modes on the Sn-Beta were measured after desorption at different temperatures. The vibrations of C-C(N) stretching modes of hydrogen-bonded (hb) and physically (ph) adsorbed pyridine were observed
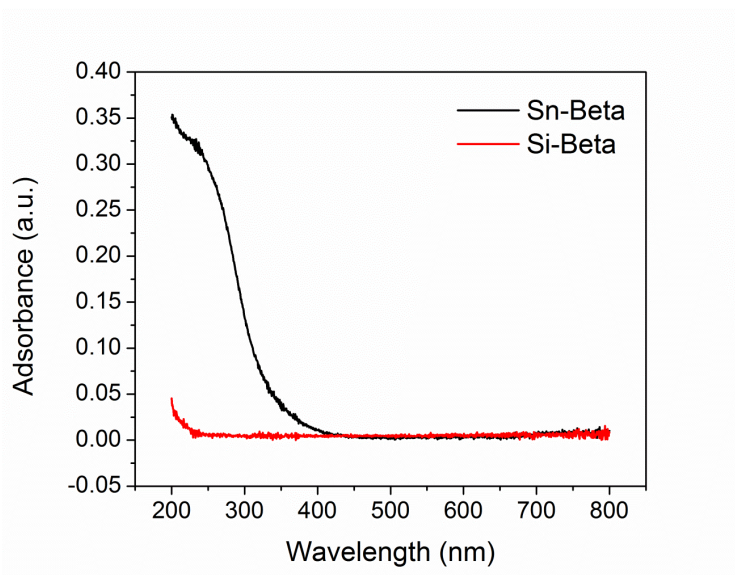
Figure 2.15 UV-Vis diffuse reflectance spectrum of synthesized Sn-Beta (140 C 48 hr) and siliceous Beta.
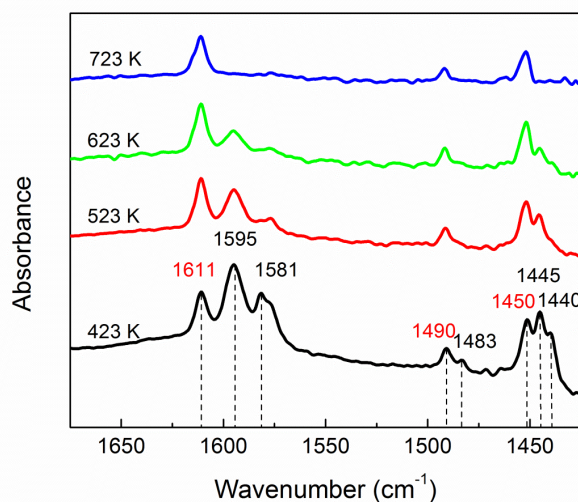
Figure 2.16 IR spectra of Sn-Beta after pyridine adsorption at 393 K for 30 min and desorption at 423 (a), 523 (b), 623 (c), and 723 K (d) for 1 h, respectively. The bands (1611, 1490 and 1450 cm^{-1}) associated to Lewis acidity are marked in red.

at 1595 cm^{-1} (hb, mode 8a), 1581 cm^{-1} (hb, ph, mode 8b), 1483 cm^{-1} (ph, mode 19b) 1445 cm^{-1} (hb, mode 19b) and 1440 cm^{-1} (ph, mode 19b), respectively.[37, 75-77] The physically adsorbed pyridine (bands at 1483 cm^{-1} and 1440 cm^{-1}) completely diminished after the desorption at 523 K. Hydrogen-bonded pyridine at 1595 cm^{-1} and 1445 cm^{-1} contributed by the hydroxyl groups (from the defects and external surface of the catalyst) decreased in intensity with increasing the desorption temperature. Absorbance at 1550 cm^{-1} associated with strong Brønsted acid sites was not observed in the sample. In addition to the hydrogen-bonded and physically adsorbed pyridine, the two distinct bands at 1611 cm^{-1} and 1490 cm^{-1} and a shoulder one at 1450 cm^{-1} were observed in all spectra. These bands are associated with the different vibration modes of the pyridine-rings adsorbed on the Sn species within zeolite beta, clearly indicating the presence of Lewis acidity in the sample.[78-80] The three bands were remained even after desorption at 723 K showing the Lewis acid sites are resistant against the relatively high temperature. The Sn-Beta synthesized here thus exhibits mainly Lewis acidity. FT-IR study of CD$_3$CN adsorption was widely used to assess the Sn coordination and Lewis acidity of Sn-containing materials.[54, 81, 82] Figure 2.17 shows the CD$_3$CN adsorbed FT-IR spectra of Sn-Beta synthesized at 140 °C for 2 day (Figure 2.17(a)) and 200 °C for 9 hr (Figure 2.17(b)) after different

desorption times at 100 °C. The band at 2263-2266 cm^{-1} can be assigned to physically adsorbed CD$_3$CN, while the band at 2276 cm^{-1} reflects the interaction of CD$_3$CN and silanol groups, and the band around 2310 cm^{-1} is attributed to the vibration related to framework Sn species.[54, 81] It has been proposed that the v(C-N) vibrations around 2310 cm^{-1} can be used to distinguish the "close" (2308
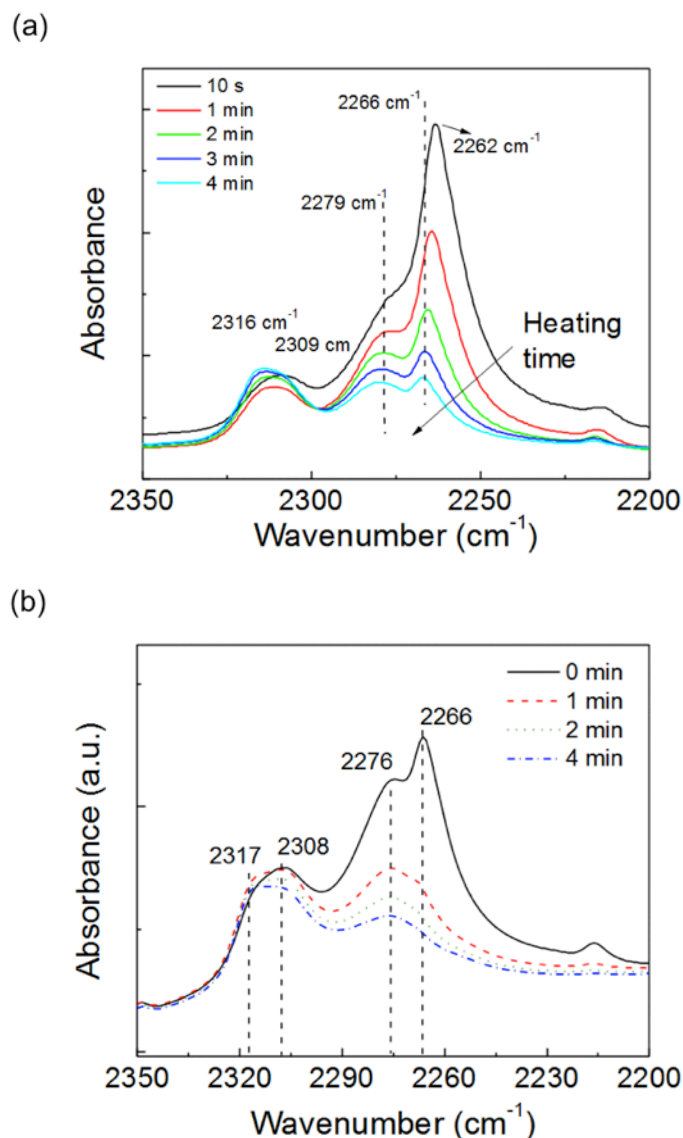
Figure 2.17 CD$_3$CN adsorbed FT-IR spectra of Sn-Beta synthesized at (a) 140 °C 48 hr and (b) 200 °C 9 hr and (c) SnO$_2$/Si-BEA. The spectra were acquired after saturation of CD$_3$CN on the samples followed by different period desorption time at 100 °C, as specified in the figures.

cm^{-1}) or "open" (hydrolyzed; 2316 cm^{-1}) Sn sites in Sn-Beta framework.[81] Two bands (2308 cm^{-1} and 2316 cm^{-1}) can be clearly observed during the desorption of CD$_3$CN for the two samples synthesized at different temperature and time, which is consistent with previous literature.[81] Upon heating, the high wavenumber band start to appear for the two samples. It should be noted that a recent report suggests the two vibration bands can also happen due to the different packing structures of CD$_3$CN rather than the difference in Sn site structures, not necessarily to be able to distinguish from close and open sites.[54] While the information about the local environment of Sn is still elusive, incorporation of Sn can be assured using this technique. Therefore, it is concluded that, Sn was incorporated into zeolite framework even when the crystallization time is as short as 9 hr.

To further confirm the coordination environment of Sn in the rapid synthesized Sn-Beta sample, glucose with deuterium substituted at the C-2 position was used in the isomerization reaction.[83] The ^{1}H-NMR spectra for unlabelled fructose and fructose isomerized from labelled glucose are shown in Figure 2.18. Presence of one resonance at δ = 3.4 ppm and the absence of other resonances at δ = 3.4-3.5 ppm corresponding to the protons at C-1 position in ^{1}H-NMR spectrum of fructose after reaction indicates that the reaction only undergoes an intramolecular hydride shift from C-2 to C-1 in water, which is consistent with previous report.[83] With the XRD, UV-Vis spectroscopy, CD$_3$CN FT-IR data, and deuterated glucose isomerization experiments, it is suggested that Sn is indeed incorporated into zeolite Beta framework, without detectable extraframework Sn species.

Based on the results presented here, it is believed that the keys to be able to greatly shorten the crystallization time from 11-40 days to 3 hr are the crystallinity, well-defined morphology of the seed crystals, and fine dispersion of the seeds in synthesis mixture. The synthesis started from a stable seed solution containing well-crystalline zeolite beta (Si/Al = 23) prepared according to the previous literature. The size of the zeolite beta seeds was around 150-200 nm as shown in Figure 2.19. In order to avoid the irreversible aggregation caused by calcination and drying, dealumination of the zeolite
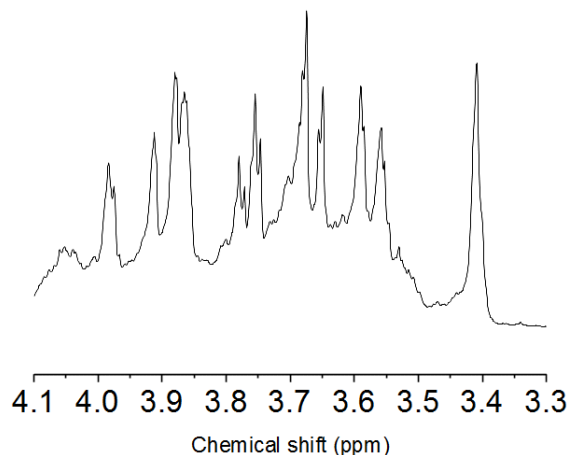
Figure 2.18 ^{1}H-NMR spectrum of fructose after isomerization reaction of deuterium substituted glucose over Sn-Beta synthesized at 200 °C for 9 hr. Reaction conditions: glucose/Sn=50, 95 °C 2hr. The separation was achieved by running the reaction mixture on HPLC (LC-20, Shimadzu) with a Biorad HPX-87C column (Ca^{2+}-type), operated at 80 °C. Water was used as mobile phase at a flow rate of 0.6 mL min^{-1}. Fructose portion was collected by a fraction collector (FRC-10, Shimadzu). The solution containing fructose was then heated in a 70 °C oven to evaporate the solvent. The obtained solids were re-dissolved in D$_2$O prior to ^{1}H-NMR measurement (AVANCE 400, Bruker).
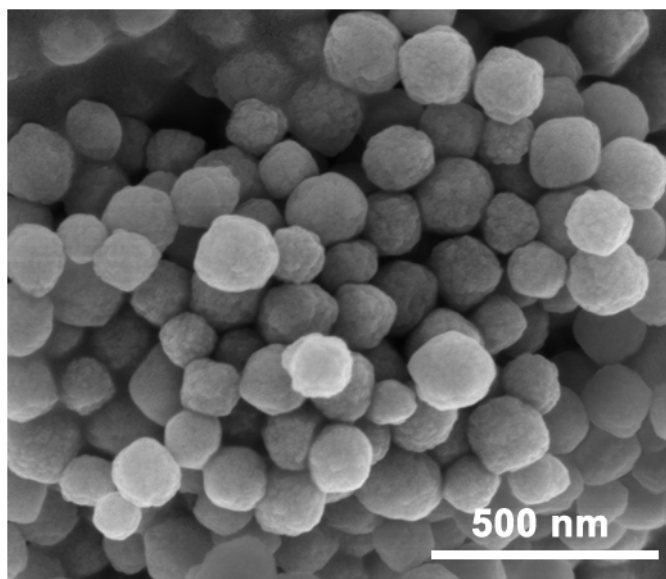
Figure 2.19 SEM image for the seed crystals applied for seeded growth of Sn-Beta.

seeds was carried out by directly treating the stable seed solution with a concentrated nitric acid solution. During the whole process, no drying or calcination were performed on the sample, which enabled us to prepare a stable suspension with well-dispersed dealuminated zeolite seeds. As shown

in Figure 2.20, the traditional seeds (dried and calcined) synthesized according to Corma et al.[26] composed of aggregated nanocrystallites with primary domain size about 20 nm, while the zeolite beta seeds from suspension has discrete crystals with about 150-200 nm. It is known that it is not easy to fully re-disperse the aggregated crystals into solution, and it avoids good dispersion in the synthesis medium.[84] The author has attempted to re-disperse dried 160 nm zeolite beta, and it takes days of sonication to reach satisfactory dispersion, and it highlights that it requires extra attention to create good suspension from once-dried crystals.

The crystallinity of the seeds showed no sign of a significant change after the dealumination process as illustrated in the XRD patterns (Figure 2.21). It should be noted that the relative peak intensities (e.g., peak at 2-theta ~ 7.5 degree ((101) plane in *BEA structure) and 22.4 degree ((302) plane in *BEA structure)) from the Figure 2.21 differ before and after dalumination, and it accompanies with appearance and disappearance of certain reflection peaks, which indicates the
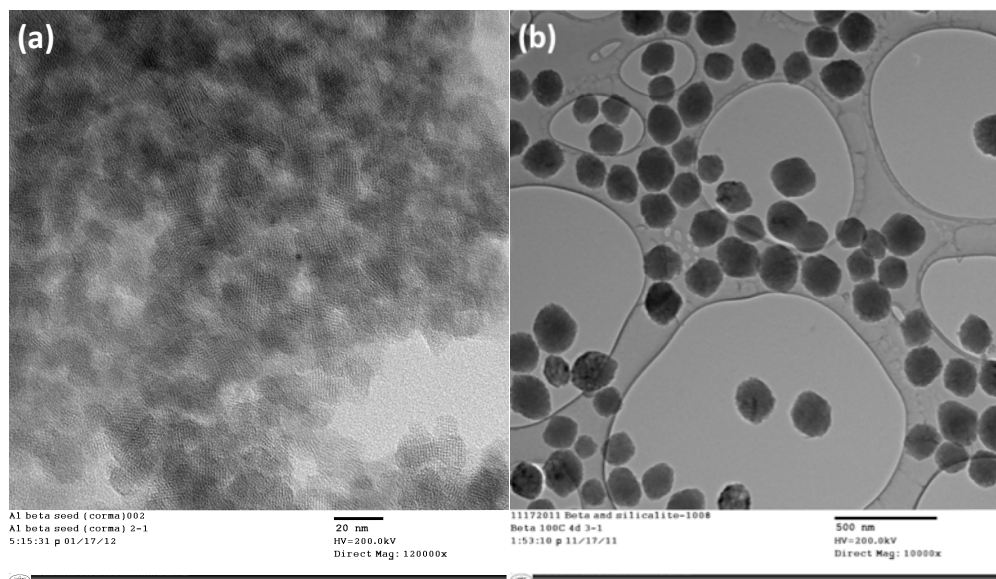
Figure 2.20 TEM images for the seed crystals made according to (a) Corma et al. and (b) Chen et al. The lattice fringe can be observed in (a), indicating the aggregation is indeed crystals, not amorphous phase.

structure directing agent utilized in the synthesis (TEA$^+$) has been simultaneously removed from the zeolite voids during the dealumination process, resulting in changes in the local electron density in the solid samples and contributing to the changes of diffraction intensity of crystal planes. The TGA and DTA analysis of the dealuminated zeolite beta seeds shown in Figure 2.22 provides further evidence. From the data, the weight change due to SDA decomposition is about 4 %, and the main loss at 250-300 °C may be attributed to Hofmann elimination of TEA$^+$ to triethylamine and ethylene from [TEA$^+$($\equiv$SiO)$^-$].[85] For the sample before dealumination, the weight loss is greater than 20 % (data not shown).

The catalytic performance of the synthesized Sn-Beta (140 °C 2 day) was tested on the isomerization of glucose and xylose in aqueous phase and isomierization-etherification of dihydroxyacetone (DHA) to methyl lactate in methanol. The reaction results are shown in Figure 2.23. The main products of the isomerization are fructose and mannose. The conversion of glucose after 2 h is 54 %, the yields of fructose and mannose are 36 % and 9 %, respectively (Figure 2.23a) Similar results were reported by Moliner et al.[9] and Lew et al.[33] In their studies, the Sn-Beta catalysts
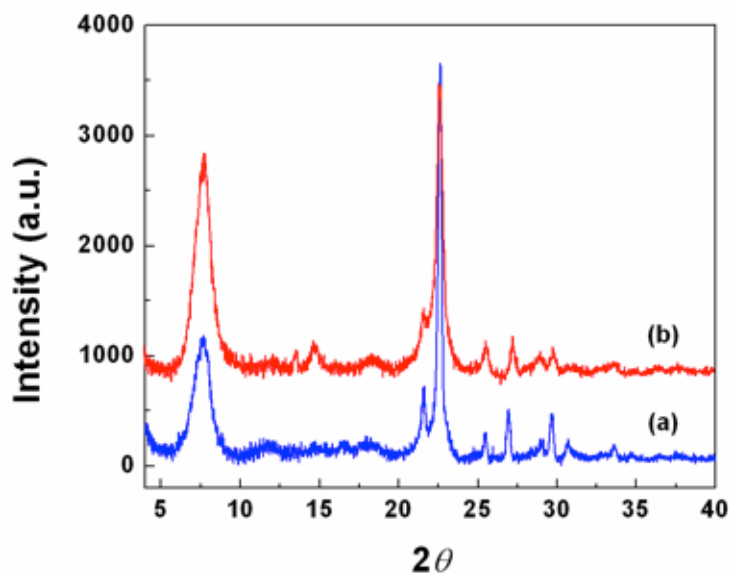
Figure 2.21 XRD patterns of the seed crystals (a) before and (b) after dealumination.
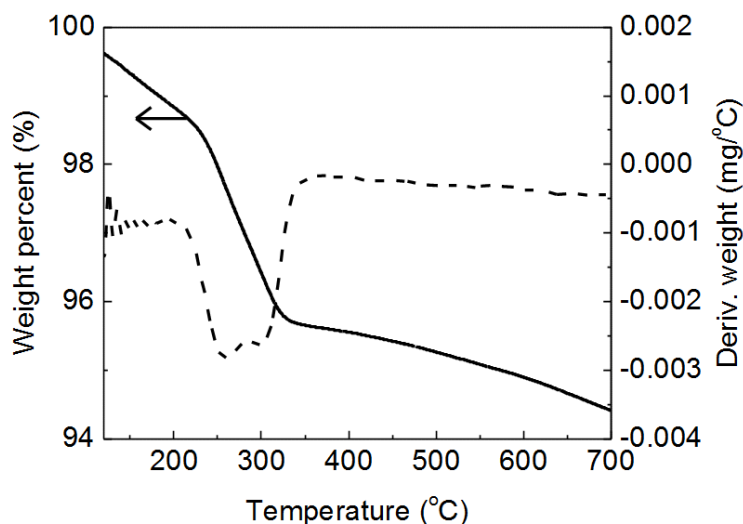
Figure 2.22 TGA and DTA data for the dealuminated seed crystals

were made by conventional method with a crystallization time from 22 days to 40 days depending on

if zeolite seeds were used. It is also known that the Sn-Beta catalyst is highly active for the

isomerization-esterification of triose sugar to methyl lactate. The Sn-Beta made in this study was used

to catalyze the reaction of dihydroxyacetone (DHA) in methanol at 70 °C (Figure 2.23b). As expected,

DHA was selectively converted to methyl lactate with a small amount of glyceraldehyde (GLA), an

isomer of DHA, in the first hour. After 7 hours, DHA was fully converted to methyl lactate,

resembling the results reported by Taarning et al.[61] In xylose isomerization reaction, the products of

the reaction are xylulose, lyxose and byproducts from degradation reactions and/or polymerization

reactions. The isomerization of xylose to xylulose catalyzed by Sn-Beta is analogous to the

isomerization of glucose to fructose as proposed by Moliner et al.[9] and Choudhary et al.[60] The

isomerization reactions reached equilibrium at 0.5 h with a maximum xylulose+lyxose yield of 35 %

at xylose conversion of 61 % (Figure 2.23c). The xylulose+lyxose yield decreased with time as a

result of side reactions consuming xylose, xylulose and lyxose. This result is also comparable to the

observation reported by Choudhary et al.[60] and Lew et al.[33] To evaluate the reproducibility of our

synthesis method, Sn-Beta made from 6 different batches were tested on the isomerization of glucose.

The standard deviation of their activity, an indicator of reproducibility, is less than 4 %, as shown in Figure 2.24.

In summary, the above data clearly indicate the Sn-Beta rapidly synthesized (2 days) from the modified seeding method resembles the catalytic property of traditional Sn-Beta (11-40 days of crystallization) and the method is highly reproducible. In addition, ammonium fluoride (NH$_4$F), a more benign fluoride alternative for hydrofluoric acid, was employed in the synthesis and also yielded
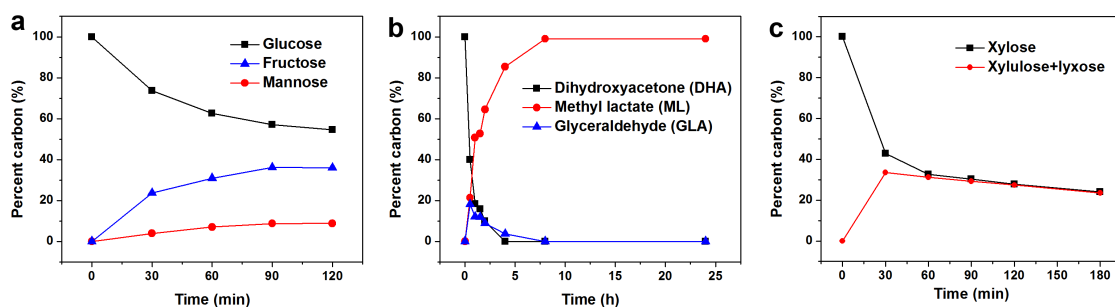
Figure 2.23 Yields of major products as a function of reaction time for the reactions of cellulosic sugars catalysed by the Sn-Beta. a), Isomerization of glucose in aqueous phase. Reaction conditions: initial glucose concentration of 10 wt%, glucose to Tin molar ratio of 50:1, 100 mg Sn-Beta, 90 °C; b), Reaction of dihydroxyacetone (DHA) in methanol. Reaction conditions: 1.25 mmol DHA, 4 g methanol, 80 mg Sn-Beta, 70 °C; c), Isomerization of xylose in aqueous phase. Reaction conditions: initial xylose concentration of 10 wt%, xylose to Tin molar ratio of 70:1, 78 mg Sn-Beta, 100 °C.
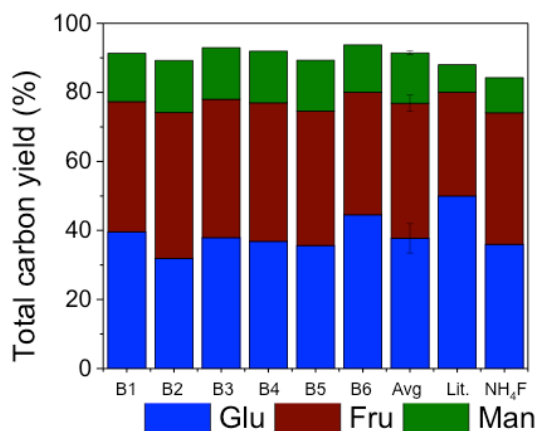
Figure 2.24 Product distribution of glucose isomerization reaction over different batches of rapid synthesized Sn-Beta compared to literature data and the sample prepared from ammonium fluoride.

active Sn-Beta material. Thus, the developed seeding method can greatly shorten the crystallization time without sacrificing catalytic properties due to well-defined crystalline zeolite Beta seeds and better dispersion of the seeds in the synthesis gel. The method can also be extended to other solid Lewis acids such as Ti- and Zr-Beta, etc.

CHAPTER 3

FLUORIDE-FREE SYNTHESIS OF TIN-BETA ZEOLITE BY DRY-GEL

CONVERSION METHOD

3.1 Background

Zeolites have been extensively used in catalysis, ion-exchange and separation due to their highly crystalline microporous structure and a large variety of available frameworks and compositions.[86-89] In addition to Brønsted acid catalysts, molecular sieves containing tetrahedrally coordinated Sn, Ti and Zr have been used for Lewis acid-catalyzed redox reactions.[9, 26, 27, 60, 61, 90, 91] In particular, Sn-BEA molecular sieve, a crystalline stannosilicate with BEA topology, exhibits extraordinary Lewis acidity for selectively activating functional groups of organic molecules involved in fine chemical syntheses.[92-98] The catalyst has shown promising activity for the catalytic oxidation of saturated and unsaturated ketones through the Baeyer-Villiger reaction and the reduction of carbonyl compounds with secondary alcohols through the Meerwein-Ponndorf-Verley reaction.[26-28] Moreover, Moliner *et al.* recently reported that Sn-BEA is water-tolerant and capable of catalyzing isomerization of glucose to fructose in aqueous phase,[9] a key intermediate step for the conversion of biomass into chemicals and fuels.[29] Similarly, Sn-BEA has also been used to catalyze the isomerization of pentose and triose sugars to form xylulose, methyl lactate and lactic acid.[60, 61, 99] The outstanding Lewis acidity of Sn-BEA catalyst in aqueous phase is likely due to the hydrophobic environment created by the defect-free siliceous surface.[95, 100, 101]

As mentioned in Chapter 1, the broad application of Sn-BEA zeolite might be hindered due to the utilization of hydrofluoric acid in the conventional synthesis. Although post-synthesis methods were reported, to our best knowledge, direct synthesis of Sn-BEA catalyst from a fluoride-free system has not been achieved so far. The challenges are mainly due to the difficulties in the crystallization of siliceous zeolite BEA in the absence of fluoride and incorporation of tetrahedrally coordinated Sn in zeolite frameworks. It has been known that during zeolite syntheses fluoride can facilitate the

mineralization of silica sources and compensate the positive charges associated with the organic structure directing agents (OSDAs) employed in the syntheses.[102] As a result, the zeolites synthesized in the presence of fluoride exhibit fewer defects and higher crystallinity than the ones made under conventional hydrothermal synthesis conditions. In order to synthesize high silica or siliceous zeolites without using fluoride, the positive charges of OSDA must be compensated by the defects located in the framework (*e.g.* ≡Si-O⁻ ⋯HO-Si≡), which is particularly challenging for relative small OSDAs, such as tetraethylammonium (TEA) used in zeolite BEA synthesis. The small OSDAs usually result in an increased number of OSDAs occluded in zeolite channels (*e.g.* 6 TEA/unit cell for BEA, while only 4 TPA/unit cell for MFI),[103, 104] which requires more defects for charge compensation and could compete with the formation of stable crystalline phases. This challenge has been partially solved by using dry gel conversion (DGC) method that was initially developed for ZSM-5 zeolite and later extended to several other zeolites including high silica zeolite BEA.[105, 106] In the DGC method, crystallization of a concentrated gel is carried out under saturated steam generated from liquid water which is not allowed to directly contact with the synthesis gel. Using this method, zeolite BEA with a wide range of Si/Al ratio has been successfully synthesized.[106] Although incorporation of other heteroatoms in zeolite frameworks by the DGC method has also been demonstrated for TS-1 and Ti-BEA,[107, 108] synthesis of Sn-BEA by the DGC method has not succeeded, likely due to the relatively large atomic size of Sn (Ti^{4+} : 0.68 Å, Sn^{4+} : 0.71 Å) and the incomparable hydrolysis rate of Sn source with silica source. These differences could lead to an amorphous phase, incredible slow crystallization and non-framework Sn as shown later in this study.

Herein, a direct and fluoride-free synthesis route is developed for Sn-BEA. We demonstrated that an active Sn-BEA catalyst can be directly synthesized by the DGC method without using any fluoride containing chemicals. The use of crystalline seeds and inorganic cations for charge compensation is essential for the crystallization of Sn-BEA in the absence of fluoride. The inorganic cations in the as-synthesized sample must be ion-exchanged to ammonium type in order to maintain the crystalline

structure of the formed catalysts during calcination. The synthesized Sn-BEA exhibits hydrophilic nature compared to the ones synthesized in the presence of fluoride.

3.2 Experimental

3.2.1 Preparation of materials

A dry gel conversion method was used to synthesize Sn-BEA in the absence of fluoride. In a typical synthesis, 0.0448 g of sodium hydroxide was dissolved in 3.09 g of 35 wt% tetraethylammonium hydroxide (TEAOH) solution and 14 g of deionized water in a plastic vessel followed by adding 1 g of fumed silica. The obtained solution was magnetically stirred for 1 h at room temperature. Tin source solution containing 0.0548 g of tin tert-butoxide ($Sn(OC_4H_9)_4$) and 0.254 mL of 30% hydrogen peroxide aqueous solution (H_2O_2) was mixed for 1 h prior to adding into the solution prepared previously. The resulting solution was stirred for 2 h at room temperature. A dealuminated zeolite BEA seed solution described in previous section (4 wt% with respect to fumed silica added, particle size of the seed is around 200 nm) was then added, and the solvent in the translucent mixture was evaporated at 80 °C with stirring in an oil bath for 24 h, leading to a dry gel. The final composition of the dry gel is SiO_2: $0.008SnO_2$: $0.22TEA_2O$: $0.034Na_2O$. The obtained dry gel (*ca.* 2 g) was ground into powder and put into a Teflon-lined stainless steel autoclave with a cup volume of *ca.* 50 mL. A portion of 0.5 mL of deionized water was added into the autoclave in a separate Teflon cup to avoid direct contact between the dry gel and water. The autoclave was then placed in an oven preheated to 140 °C for crystallization. The as-made sample was washed by filtration with 1 L of deionized water and dried at 100 °C overnight (denoted as Sn-BEA-AM). Ion-exchange was carried out by treating 0.25 g of as-made zeolites with 25 mL of 1 M ammonium nitrate (NH_4NO_3) solution for 2 h at 80 °C. The process was repeated five times. Removal of OSDA and ammonium ions was obtained by calcining the powder in a muffle furnace at 550 °C for 12 h with a ramping rate of 1 °C min^{-1} (denoted as Sn-BEA-IE). Synthesis of Sn-BEA (denoted as Sn-BEA-F, Si/Sn = 125) from a fluoride medium was achieved by using the method reported in Cahpter 2.[35] Extra-framework SnO_2 in siliceous zeolite BEA sample (SnO_2/Si-BEA, Si/Sn=125) were prepared

according to according to Bermejo-Deval et al.[109] The procedure is the same as preparation of Sn-BEA-F, except for that SnO_2 (-325 mesh, Aldrich) was added as Sn source. The Si/Sn ratio was designed to be 125.

3.2.2 Characterizations

Samples were characterized by X-ray diffraction (XRD), scanning electron microscopy (SEM), transmission electron microscopy (TEM), nitrogen sorption measurements, thermogravimetric analysis (TGA), diffuse reflectance ultraviolet-visible spectroscopy (DR UV-Vis), FT-IR spectroscopy and inductively coupled plasma mass spectroscopy (ICP-MS). Details can be found in Section 2.2.

3.3 Results and discussions

Synthesis of Sn-BEA by the DGC method was first performed with or without adding zeolite BEA seeds. As shown in Figure 3.1, characteristic XRD peaks corresponding to the BEA topology are observed for the sample synthesized with adding zeolite BEA seeds after 5 days of crystallization, revealing highly crystalline BEA zeolite has been synthesized without any impurity phase. Crystallization is apparently slow in the absence of zeolite seeds, and an unidentifiable reflection peak dominates the spectrum after 5 days of crystallization. Longer crystallization time (20 days) does not yield pure BEA phase. These results indicate that adding zeolite BEA seeds not only facilitates the crystallization but also directs the formation of desired crystal structure under the present synthesis conditions. Thus, it is concluded that the seeding approach plays an essential role in the crystallization of pure Sn-BEA phase from the dry gel.
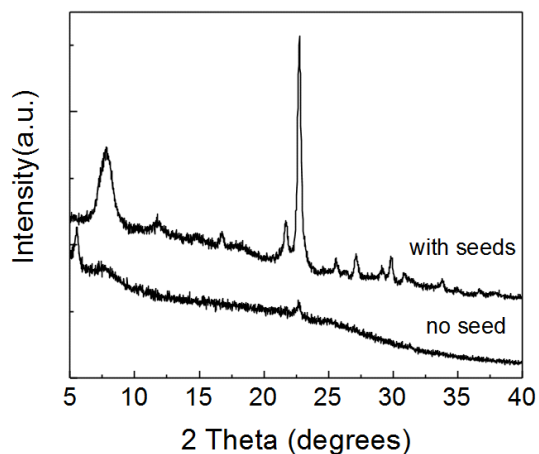
Figure 3.1 XRD patterns of the samples prepared with and without using zeolite BEA seeds after dry gel conversion at 140 °C for 5 days.
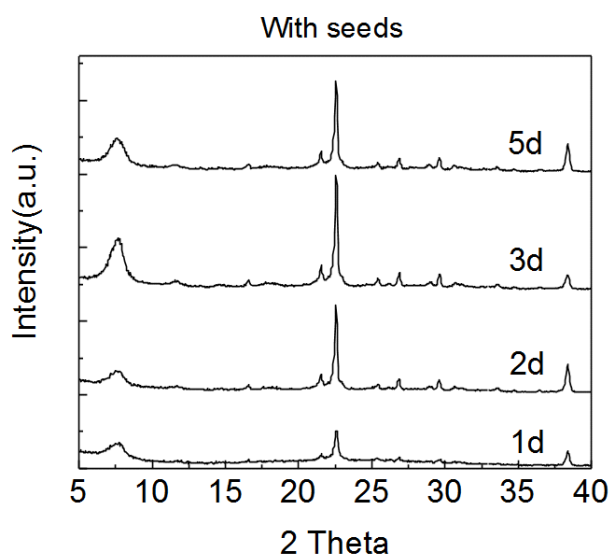
Figure 3.2 XRD patterns for the samples prepared with using zeolite BEA seeds after dry gel conversion at 140 °C for different treatment time.

Examining the crystallization time suggests that the Sn-BEA sample is fully crystallized after 3 days of SAC treatment, as shown in the XRD pattern in Figure 3.2.

It is also found that the use of alkali ions is crucial for the crystallization of Sn-BEA via the DGC method. As revealed in Figure 3.3, only very weak reflections can be observed in the samples when no alkali ion was added, and the signals are likely attributed to the seed crystals present in the

47

synthesis mixture. Figure 3.4 reveals the XRD patterns of as-made Sn-BEA (Sn-BEA-AM), Sn-BEA after direct calcination (Sn-BEA-DC) and Sn-BEA after ion-exchange and calcination (Sn-BEA-IE). Sn-BEA-AM shows typical diffraction peaks corresponding to zeolite BEA phase. However, much weaker peaks are observed in the XRD pattern of Sn-BEA-DC which is made by direct calcination without ion-exchange, indicating the crystalline structure of the sample was significantly damaged. The partial collapse of crystalline structure during calcination might be attributed to the inherent defects ($\equiv$SiO$^-$) generated for compensating the positive charges from the TEA$^+$ ions. Because of no aluminum in the zeolite framework, positive charges from the TEA$^+$ occluded within Sn-BEA samples can generate much more framework defects ($\equiv$SiO$^-$) than Al-BEA. Formation of BEA
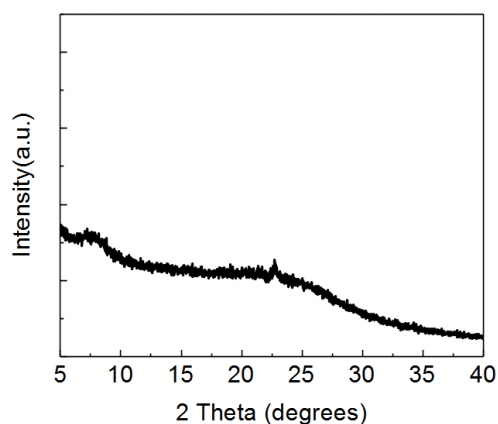
Figure 3.3 XRD pattern for the sample without adding sodium ion.
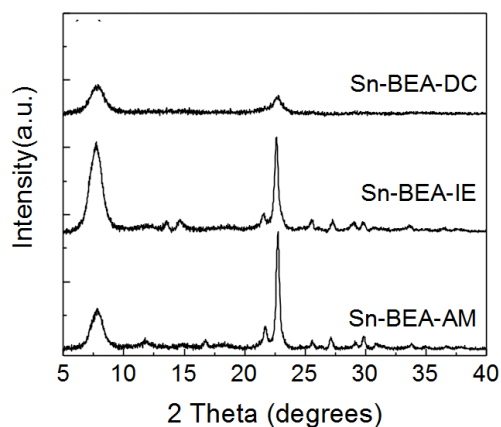
Figure 3.4 XRD patterns of Sn-BEA-AM, Sn-BEA-IE, and Sn-BEA-DC.

48

crystalline phase under the conditions thus requires use of alkali ions (*e.g.* Na^+, K^+ and Li^+) to compensate the additional defects as shown previously. It is interesting that even though crystalline phase can be achieved using Na^+ in the synthesis solution, the $\equiv$Si-O-Na structure could not undergo condensation with adjacent defect sites ($\equiv$Si-O-H or $\equiv$Si-O-Na) to form $\equiv$Si-O-Si$\equiv$ during calcination. As a result, the crystalline structure collapsed after the removal of TEA^+ (Sn-BEA-DC) by calcination. Interestingly, it is found that the crystalline structure can be well retained by the ion-exchange of Na^+ with NH_4^+ before the calcination.[108] Sn-BEA-IE sample made by the ion-exchange of Sn-BEA-AM with ammonium nitrate (NH_4NO_3) solution and subsequent calcination exhibits well-crystalline BEA structure (Figure 3.4). It is believed that the Na^+ was replaced by NH_4^+ during the ion-exchange. Upon further heat treatment, $\equiv$Si-O-NH_4 could be transformed into $\equiv$Si-O-H. Subsequent dehydration/condensation of the silanol groups could lead to the formation of $\equiv$Si-O-Si$\equiv$ bond, which benefits retaining the crystallinity and microporous structure of Sn-BEA (Scheme 3.1). This result clearly suggests that exchanging alkali ions from the zeolite samples by NH_4^+ is indispensable for obtaining highly crystalline Sn-BEA catalyst under the synthesis route used in this study. The method might also be applicable for retaining the crystallinity of other high silica or siliceous zeolites that have a large number of OSDAs and defects in the as-made forms. It was also attempted to replace the alkali ions (*e.g.* Na^+, K^+, Li^+) by NH_4^+ ion in the synthesis mixture as the charge compensator to avoid the ion-exchange process. However, no crystalline phase was achieved under the synthesis conditions (Figure 3.5). The ineffectiveness of NH_4^+ ion for stabilizing zeolite structure during crystallization might be due to the steric hindrance with TEA^+ ion within zeolite BEA framework.

Fig. 3.6 shows the SEM and TEM images of Sn-BEA-IE sample. Discrete truncated bipyrimidal crystals with a size of around 400-700 nm can be observed in the sample (Figure 3.7). Sn-BEA-F
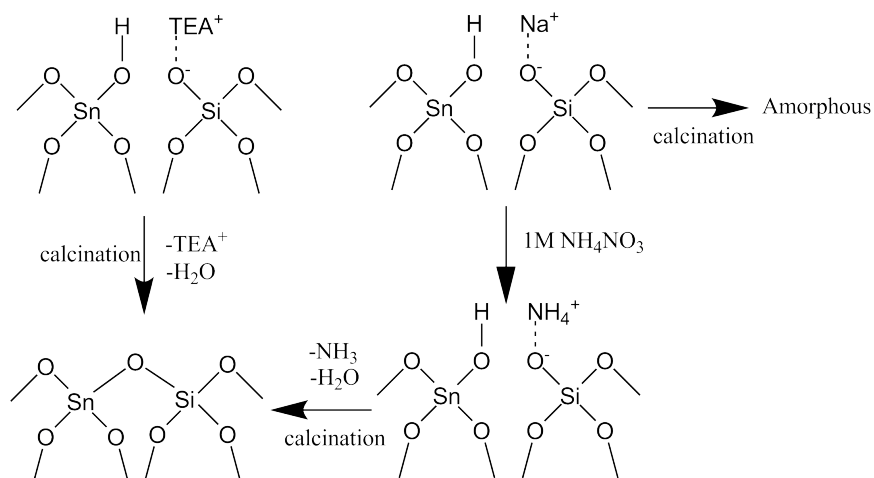
Scheme 3.1 Illustrative representation of the effect of NH_4^+ ion-exchange on crystal structure of the final product.
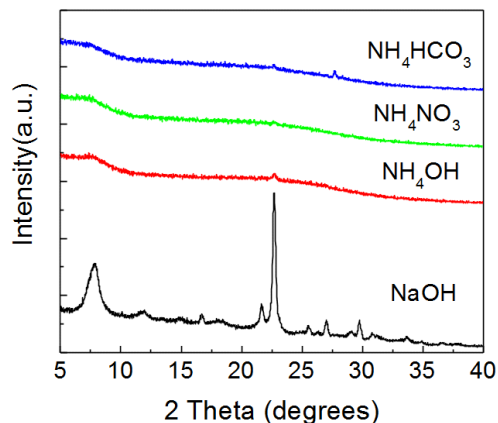
Figure 3.5 XRD pattern of sample synthesized with ammonium hydrogen carbonate, ammonium nitrate, ammonium hydroxide and sodium hydroxide (Na_2O/SiO_2 or $(NH_4)_2O/SiO_2$ ratio is 0.096) after 5 days of DGC at 140 °C. Only very weak reflections can be observed except for sodium hydroxide case, and they could originate from the seed crystals added in the gel. The data clearly indicate that the alkali ions are essential for the synthesis from dry gel conversion.
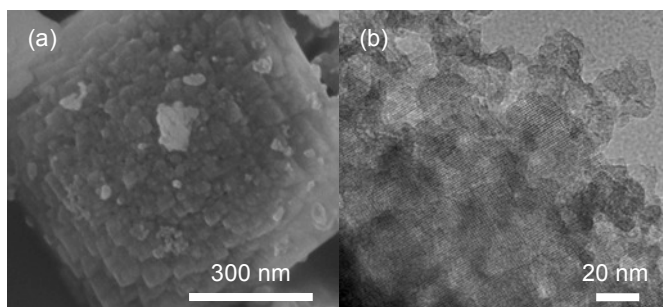
Figure 3.6 (a) SEM and (b) TEM images of Sn-BEA-IE synthesized from the dry gel conversion (DGC) method.

catalyst synthesized from a fluoride medium (See Chapter 2) also shows truncated bipyrimidal crystals (600 nm to 1 μm) but with highly intergrown morphology. The images suggest that Sn-BEA-IE consists of more discrete and smaller crystal domains compared with conventional Sn-BEA, which is consistent with its higher surface area obtained from N_2 sorption experiments. In addition, lattice fringes can be clearly observed in the TEM image (Figure 3.6(b)), confirming that the sample is a highly crystalline material. Based on the observations above, it is concluded that Sn-BEA-IE features a well-crystalline structure and a large surface area. The elemental analysis shows that Sn-BEA-IE has a Si/Sn ratio of 102.
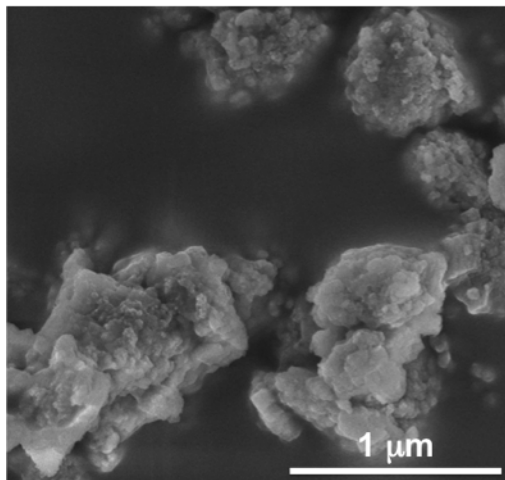
Figure 3.7 Representative SEM image for Sn-BEA-IE.

A series of characterization techniques were used to study the structures of Sn site in the Sn-BEA samples from DGC method. UV-Vis spectroscopy has been shown to be an effective method to distinguish the coordination environment of Sn in zeolites.[37, 73, 109] The absorbance at ~200-210 nm corresponds to tetrahedrally-coordinated Sn (framework Sn), absorbance at ~240 nm results from extra-framework Sn species, and the band at ~280 nm is assigned to Sn in tin dioxide.[109] Figure 3.8 shows the UV-Vis spectra for Sn-BEA-IE and Sn-BEA-DC samples. As seen in the plot, the intensified absorbance at ~200 nm suggests that most Sn in Sn-BEA-IE locate in the framework
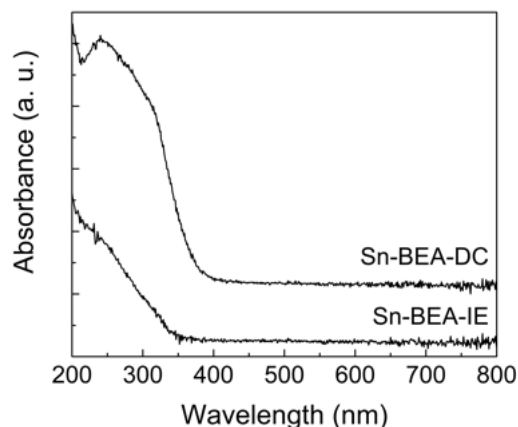
Figure 3.8 DR UV-Vis spectra for Sn-BEA-IE and Sn-BEA-DC. The spectrum of Sn-BEA-DC was shifted 0.05 unit for clarity.

position (SnO$_4$ tetrahedral), while there are several different coordination states of Sn observed in Sn-BEA-DC sample. It is plausible that multiple Sn species are formed after zeolite structure collapses during calcination. The result also indicates that the ion-exchange/calcination treatment can preserve the micropore structures of the zeolite samples and the local environment of Sn.

FT-IR study of CD$_3$CN adsorption was employed to assess the Lewis acidity of Sn-containing materials.[54, 81, 82] The CD$_3$CN adsorbed FT-IR spectra for different Sn-BEA samples, including Sn-BEA-IE, Sn-BEA-F (sample made from the rapid synthesis method) and SnO$_2$/Si-BEA (tin oxide was used as tin source in the rapid synthesis method, XRD pattern shown in Figure 3.9), are shown in Figure 3.10. The data for Sn-BEA-IE after different desorption times at 100 °C are shown in Figure 3.10(a). The band at 2265 cm^{-1} can be assigned to physically adsorbed CD$_3$CN, while the band at 2275 cm^{-1} reflects the interaction of CD$_3$CN and silanol groups, and the band around 2310 cm^{-1} is attributed to the vibration related to framework Sn species.[54, 81] It has been proposed that the v(C-N) vibrations around 2310 cm^{-1} can be used to distinguish the "close" (2308 cm^{-1}) or "open" (hydrolysed Sn-O-Si; 2316 cm^{-1}) Sn sites in Sn-BEA framework.[81] Interestingly, our data reveal a main band at 2309 cm^{-1}, and no other band at higher wavenumber is observed during the course of CD$_3$CN
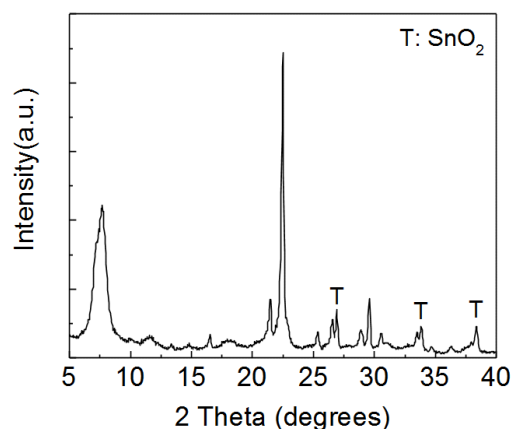
Figure 3.9 XRD pattern of SnO$_2$/Si-BEA (Si/Sn=125) sample. The XRD shows that the sample has zeolite BEA topology and reflections from SnO$_2$.
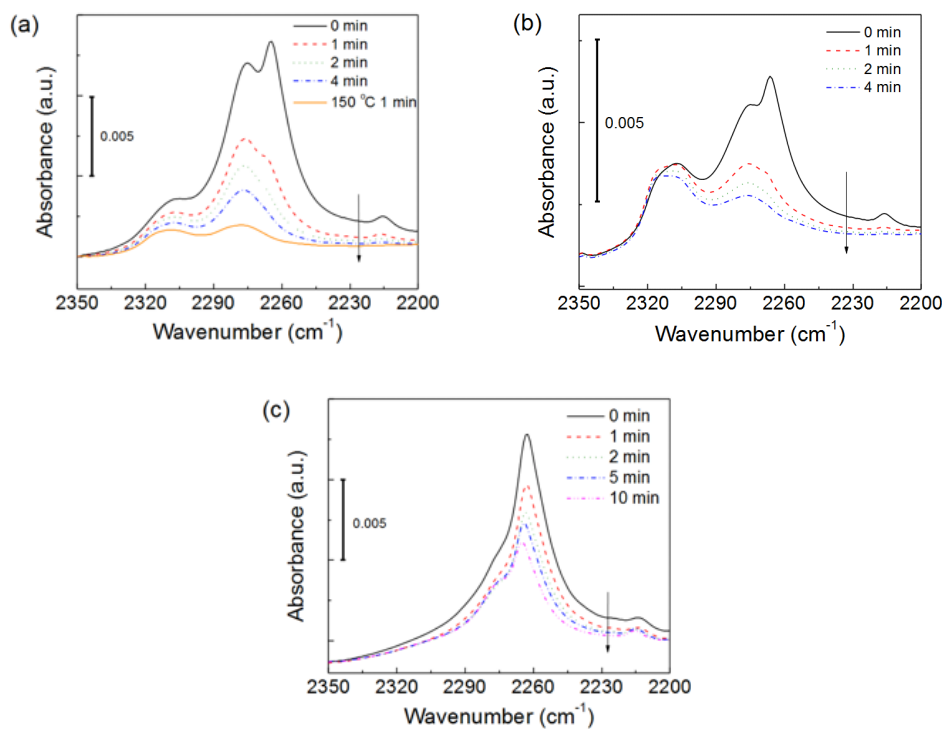
Figure 3.10 CD$_3$CN adsorbed FT-IR spectra of (a) Sn-BEA-IE, (b) Sn-BEA-F and (c) SnO$_2$/Si-BEA. The spectra were acquired after saturation of CD$_3$CN on the samples followed by different period desorption time at 100 °C, as specified in the figures.

desorption, even when desorption temperature was at 150 °C. In contrast, two bands (2308 cm^{-1} and 2316 cm^{-1}) can be clearly observed during the desorption of CD$_3$CN for Sn-BEA-F (Figure 3.10(b)),

53

which is consistent with previous literature.[81] In addition, the spectra from the sample intentionally made with SnO_2 as extra-framework Sn site did not show absorption at 2305-2315 cm^{-1} range (SnO_2/Si-BEA, Figure 3.10(c)). These results clearly indicate that the Sn-BEA-IE sample prepared from the DGC method indeed possesses framework Sn, while the local Sn environment could be different from the Sn-BEA-F sample made from fluoride medium. It should be noted that a recent report suggests the two vibration bands can also happen due to the different packing structures of CD_3CN rather than the difference in Sn site structures.[54] In addition, the locations and distribution of Sn in zeolite frameworks might also affect their FT-IR spectra. At this point, it can be concluded that Sn-BEA-IE does have framework Sn site, however the local environment of Sn and its difference from the Sn-BEA-F are still elusive, and require further investigation.

To further confirm the coordination environment of Sn in the synthesized Sn-BEA-IE sample, glucose with deuterium substituted at the C-2 position was used in the isomerization reaction.[83] The ^{1}H-NMR spectra for unlabelled fructose and fructose isomerized from labelled glucose are shown in Supplementary Information (Figure 3.11). The absence of resonances at δ = 3.4-3.5 ppm corresponding to the protons at C-1 position in ^{1}H-NMR spectrum of fructose after reaction indicates that the reaction only undergoes an intramolecular hydride shift from C-2 to C-1 in water, which follows the same mechanism as the Sn-BEA-F.[83] The finding from ^{1}H-NMR measurement is consistent with the DR UV-Vis and CD_3CN FT-IR measurements, showing most Sn are incorporated into the zeolite framework with a tetrahedral coordination and able to catalyze the glucose isomerization reaction *via* an intramolecular hydride shift pathway. With these characterization results, it is concluded that the Sn-BEA-IE synthesized in this study possesses framework Sn in siliceous BEA framework, and the isolated metal centers exhibit Lewis acidity capable of catalyzing the sugar isomerization in aqueous phase.

It has been suggested that the hydrophobic environment is a key factor for adsorbing glucose from aqueous phase into hydrophobic Sn-BEA catalyst and catalyzing the isomerization reactionfrom
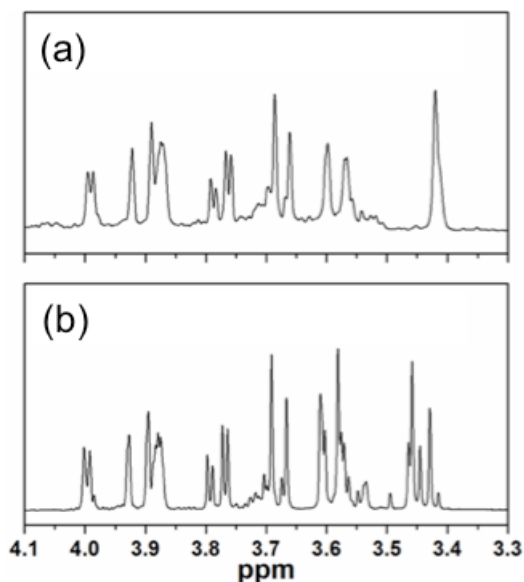
Figure 3.11 ^{1}H-NMR spectrum of (a) fructose after isomerization reaction of deuterium substituted glucose over Sn-BEA-IE and (b) unlabeled fructose. Reaction conditions are the same as described in the manuscript, except for longer reaction time (2 h). The separation was achieved by running the reaction mixture on HPLC (LC-20, Shimadzu) with a Biorad HPX-87C column (Ca^{2+}-type), operated at 80 °C. Water was used as mobile phase at a flow rate of 0.6 mL min^{-1}. Fructose portion was collected by a fraction collector (FRC-10, Shimadzu). The solution containing fructose was then heated in a 70 °C oven to evaporate the solvent. The obtained solids were re-dissolved in D$_2$O prior to ^{1}H-NMR measurement (AVANCE 400, Bruker).

glucose to fructose.[101, 110, 111] The Sn-BEA catalyst synthesized from the DGC method (Sn-BEA-IE) is expected to have more silanol defects than the sample made from a fluoride medium, and exhibits different hydrophobicity from Sn-BEA-F. This is because the charge of occluded TEA$^+$ ions in the Sn-BEA-IE synthesized from caustic medium must be compensated by framework defects ($\equiv$Si-O$^-$), while in Sn-BEA-F, F$^-$ can form a pair with TEA$^+$ and generates fewer defects. As discussed in the previous paragraph, the framework defects ($\equiv$Si-O$^-$) can be reduced by reacting with adjacent silanol groups in Sn-BEA-IE sample during ion-exchange and calcination processes. However, Sn-BEA-F still has fewer silanol groups ($\equiv$Si-OH) than Sn-BEA-IE, as shown in a TGA study and FT-IR sepctra (Figure 3.12). The TG experiments (Figure 3.12(a)) clearly suggest that Sn-BEA-IE adsorbs more water (4% *vs.* 2% weight loss at 400 °C) and has more hydroxyl condensation at higher temperature (~2% *vs.* 0.5% weight loss above 450 °C) than Sn-BEA-F. The FT-IR spectra in the OH stretching

region for degassed samples are shown in Figure 3.12(b). 3738 and 3745 cm^{-1}, which can be assigned to terminal silanol groups (weakly hydrogen bonded and free Si-OH, respectively).[112] A small shoulder at 3701 cm^{-1} corresponding to weakly hydrogen bonded silanols in zeolites is also observed for Sn-BEA-IE. By directly comparing the normalized spectra, it is obvious that Sn-BEA-IE possesses more silanol groups than Sn-BEA-F does. These results indicate that Sn-BEA-IE has more defects and more hydrophilic surface compared to the sample made in the presence of fluoride.[101, 110]

The catalytic activity of the Sn-BEA-IE sample was examined by glucose isomerization and PA reaction in water and compared with hydrophobic Sn-BEA-F. The reaction results are summarized in
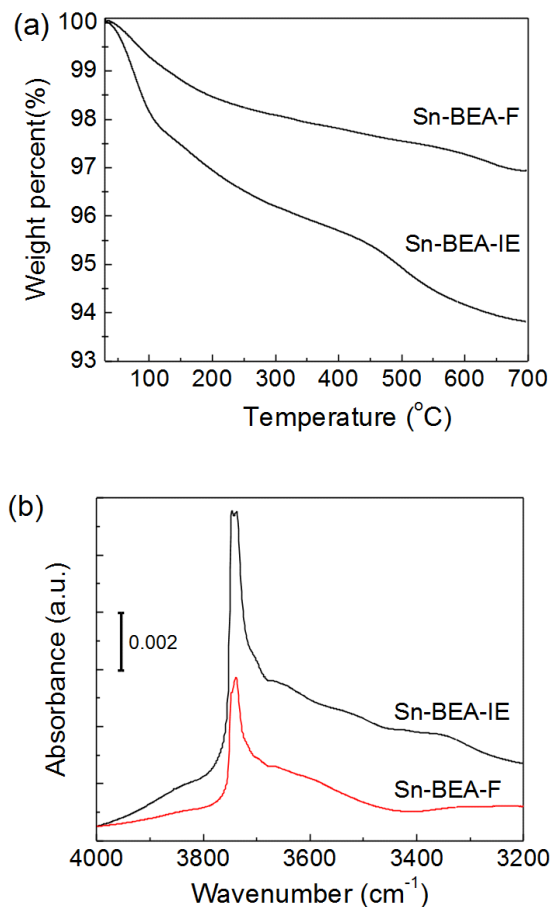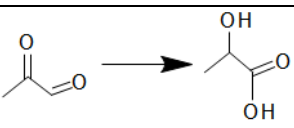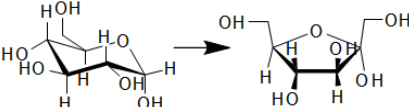
Figure 3.12 (a) TGA curves and (b) FT-IR spectra for Sn-BEA-IE and Sn-BEA-F. Samples were contacted with liquid water and dried in a 70 °C overnight prior to TG measurements. FT-IR spectra were acquired at 30 °C after degassing.

Table 3.1. The product distributions for different reactions are listed in Table 3.2 and 3.3. As expected, the TOF for the isomerization of glucose into fructose in aqueous phase on Sn-BEA-IE is only ~25% of that of Sn-BEA-F. The low reaction rate is likely due to the hydrophilic surface of Sn-BEA-IE catalyst disfavoring adsorption of glucose, which is in good agreement with previous literature.[110] On the other hand, the activity of Sn sites in Sn-BEA-IE for the conversion of PA into lactic acid (LA) (1.20 min^{-1}) is still lower than that in Sn-BEA-F (1.52 min^{-1}), but the difference is much less significant compared to the glucose reaction. The production of LA is similar for the two catalysts under the reaction conditions (18.3% *vs.* 18.9% yield). It has been known that the reaction from PA to LA undergoes hydration of PA in aqueous phase followed by intramolecular 1,2 hydride-shift reaction on the Lewis acid sites of Sn-BEA.[61] Hence, it is reasonable that the hydrophilic material shows improved activity due to the enhanced adsorption of water in micropores. However,

Table 3.1 Turnover frequencies (TOF, min^{-1}) of Sn-BEA catalysts for sugar isomerization reactions

Substrate	Reaction Scheme	Sn-BEA-IE	Sn-BEA-F
Pyruvaldehyde^a		1.20	1.52
Glucose^b		0.25	0.99

^{a} 70 °C, 15 min, 20 mg catalyst with 56.3 mg PA solution (40 wt%) in 1 g water
^{b} 95 °C, 15 min, 68 mg catalyst with 0.8 g 10 wt% glucose solution

Table 3.2 Product distribution of pyruvaldehyde over Sn-BEA catalysts (conditions: refer to table 3.1)

Reaction time 15 min	Si/Sn	PA (%)	LA (%)	TOF (min^{-1})
Sn-BEA-IE	102	81.2	18.3	1.20
Sn-BEA-F	126	79.8	18.9	1.52

Table 3.3 Product distribution of glucose over Sn-BEA catalysts (conditions: refer to table 3.1)

Reaction time 15 min	Si/Sn	Glucose (%)	Mannose+Fructose (%)	TOF (min^{-1})
Sn-BEA-IE	102	90.8	9.1	0.25
Sn-BEA-F	126	66.3	34.7	0.99

we have to point out that the local environment of Sn sites including "open/close site", distribution and location might be different for the two Sn-BEA catalysts as revealed in CD_3CN adsorbed FT-IR study which could also affect the catalytic activity of the materials.[27, 113] Although it is evident that most Sn atoms are incorporated in framework, the discrepancies in activities for different reactions reported here might result from a combinatorial effect of active site nature and surface properties (hydrophobicity).

In summary, highly crystalline Sn-BEA with tetrahedrally coordinated Sn was successfully synthesized from a non-fluoride medium for the first time by a dry gel conversion method. The sample exhibits a higher surface area than the conventional Sn-BEA synthesized from a fluoride medium. It is found that the use of seed crystals, addition of alkali ions and ion-exchange with ammonium nitrate before calcination are essential for obtaining a highly crystalline Sn-BEA catalyst. The Sn-BEA catalyst shows lower catalytic activity than the conventional Sn-BEA for glucose isomerization and comparable activity for pyruvaldehyde reaction in aqueous phase. The difference in catalytic activity could be attributed to the different hydrophobic nature and local Sn environment in the catalysts prepared from different synthesis routes. The current work provides an alternative and a more environment-friendly approach to synthesize Sn-BEA catalyst.

CHAPTER 4

DEVELOPMENT OF CATALYSTS FOR RENEWABLE PARA-XYLENE

PRODUCTION FROM 2, 5-DIMETHYLFURAN AND ETHYLENE

4.1 Background

p-Xylene is used for the production of terephthalic acid,[43] which is used as a feedstock for polyester and polyethylene terephthalate plastics (e.g., plastic bottles)[5] and is currently produced from the separation of mixed aromatics (isomers of xylene and ethylbenzene) from the naptha fraction of petroleum. *p*-Xylene can also be selectively produced from toluene through the use of ZSM-5 catalysts[44] in combination with membrane separation.[45] New processes are currently being implemented to produce *p*-xylene from renewable resources using a hybrid process that combines fermentation and heterogeneous catalysis.[46, 47]

p-Xylene can potentially be produced renewably starting from glucose as shown in Scheme 1.1. As the last step of this scheme, the conversion of dimethylfuran (DMF) to *p*-xylene by a two-step process (cycloaddition + dehydration) is crucial for the efficient production of high-value chemicals from biomass-derived sugars. Williams and Dauenhauer collaborated with our lab and demonstrated the chemistry using zeolite catalysts.[15] Under mild temperature (200-300 °C) and high ethylene pressure (57-62 bar), the authors demonstrated the temperature dependence of the product distribution, the higher the temperature, the higher the *p*-xylene selectivity, as shown in Figure 4.1. 51% of *p*-xylene selectivity at 95% conversion at 300 °C was achieved in a pure DMF system. Furthermore, when the reaction is carried out with heptane solvent, the selectivity of *p*-xylene can be further increased to 75 %. It was also found under the reaction conditions, the reaction is rate-controlled by the uncatalyzed Dields-Alder (DA) cycloaddition step with dehydration step catalyzed by Brønsted acids. The results is consistent with the computational work by Nikbin *et. al*. (DFT calculation in gas phase),[18] in which the authors have shown that with Brønsted acid, the reaction

59
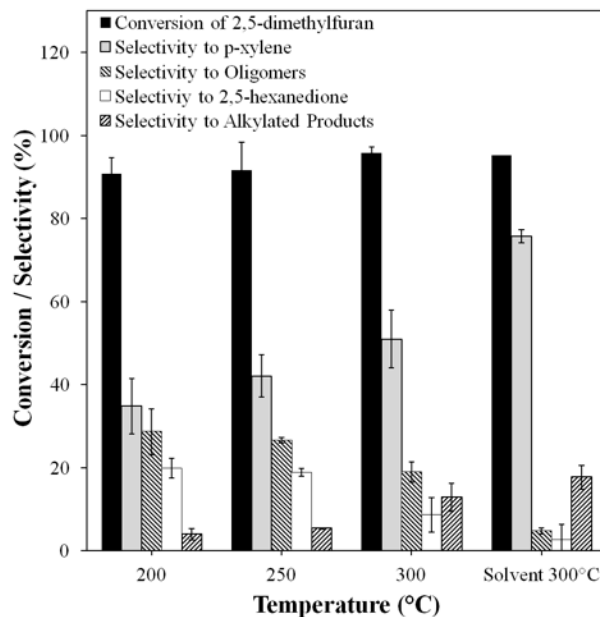
Figure 4.1 Demonstration of dimethylfuran cycloaddition at high Conversion. Increase of reaction temperature from 200 to 300 °C with H-Y zeolite (Si/Al=2.6) and 900 psig C_2H_4 with pure dimethylfuran exhibits increasing selectivity to *p*-xylene for high conversion of dimethylfuran, X_{DMF}>90%. Yield of *p*-xylene further increases by the addition of n-heptane solvent (25 vol% DMF / 75 vol% n-heptane) at 300 °C.

barrier for dehydration is greatly reduced, from 59 kcal/mol to 17 kcal/mol, while the DA reaction still renders uncatalyzed. When Lewis acid (specifically alkali ion exchanged zeolites) is modeled, the results indicates it can slightly decrease the activation energy of the DA reaction (24.7 to 16.9 kcal/mol for Li^+ exchanged zeolite) and some enhancement on the dehydration step due to stabilization of intermeidiates. The authors proposed a bifunctional catalyst featuring both Lewis (high DA rate) and Brønsted acidity (high dehydration rate) could potentially enhance the production of *p*-xylene from DMF and ethylene.

Do *et. al.* has revealed the mechanism of the reaction over zeolite Y catalyst, as shown in Scheme 4.1.[16] The desired pathway, as described previously, consists of [4+2] Diels-Alder cycloaddition of DMF and ethylene followed by a dehydration reaction to form *p*-xylene. Other byproduct includes 2, 5- hexanedione, a hydrolysis product from DMF, alkylated products (such as 4-propyltoluene) formed from an alkylation reaction of ethylene and protonated cycloadduct and oligomers (such as 1, 4-

dimethyl-2-(4-methylbenzyl)benzene) is produced from a Friedel-Craft type reaction between DMF and cycloadduct derivatives. According to the reaction network, the author suggested by removing water from the system, carefully selecting catalysts with adequate acid strengths and tuning dielectric properties of the solvents, the selectivity towards *p*-xylene can be further enhanced. Elucidation of the reaction pathways has revealed three competing side reactions to the main pathway to *p*-xylene: (1) hydrolysis of DMF to 2,5-hexanedione, (2) secondary addition of DMF to produce dimers, and (3) secondary reactions of ethylene to alkylated aromatics. From this analysis, further improvement in selectivity to *p*-xylene can be specifically defined as: (a) elimination of the hydrolysis side reaction or (b) reduction in secondary addition of either the dienophile (e.g. ethylene) or the diene (e.g. DMF).

Here, we examined various common zeolites (zeolite Y, ZSM-5, zeolite BEA) and acidic catalysts (niobic acid and γ-Al$_2$O$_3$) in this reaction to illustrate the effect from different zeolite framework and kinds of acids on the production of *p*-xylene from the tandem Diels-Alder cycloaddition/dehydration reactions.
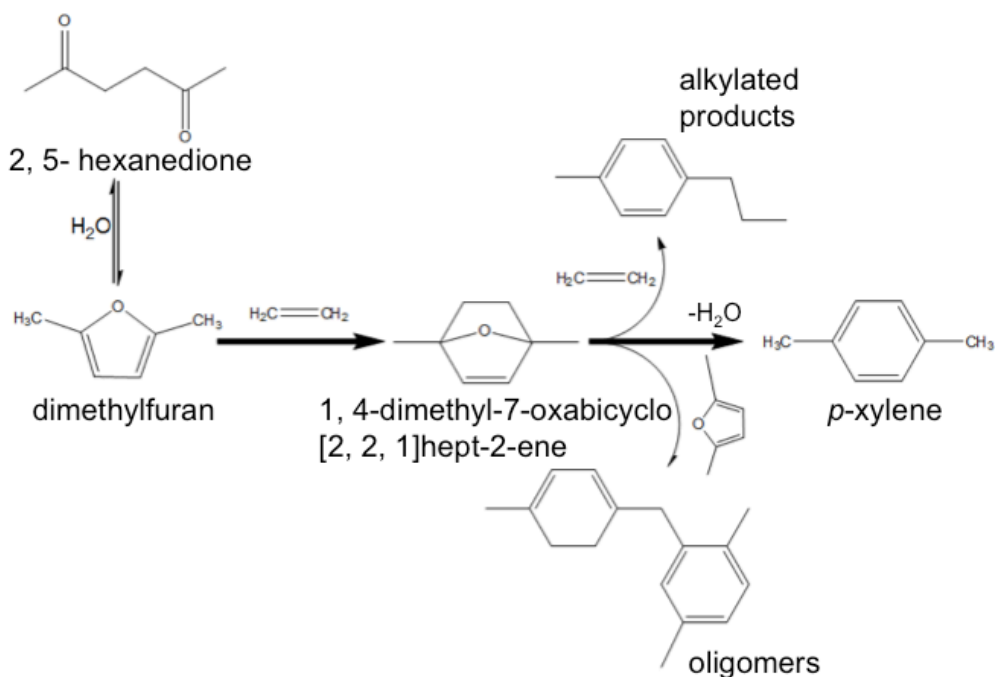
Scheme 4.1 Simplified proposed reaction pathway of *p*-xylene formation from DMF and ethylene over zeolite Y.

4.2 Experimental

4.2.1 Catalyst preparation

CBV600 (FAU, Si/Al=2.6), CP814C (BEA, Si/Al=19), CP814E (BEA, Si/Al=12.5) and CBV3024E (MFI, Si/Al=15) were obtained from Zeolyst. Prior to reactions, the catalysts were calcined in a tube furnace under air flow with an online drierite tube to remove moisture present in the gas. The calcination was carried at 550 °C for 12h with a ramping rate of 1 °C min^{-1}. Gamma alumina (STREM) was pretreated at 500 °C for 12h with the same ramping rate. Niobic acid (HY-340, CBMM) was pretreated for 3 h at 100 °C.

4.2.2 Brønsted acid sites and total acid sites measurement

Physiochemical properties of the catalysts are included in Table 4.1. The numbers of Brønsted acid site of the catalysts were determined by temperature programmed desorption (TPD) of isopropylamine (IPA, Aldrich) in conjunction with thermal gravimetric analysis (TGA) in a thermal analyzer (SDT600, TA instrument). Around 10 mg of catalyst was first cleaned at 550 °C for 1 h under helium flow. After the sample cooled down at 120 °C, isopropylamine was bubbled with helium at room temperature into the furnace for adsorbing on the catalysts. The stream was then switched to pure helium and kept flowing for 1 h to remove weakly adsorbed species. After that, the temperature programmed desorption/decomposition of isopropylamine was carried out with a ramping rate of 10 °C min^{-1} to 700 °C. The Brønsted acid site concentrations were then determined by the weight difference between 300 °C and 400 °C, which is the temperature range corresponding the decomposition of isopropylamine on Brønsted acid sites.[114]

The numbers of total acid sites were measured by FT-IR measurement on pyridine-adsorbed catalysts. The spectra were collected on Equinox 55 (Bruker) with a resolution of 2 cm^{-1}. Briefly, the catalysts were loaded in the High Temperature Reaction Chamber (Harrrick) on Praying Mantis^{TM} DRIFTS attachment (Harrick) and degassed at 550 °C for 1 hr under helium flow. Pyridine vapor was then bubbled into the chamber and contacted with the catalysts for 10 min. The catalysts were heated

up to 150 ^{o}C and held for 1 hr under a flow of helium, and the spectra were all recorded at 120 °C. The Brønsted/Lewis acid site ratio was determined by integrating the adsorbance bands corresponding to Brønsted acid site (~1545 cm^{-1}) and Lewis acid site (~1454 cm^{-1}) and applications of molar extinction coefficients (1.67 cm μmol^{-1} and 2.22 cm μmol^{-1}, respectively). Detailed procedure can be found in the work by Emeis.[115] The numbers of total acid sites were calculated by using the Brønsted acid to Lewis acid site ratio and Brønsted acid site concentrations obtained from the IPA-TGA measurement,.

Table 4.1. Physicochemical properties of the catalysts

Catalyst	Si/Al Ratio[a]	surface area[a] (m^2 g^{-1})	Na$_2$O content[a] (wt.%)	Brønsted acid sites[c,d] (mmol g^{-1})	Total acid sites[d] (mmol g^{-1})
H-BEA (CP814E)	12.5	680	0.05	0.70	1.12[e]
H-BEA (CP814C)	19	710	0.05	0.56	1.21
H-Y (CBV600)	2.6	660	0.2	0.36	0.99
H-ZSM-5 (CBV3024E)	15	405	0.05	0.71	1.10
Niobic Acid	NA	118[b]	-	0.05[b]	0.13[b]
γ-Al$_2$O$_3$	NA	200[b]	-	-	0.21[b]

[a] Zeolyst; [b] D. Wang et al.[17]; [c] measured by isopropylamine TPD-TGA; [d] C. L. Williams et al.[15] [e] pyridine FT-IR.

4.2.3 Reaction details

The detailed schematic of the reactor design can be found in our previous work.[15] In dimethylfuran (DMF, Alfa Aesar or Acros Organics, >98%) reactions, 100 mL of ~1.3±0.1M of DMF in n-heptane (Alfa Aesar, 99%) with n-tridecane (Acros Organics, 99%) was enclosed in a 160 mL mini bench-top reactor (Parr) with 0.45±0.05 g of catalyst, and the reaction vessel was purged by nitrogen. For furan (Aldrich, 99%) and methylfuran (MF, Alfa Aesar, 98%) experiments, 100 mL of 1.0 M furanic feedstock in n-heptane with tridecane was used with 0.45±0.05 g of catalysts. The mixture was then stirred at 950±50 rpm with a gas entrainment impeller to ensure facile mass transfer

in the system and heated up to 250 °C, controlled by 4848 control unit (Parr). The reactor was then pressurized with 14 bar (partial pressure) of ethylene gas (Airgas), and the total pressure the system was kept at ~62 bar over the reaction period. Liquid was sampled by a double block sampling system at designed reaction times. The composition of the sample was then analyzed on an Agilent 6890A or 7890A gas chromatograph with column equipped with flame ionization detector. The products were identified by comparing the retention times with standard chemicals. The concentrations of alkylated products and oligomers were estimated by using the response factor (RF) for p-xylene, toluene, or benzene and the additive RF of the aforementioned products and the furanic feedstock (based on the reaction scheme).[16] The conversion of furanic compounds and selectivity to the products are defined as following:

$$X_{furans} (\%) = 100 \times \frac{C_{furans,t_0} - C_{furans}}{C_{furans,t_0}}$$

$$Selectivity_{product\ i}(\%) = 100 \times \frac{C_i}{\Sigma_i\ C_i}$$

$$Carbon\ balance(\%) = 100 \times \frac{C_{furans} + \Sigma_i\ C_i}{C_{furans,t_0}}$$

where C is concentration of the chemicals.

4.3 Results and disucssions

As shown in Figure 4.2, initial catalytic reaction rates reveal the activity of several solid-acid catalysts at 250 °C in heptane solvent at low conversion (X_{DMF}, the conversion of DMF, <20%). While previous studies using pure DMF reactant at 300 °C have indicated that Y-zeolite is more active than H-BEA,[15] the reaction with H-BEA (47 mmol (g-cat hr)$^{-1}$) in the presence of heptane solvent at 250 °C is at least 50% more active than H-Y zeolite. Additionally, several other catalysts including H-ZSM-5, niobic acid, and γ-Al$_2$O$_3$ are nearly an order of magnitude less active than H-BEA, at these conditions. Initial kinetics of solid-acid catalyzed cycloaddition in heptane solvent support the previously proposed mechanism of p-xylene production, and highlight the importance of
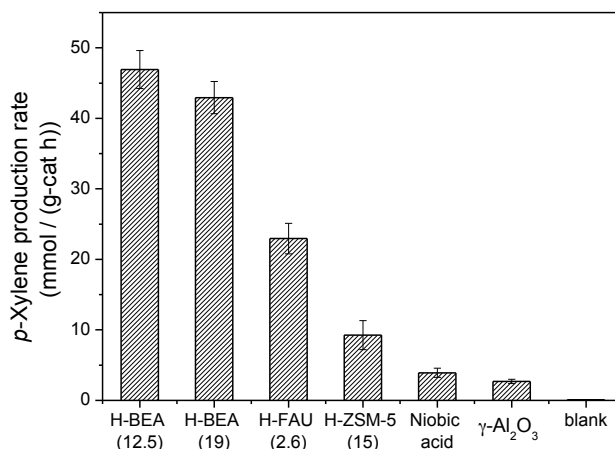
Figure 4.2 Initial reaction rates of *p*-xylene formation for the reaction of DMF in heptane with ethylene (62 bar) at 250 °C with various catalysts. Si/Al ratios of catalysts shown in parentheses.

H-BEA. As shown in Figure 4.2, the initial reaction rate of *p*-xylene is independent of Si/Al ratios within given materials such as BEA, which indicates that the overall reaction rate (at low conversion) is independent of the total number of Brønsted acid sites, for the considered reaction conditions. However, it was shown previously that materials require a Brønsted acid site to exceed the rate of cycloaddition/dehydration occurring within the non-catalyzed system.[15] The necessity for a Brønsted acid site for which site-density does not correlate with activity (at high catalyst loading) is consistent with the proposed mechanism of rate-limiting, non-catalyzed Diels-Alder cycloaddition, described previously.[15]. H^+ has been shown to exhibit no potential for decrease in the cycloaddition reaction barrier both experimentally and by DFT.[18, 116] With this in mind, comparison of H-BEA activity (R_{DMF}, the initial reaction rate of DMF, = 47±3 mmol-*p*X (g-cat hr)$^{-1}$) with other non-porous materials such as WOx-ZrO$_2$ (R_{DMF} = 50-55 mmol-*p*X (g-cat hr)$^{-1}$) indicates comparable reaction activity at the same temperature (250 °C).[17]

The potential of H-BEA for combined cycloaddition/dehydration chemistry relative to other materials is further revealed by long-time experiments examining high conversion of DMF. As shown in Figure 4.3, most catalytic materials at 250 °C in heptane solvent exhibit similar behavior
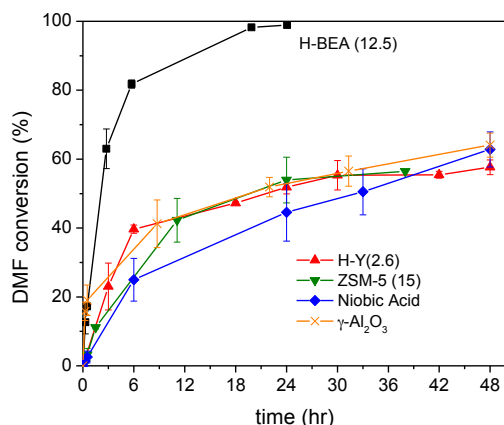
Figure 4.3 Conversion of DMF as a function of time for the reaction of DMF in heptane with ethylene (62 bar) at 250 °C with various catalysts. Si/Al ratios of catalysts shown in parenthese.

with significant deactivation after ~10 hours. Niobic acid, γ-Al_2O_3, H-Y zeolite, and H-ZSM-5 all exhibit only ~50-60% conversion after 30 hours. In contrast, H-BEA exhibits significantly different catalytic behavior and rapidly achieves high conversion of ~90% in 10 hours for these same conditions.

The benefit of high activity of H-BEA relative to other considered materials is higher selectivity to *p*-xylene of ~90% on a carbon basis. As shown in Figure 4.4, selectivity to *p*-xylene increases with DMF conversion. At X_{DMF} = 20%, selectivity to *p*-xylene is only 60%, and the hydrolysis product (2,5-hexanedione), alkylated products and oligomers comprise the remaining 40%, within experimental error. However, as X_{DMF} increases to >99%, selectivity to *p*-xylene exceeds 90% (concentration profiles for other catalysts can be found in Figure 4.5-8). This counter-intuitive behavior can be partially explained by the concentration of the hydrolysis side-product, 2,5-hexanedione, as revealed in Figure 4.4(a). For X_{DMF} < 60%, the concentration of all side products increase in step with DMF conversion. However, while no change in concentration is observed for the alkylated products and oligomers after X_{DMF}>80%, the concentration of 2,5-hexanedione decreases from 0.08 M for X_{DMF}>60% and reduces to nearly zero concentration as X_{DMF}>99%. This behavior is consistent with the hydrolysis reaction equilibrium between DMF/water and 2,5-hexanedione;[117] as

66
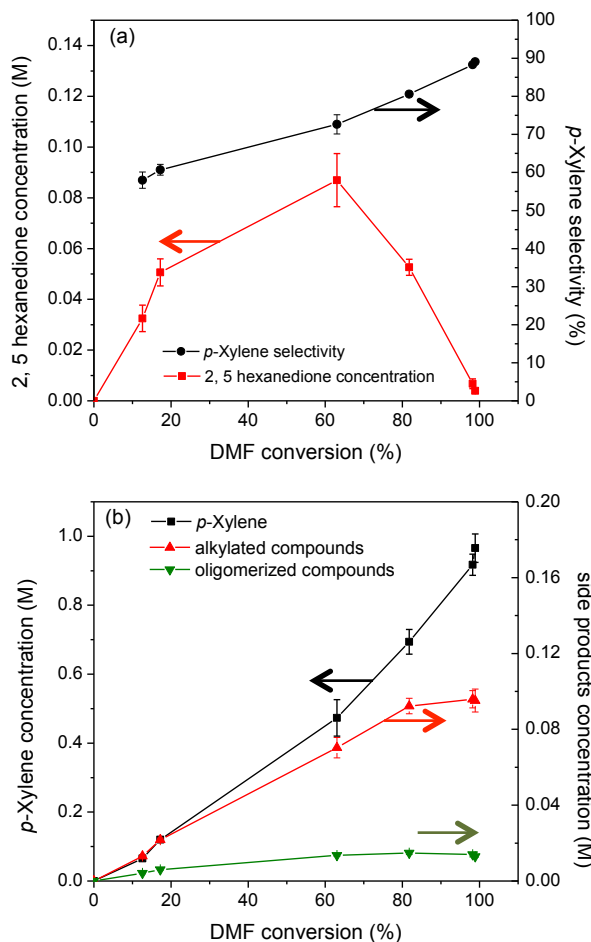
Figure 4.4 (a) Selectivity of *p*-xylene and concentration of 2,5-hexanedione and (b) concentration of other products as a function of DMF conversion for the reaction of DMF in heptane with ethylene (62 bar) at 250 °C with H-BEA (Si/Al=12.5).

DMF reacts with ethylene, 2,5-hexanedione reforms DMF to maintain equilibrium. *p*-Xylene formation is highly favourable thermodynamically,[15, 18] and all reactants including side products in equilibrium will yield *p*-xylene at high conversion. This was confirmed by a separate experiment starting with 2,5-hexandione and water in heptane in the reaction with ethylene at 250 °C, as shown in Figure 4.9. The experiment to confirm the formation of *p*-xylene from 2,5-hexanedione was carried out by using 100 mL of reactant containing 0.12 M of 2, 5-hexanedione and 1.0 M of water in heptane with 0.5 g of H-BEA (Si/Al=12.5) at 250 °C. 2, 5-hexanedione undergoes cyclization to form DMF even with presence of water during the heating process (point "RT" to time = 0), similar to
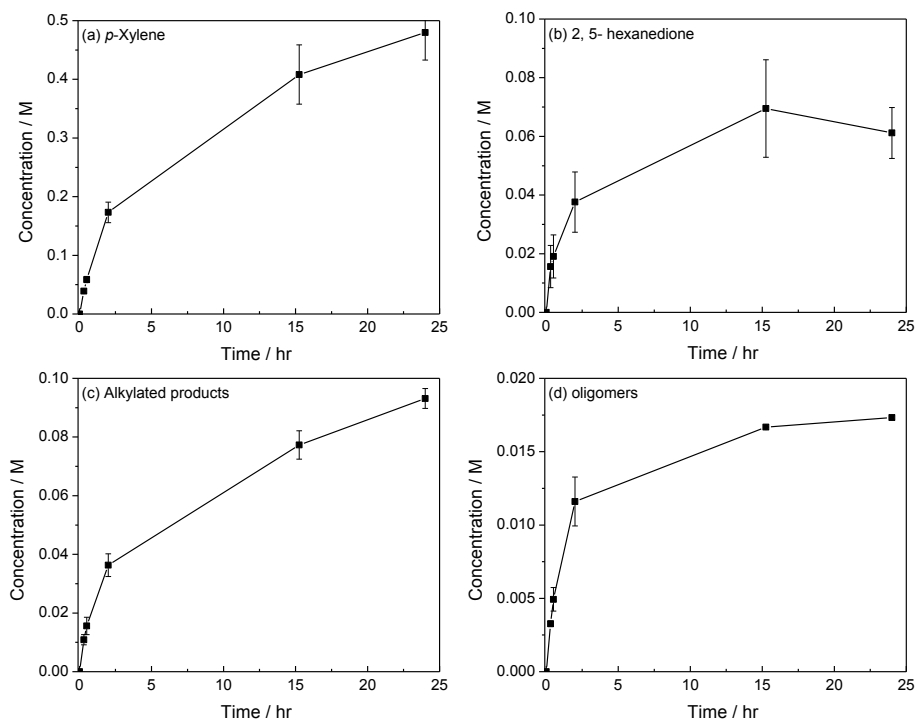
Figure 4.5 Concentration of products as a function of time for the reaction of DMF over H-FAU (Si/Al=2.6).
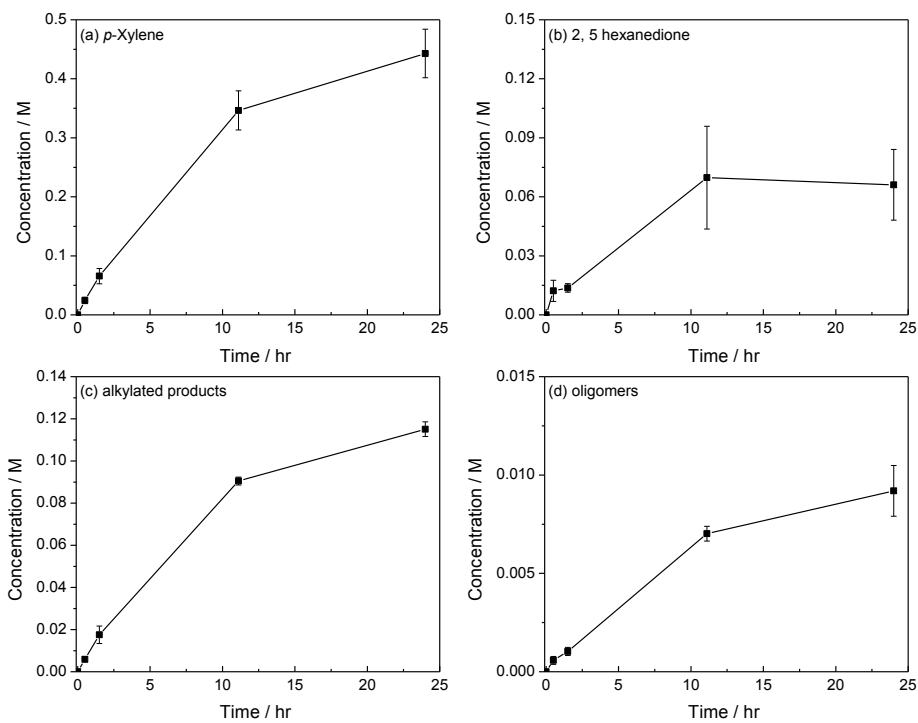
Figure 4.6 Concentration of products as a function of time for the reaction of DMF over H-ZSM-5 (Si/Al=15).

68
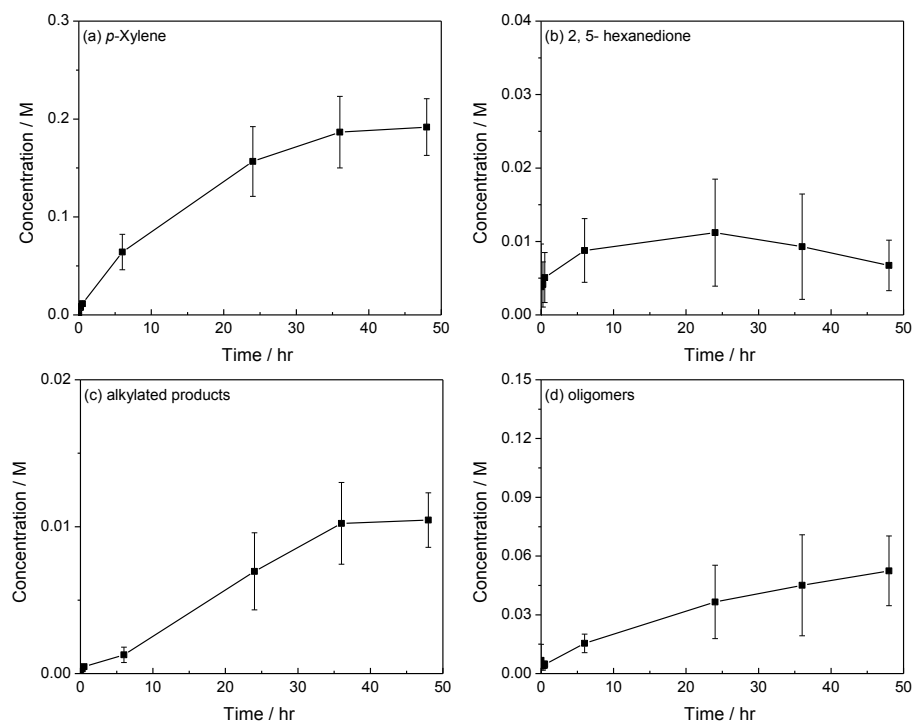
Figure 4.7 Concentration of products as a function of time for the reaction of DMF over niobic acid.
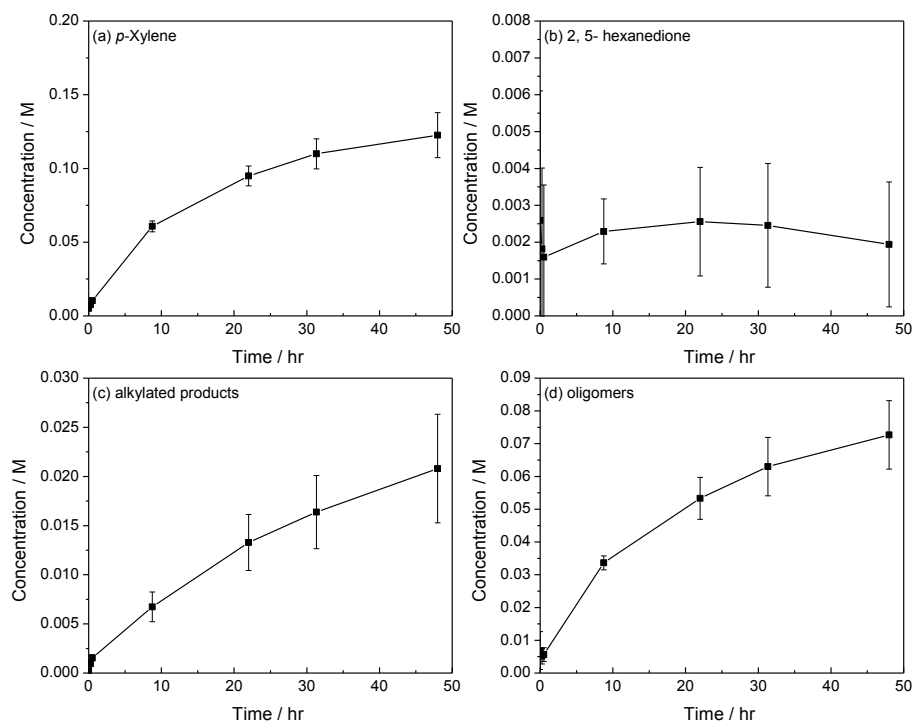
Figure 4.8 Concentration of products as a function of time for the reaction of DMF over γ-Al$_2$O$_3$.
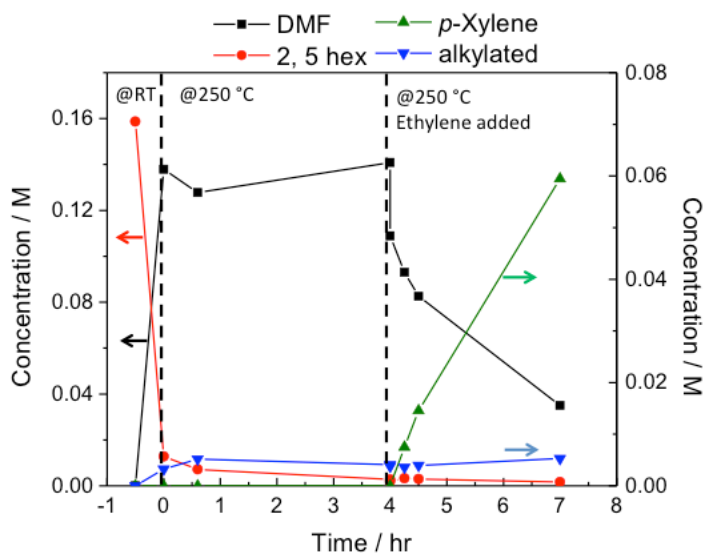
Figure 4.9 Concentration of products as a function of time for the reaction of 2,5-hexanedione , water, and ethylene over H-BEA (Si/Al=12.5) at 250 °C.

diketone cyclization described in literature,[117] and the composition did not change significantly after held at 250 °C for about 4 hrs. Once ethylene was introduced into the reactor (at 4 hours), the formed DMF started to be converted into *p*-xylene, and it supports the postulation that 2,5-hexanedione, the product from hydrolysis of DMF, can be cyclized back to DMF during the reaction and subsequently form *p*-xylene. The discrepancy between the 2,5-hexanedione concentration and DMF concentration might be a result of the condensation reaction of the diketone over the catalysts.

By the DMF hydrolysis reaction, carbon, which appears lost to the side product 2,5-hexanedione at low conversion, is recovered and results in high selectivity to *p*-xylene at high conversion of DMF. The superior performance of H-BEA for selective production of *p*-xylene can therefore be attributed to: (a) its resistance to deactivation, allowing for high conversion of DMF (Figure 4.3), (b) its superior activity relative to other solid-acid materials (Figure 4.2), and (c) its ability to catalyze dehydration of the Diels-Alder cycloadduct without catalyzing important side reactions. *p*-Xylene, once formed from DMF, does not readily isomerize to *o*- or *m*-xylene at the considered reaction

conditions (verified on GC-FID) which provides a significant process advantage by eliminating the expensive separation of xylene isomers.

The high activity of H-BEA is more pronounced for the conversion of DMF to *p*-xylene than for the reaction of 2-methylfuran (MF)/ethylene to toluene or the reaction of furan/ethylene to benzene. For the reaction of MF and ethylene, conversion of MF was 93% with H-BEA and 71% with H-Y after 24 hours of reaction at identical conditions to the experiments in Figure 4.3. Similarly, conversion of furan with ethylene was 54% with H-BEA and 50% with H-Y after 24 hours (see Figure 4.10-13). Figure 4.14 compares the product selectivity for conversion of DMF and MF at $X_{DMF,MF}$ >90% and furan at X_{furan} >70% at 250 °C. While 90% selectivity to *p*-xylene is achieved for conversion of DMF, only 46% selectivity to toluene and 35% selectivity to benzene are observed. Significant loss of carbon occurs in the reaction of MF and furan due to increased reactions between the furans forming dimers (e.g. benzofuran) and larger oligomers.[17] The increase in these reactions is likely due to the absence of methyl groups at the furan α-carbon positions, which inhibit these side reactions.
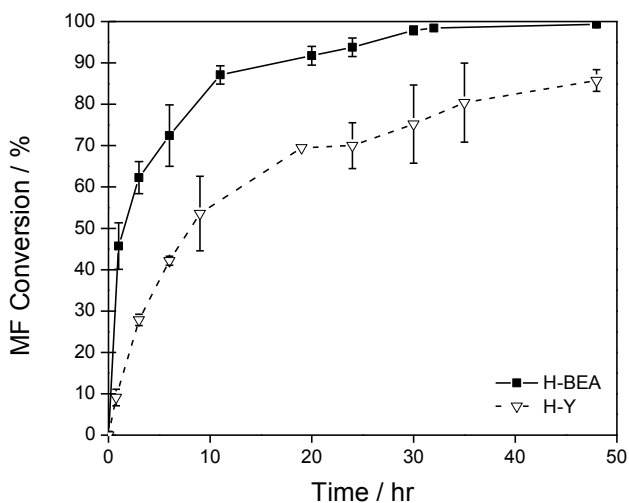
Figure 4.10 Conversion of MF as a function of time for the reaction of MF and ethylene over H-BEA (Si/Al = 12.5) and H-Y (Si/Al = 2.6) at 250°C.
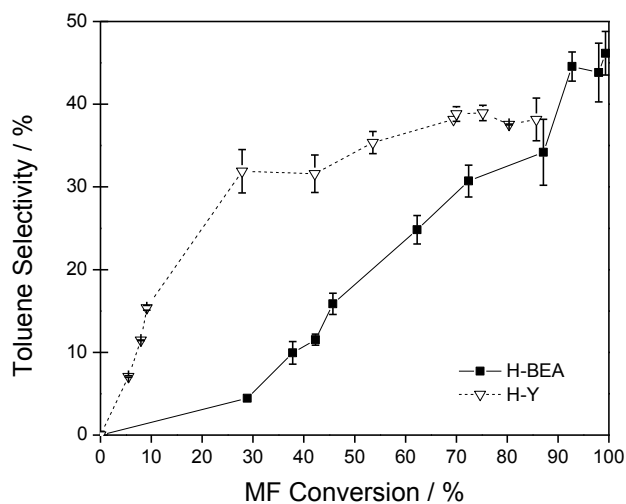
Figure 4.11 Selectivity to toluene as a function of MF conversion for the reaction of MF and ethylene over H-BEA (Si/Al = 12.5) and H-Y (Si/Al = 2.6) at 250°C.
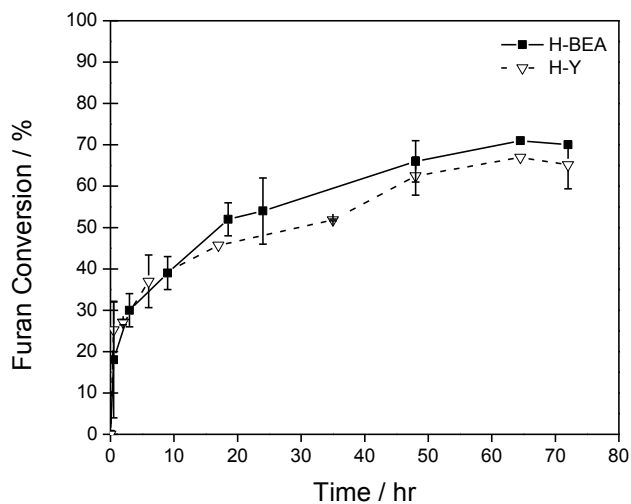
Figure 4.12 Conversion of furan as a function of time for the reaction of furan and ethylene over H-BEA (Si/Al = 12.5) and H-Y (Si/Al = 2.6) at 250°C.

The discovery that H-BEA in heptane exhibits high selectivity with high catalytic reaction rate significantly improves the potential for lignocellulosic biomass to serve as a renewable feedstock for aromatic chemicals. Techno-economic analysis of the process to convert glucose to HMF and eventually *p*-xylene indicates that the use of H-BEA addresses two of the three most important design
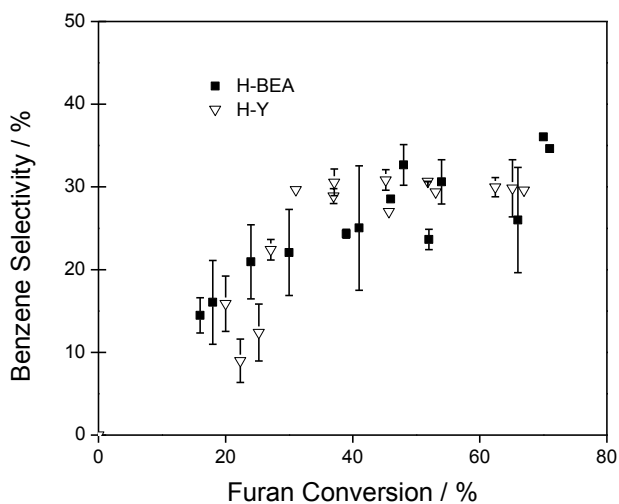
Figure 4.13 Selectivity to benzene as a function of time for the reaction of furan and ethylene over H-BEA (Si/Al = 12.5) and H-Y (Si/Al = 2.6) at 250°C.
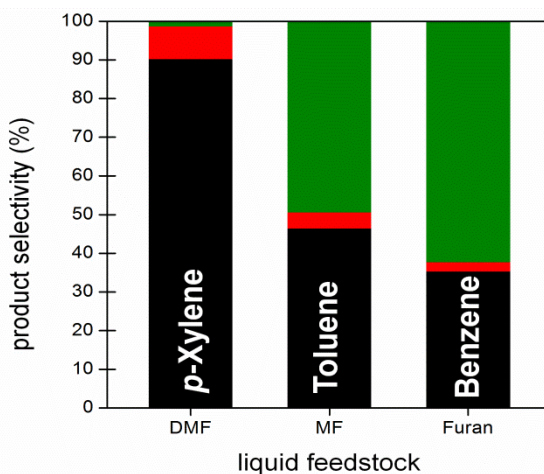
Figure 4.14 Product selectivity to (■) *p*-xylene, toluene, and benzene; (■) alkylated compounds; and (■) oligomer compounds at high conversion (>99% DMF & MF, 70% furan). Reaction conditions: 1M furanic feedstock in heptane with ethylene (62 bar) at 250°C with 0.45±0.05g catalyst. Error bars were less than 2% for each compound.

parameters for improved economics.[19, 118] First, high selectivity to *p*-xylene reduces the loss of feedstock carbon, which has been identified as the largest process cost. Second, the ability to utilize the side product, 2,5-hexanedione, by dehydration to DMF allows for the recovery of carbon within the process and raises the value of the ring-opened side product.

Later, during the optimization of reaction conditions, it is observed that the turnover frequency increase at lower catalyst loading, reaches a maximum, and start to decrease. Examine closely the raw reaction data, it is found that there exists a dependence of the reaction rate on the amount of catalysts. Figure 4.15 shows the initial reaction rates versus the concentration of Brønsted acid sites present in the reaction system over various catalysts, including different Si/Al ratio zeolite Beta and Y, ZSM-5 (CBV 3024, Zeolyst), Gamma alumina (STREM), niobic acid (HY-340, CBMM), tunstated zirconia (MEL chemicals) and 3DOm-i zeolite beta prepared in-house[58, 119] are tested as well. The reactions were carried out in a high pressure Parr benchtop reaction operated at 250 °C, 1.4 M DMF in heptane and ~62 bar of ethylene gas. The concentrations of Brønsted acids in the catalysts are determined by using isopropylamine TPD-TGA or literature.[15, 114, 120] As we can see in the plot, there are two kinetic regimes in the reaction. When the acid concentration is low, the reaction rate is linearly dependent of the acid concentration. However, the reaction rate does not vary and hit a plateau at high acid loading, irrespective of catalyst applied in the reaction. The interesting phenomena can be explained by the two-step reaction, DA cycloaddition and subsequent dehydration reactions, from DMF reacting with ethylene to p-xylene, as shown in Scheme 3.1. In the low catalyst loading region, the reaction is limited by dehydration reaction, while at high loading, the
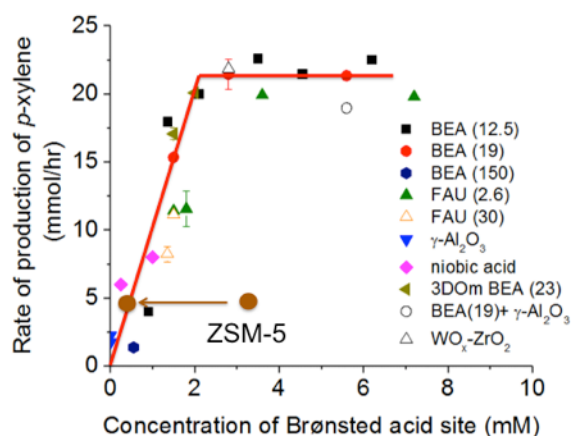
Figure 4.15 Dependence of the initial reaction rate vs. the concentration of Brønsted acid present in the system

cycloaddition reaction is the rate-limiting step. The results once again imply that Brøsted acid cannot catalyze the cycloaddition reaction, and none of the tested catalysts were able to enhance the rate of cycloaddition. One outlier on the plot is ZSM-5, as indicated in Figure 4.15. The reaction rate of ZSM-5 matches the plot when only acid sites on external surface are considered, and this suggests that the cycloaddition cannot happen within the zeolite pore structure or the cycloadduct is not able to diffuse into the zeolite and react with internal acid sites due to narrow pore openings of ZSM-5.

The particle size effect on the initial production rate of the tandem reaction was studied by synthesizing different particle sizes of aluminosilicate zeolite Beta. Mesoporous (3DOm-i) and 200 nm zeolite Beta were prepared according to Chen et al.[58] Micron-sized zeolite Beta were synthesized based on Camblor et al.[62] and the seeding growth method described in Chapter 2 to control the paricle size. The size of the particle was determined by scanning electro microscopy, and the representative images are shown in Figure 4.16. 3DOm-i zeolite beta consists of primary particle around 30 nm in ordered face center cubic packing, and the window size in around 10 nm.[58, 119] The larger crystals show typical truncated bipyrimidal morphology of zeolite Beta. Figure 4.17 reveals the initial reaction rate of the formation of *p*-xylene at the same acid site concentration in the system (1.5 mM, in dehydration limited regime), and a clear size dependence can be observed. The mesoporous and 200 nm samples shows similar reaction rate, while when large crystals were employed (> 800 nm), the reaction rate decreases. The data suggest there exists diffusion limitation when the particle size of zeolite Beta is larger than 800 nm. Thus, to design a suitable catalyst for the system, it should be mesoporous or nanocrystalline for zeolite Beta to achieve high production rate of *p*-xylene.

The performances for different zeolites are also studied in long reaction time to investigate the micropore structure effect. As shown in Figure 4.18, at the same concentration of Brønsted acid site, among the catalysts, zeolite Beta shows the best performance and can avoid fast deactivation, reaching 99 % conversion in 24 h, while the other two fail to keep up with zeolite Beta. For ZSM-5, since only external acid sites take effect, it is rational to behave faster deactivation and showing indications of non-efficient use of the catalyst due to relative small micropore dimensions. For zeolite
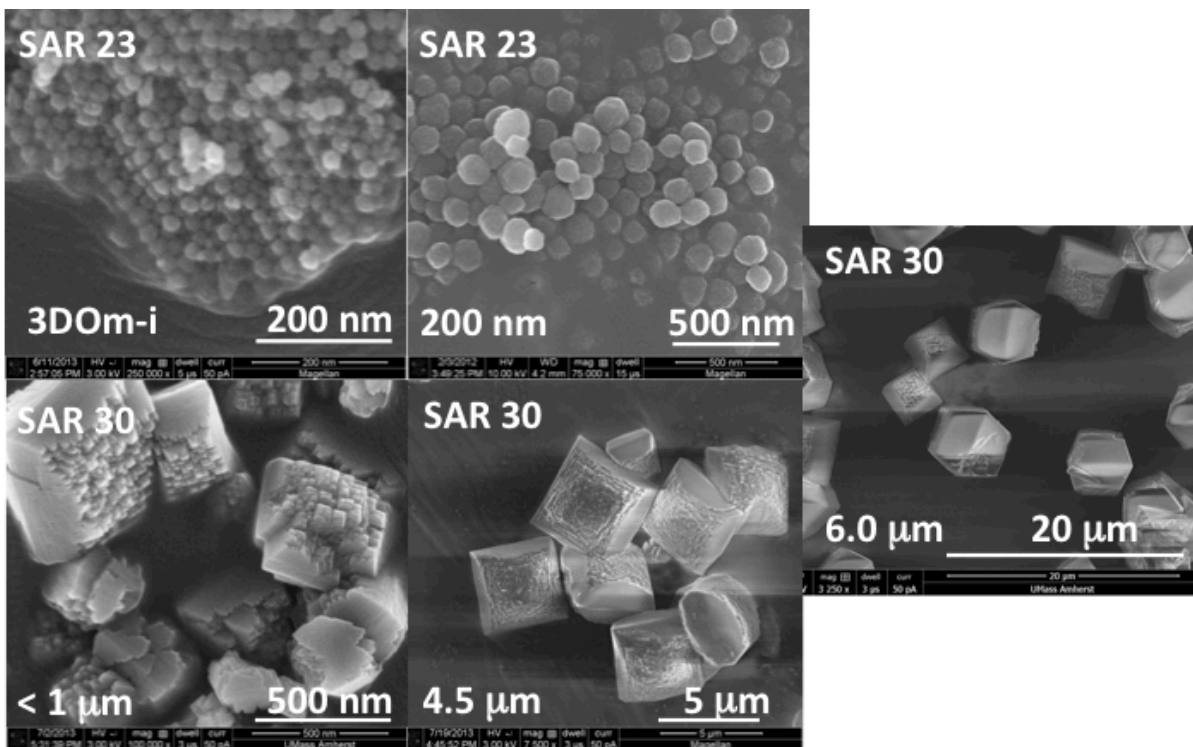
Figure. 4.16 SEM images for different sizes of zeolite Beta: mesoporous (3DOm-i), 200nm, 800 nm, 4.5 μm, and 6 μm.
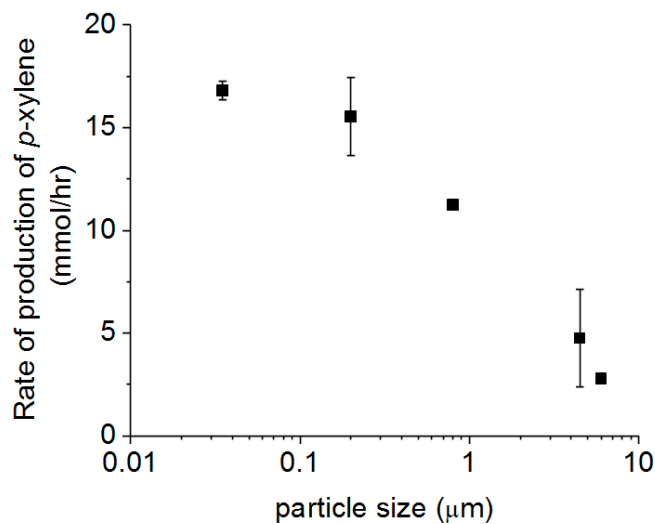
Figure. 4.17 Rate of *p*-xylene production with different sizes of zeolite Beta. Reactions with 1.5 mM of Brønsted acid sites in the reaction system (1.3 M DMF in heptane, 62 bar ethylene, 250 °C.)

Y, we hypothesize the faster deactivation is due to its super cage structure such that it facilitates byproduct formation. Zeolite Beta's long life might be due to its adequate pore structure. More
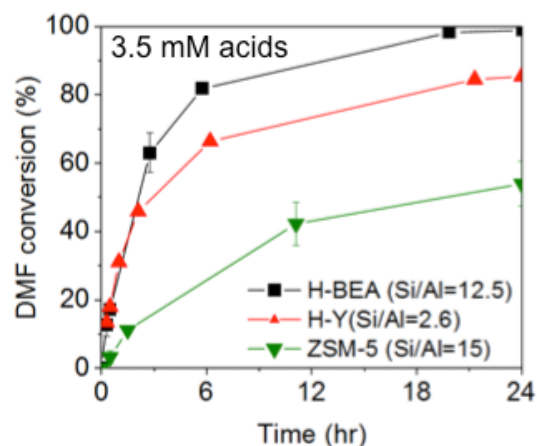
Figure. 4.18 Reaction kinetics of zeolite Beta, zeolite Y and ZSM-5 in DMF to *p*-xylene reaction. The reaction conditions are described previously.

importantly, the selectivity to *p*-xylene in detectable compounds can reach 90% (on a carbon basis) at

99% conversion of DMF for zeolite Beta, as shown in Figure 4.4. These data clearly suggest that the

pore structure indeed impact the Diels-Alder cycloaddition/dehydration tandem reaction to form *p*-

xylene, and zeolite Beta presents the most promising performance.

CHAPTER 5

LEWIS ACID ZEOLITES CATALYZE PRODUCTION OF RENEWABLE PARA-XYLENE FROM 2,5-DIMETHYLFURAN AND ETHYLENE

5.1 Background

p-Xylene is an important commodity chemical for the synthesis of terephthalic acid which is the monomer for synthesis of polyethylene terephthalate (PET). PET has been widely utilized to commercially manufacture synthetic fibers and plastic bottles due to their outstanding mechanical and chemical properties. [57, 121, 122] As the third largest chemical in volume on the world produced from petroleum-derived feedstock (catalytic reforming of naphtha) and the increasing demand (6-8 % per year),[6] there are now ongoing worldwide efforts developing alternative routes for producing *p*-xylene from renewable biomass resources.[14, 15, 17, 48, 123-128] For example, Lyons et al. demonstrated that *p*-xylene can be synthesized from ethylene (from dehydration of bio-ethanol) by a multi-step reaction pathway including trimerization of ethylene, Diels-Alder reaction of 2,4-hexadiene with ethylene and dehydrogenation of 3,6-dimethylcyclohexene; Shiramizu and Toste also reported that *p*-xylene can be selectively produced from 2,5-dimethylfuran (DMF, from hydrogenolysis of cellulosic biomass-derived 5-hydroxymethylfurfural (HMF)) and acrolein (from glycerol, a biodiesel byproduct).[48, 126]

In our previous studies we have reported a renewable reaction pathway to produce *p*-xylene from lignocellulosic biomass over solid acid catalysts. The Diels-Alder dehydration reaction pathway includes the cycloaddition of biomass-derived dimethylfuran (DMF) with ethylene, and subsequent dehydration of the formed Diels-Alder adduct to *p*-xylene (Scheme 1).[14-16, 18, 120] Competing reactions involving hydrolysis of DMF to 2,5-hexanedione and reactions between the cycloadduct, DMF (oligomers) and ethylene (alkylated products).[16] The reaction network can be 100% based on biomass resources since DMF can be produced from the hydrolysis of cellulose followed by dehydration of glucose or fructose to HMF, and hydrodeoxygenation of HMF to DMF[1], and ethylene can be produced from the dehydration of bio-ethanol.[129, 130] We have demonstrated that a nearly 90%

selectivity of *p*-xylene can be achieved by running the Diels-Alder dehydration reaction over Brønsted acid zeolite catalysts (i.e. Al-BEA zeolite) in n-heptane solvent environment.[14] Toluene and benzene can also be produced with a similar chemistry, but starting with 2-methylfuran and furan, respectively. Computational study (density functional theory (DFT) or quantum mechanics/molecular mechanics (QM/MM)) revealed that the formation of oxanorbornene cycloadduct intermediate by the addition of ethylene to DMF may not be catalyzed by Brønsted acid of zeolite catalysts.[15, 131, 132] However, the Brønsted acid of zeolite catalyst can effectively catalyze the dehydration of the cycloadduct intermediate and decrease the activation energy from 58-60 kcal/mol to 14-19 kcal/mol, leading to a significantly increased reaction rate.[15, 18, 131] Although Brønsted acid zeolite catalysts exhibit promising catalytic performance, the relatively slow reaction rate compared with homogeneous catalyst and catalyst deactivation present technical challenges for the commercialization of the catalytic process. The slow reaction rate is partially due to the tandem reaction pathway and the uncatalyzed Diels-Alder reaction. The catalyst deactivation observed over Brønsted acid zeolite catalysts is mainly due to the hydrolysis of DMF to 2,5-hexanedione and formation of alkylated and oligomer side products. There are thus persistent needs for improving the reaction rate by developing catalysts which can catalyze the Diels-Alder reaction to increase the
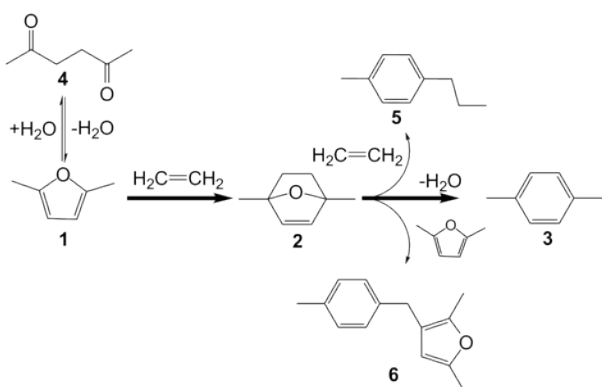
Scheme 5.1 Simplified reaction scheme for synthesis of *p*-xylene from DMF and ethylene. **1**: DMF; **2**: cycloadduct; **3**: *p*-xylene; **4**: 2,5-hexanedione; **5**: representative alkylated product; **6**: representative oligomer.

production rate of cycloadduct intermediate, and better dehydration catalyst for reducing the side product formation.

Several previous studies have suggested that Lewis acid can coordinate with dienes to catalyze the Diels-Alder reaction.[48-52] DFT study on the production of *p*-xylene from DMF also suggested that Lewis acid can coordinate with ethylene to catalyze the Diels Alder reaction to form cycloadduct intermediate, oxanorbornene.[18, 53] In addition, experimental and theoretical studies have also suggested that solid Lewis acid catalysts are capable of catalyzing the dehydration of cycloadduct intermediate and other alcohols.[18, 53-55]. Using Fe^{3+}-exchanged montmorillonite K10 clay as a Lewis acid catalyst for the aromatization of oxabicyclic derivatives has also been reported.[52, 56] Lewis acid zeolite catalysts, in particular Sn-BEA and Zr-BEA, have also shown superior catalytic activity for the synthesis of terephthalic acid via Diels-Alder reactions with oxidized variants of 5-hydroxymethylfurfural.[57]

Motivated by the experimental and theoretical studies, Lewis acid catalysts were employed in the Diels-Alder cycloaddition-dehydration reaction pathway for producing *p*-xylene from DMF and ethylene. We demonstrated that Lewis acid zeolite catalysts are active for producing *p*-xylene due to their catalytic activities for both Diels-Alder cycloaddition and dehydration reactions. Zr-BEA catalyst, in particular, exhibited a high selectivity of 90% to *p*-xylene and slow deactivation due to the low production rate for the hydrolysis by-product, 2,5-hexanedione. It is also evidenced that Zr-BEA can effectively enhance the formation of cycloadduct from DMF and ethylene, resulting in the highest *p*-xylene production rate.

5.2 Experimental

5.2.1 Preparation of the catalysts

The solid Lewis acid zeolite catalysts employed in this study were prepared according to previous published research and Chapter 2 based on a seeded growth method developed for Sn-BEA.[35, 90, 112]

5.2.1.1 Preparation of Zr-BEA

Typically, a portion of 23.72 g tetraethylorthosilicate (TEOS, 99%, Alfa Aesar) was added to 27.39 g of tetraethylammonium hydroxide solution (TEAOH, 35 wt.%, SACHEM) and magnetically stirred in a plastic beaker. After a homogeneous solution was obtained (about 1 h), 0.3 g of zirconium(IV) oxychloride octahydrate ($ZrOCl_2\bullet8H_2O$, Sigma-Aldrich) was dissolved in 1.92 g water and added dropwise into the silicate solution. The mixture was kept stirring in a fumed hood until desired amount of water and ethanol (generated from hydrolysis of TEOS) were evaporated. To this solution, 1.712 mL of zeolite BEA seed suspension (0.163 g of seed crystal per mL; corresponding to 4 wt.% seed with respect to silica) was added and mixed with a plastic spatula. Lastly, 2.36 mL of hydrofluoric acid (49 %, Alfa Aesar) was added and mixed with a plastic spatula, and a hard gel was formed. The final composition of the gel is SiO_2: 0.008 ZrO_2: 0.56 TEAOH: 0.56 HF: 7.5 H_2O. The hard gel was transferred to Teflon lined stainless steel autoclave and heated in a preheated convection oven at 140 °C for 4 days with 2 rpm rotation. The solids were washed with 1 L of deionized water by filtration and dried in an 80 °C oven overnight. The organic template was removed by calcining the as-made catalyst at 550 °C with a ramping rate of 1 °C/min for 12 h under flowing dry air (Grade 0.1, Middlesex Gases & Technologies, Inc.).

5.2.1.2 Preparation of Sn-BEA

Please see Chapter 2 for the details. The sample was prepared at 140 °C for 4 day. The organic template was removed by calcining the as-made catalyst at 550 °C with a ramping rate of 1 °C/min for 12 h under flowing dry air.

5.2.1.3 Preparation of Ti-BEA

Typically, a portion of 24.66 g of TEOS was added to a mixture of 26.76 g of TEAOH solution and 4.24 g of hydrogen peroxide solution (H_2O_2, 30 %, Fisher) and magnetically stirred in a plastic beaker. After a homogeneous solution was obtained (about 1 h), 0.45 g of Titanium (IV) ethoxide (Aldrich) was added dropwise into the silicate solution. The mixture was kept stirring in a fumed

hood until desired amount of water and ethanol were evaporated. To this solution, 1.708 mL of zeolite BEA seed suspension (corresponding to 4 wt.% seed with respect to silica) was added and mixed with a plastic spatula. Lastly, 2.306 mL of hydrofluoric acid (49 %, Alfa Aesar) was added and mixed with a plastic spatula, and a hard gel formed. The final composition of the gel is SiO_2: 0.008 TiO_2: 0.54 TEAOH: 0.54 HF: 7.5 H_2O. The hard gel was transferred to Teflon lined stainless steel autoclave and heated in a preheated convection oven at 140 °C for 8 days with 2 rpm rotation. The solids were washed with 1 L of deionized water by filtration and dried in an 80 °C oven overnight. The organic template was removed by calcining the as-made catalyst at 550 °C with a ramping rate of 1 °C/min for 12 h under flowing dry air.

5.2.1.3 Preparation of Al-BEA

Aluminosilicate zeolite BEA (CP814E, Si/Al=12.5) was obtained from Zeolyst for comparison. The catalyst was calcined at 550 °C with a ramping rate of 1 °C/min for 12 h under flowing dry air prior to the reaction.

5.2.2 Characterizations of the catalysts

The crystalline phase of the Lewis acid catalysts were examined by powder x-ray diffraction (PXRD) on a diffractometer (X'Pert Pro, PANalytic) operated at a voltage of 40 kV and a current of 45 mA with an X'cellerator detector scanning from 4° to 40°. The amount of Lewis acid site in the Lewis acid zeolites was determined by diethylether temperature programmed desorption thermogravimetric anlaysis (TPD-TGA) except for Ti-BEA. Ti-BEA interacted weakly with the probe molecules, and can't provide the Lewis acid site information. The elemental analyses were carried out in Analytical Geochemistry Lab, Department of Earth Sciences in University of Minnesota using ICP-OES (iCAP 6500 duo view, Thermo Scientific).

5.2.3 Reaction tests

The protocol is the same as described in Chapter 4 and in our previous reports.[14, 15] Typically in DMF (Alfa Aesar) reactions, 100 mL of 1.3 M of DMF in n-heptane (Alfa Aesar) with 0.08 M n-tridecane (Alfa Aesar) was enclosed in a 160 mL bench-top reactor (Parr), and the reaction vessel was purged by nitrogen. The acid concentration present in the system was defined as the total acid site number of the catalyst divided by the reactant volume. The mixture was then stirred at 1000 rpm with a gas entrainment impeller to ensure facile mass transfer in the system and heated up to 250 °C, controlled by 4848 control unit (Parr). The reactor was then pressurized with 38 bar (partial pressure) of ethylene gas (Airgas), and the total pressure the system was kept at 62 bar over the reaction period. Liquid was withdrawn by a double block sampling system at designed reaction times. The composition of the sample was then analyzed on an Agilent 6890A gas chromatograph with a Rtx-VMS (Restek) column equipped with flame ionization detector. The products (DMF, p-xylene, 2,5-hexanedione) were identified by comparing the retention times with standard chemicals. The concentrations of alkylated products and oligomers were estimated by using the response factor (RF) for p-xylene and the additive RF of p-xylene and the DMF (based on the reaction scheme), respectively.[16] Cycloadduct of DMF and ethylene was identified on a GC/MS system (5890 GC/5972 series mass selective detector, HP) and by comparing the electron ionization spectrum to literature, and the concentration of the cycloadduct was estimated by using the RF for p-xylene.[16] The conversion of DMF and selectivity to the products are defined as following:

$$X_{DMF} (\%) = 100 \times \frac{C_{DMF,t_0} - C_{DMF}}{C_{DMF,t_0}} \tag{5.1}$$

$$Selectivity_i (\%) = 100 \times \frac{C_i - C_{i,t_0}}{\Sigma_i (C_i - C_{i,t_0})} \tag{5.2}$$

$$Yield_i (\%) = 100 \times \frac{C_i}{C_{DMF,t_0}} \tag{5.3}$$

where t_0 is the time after ethylene added to the reactor and C_i is concentration of the chemical i.

For the reaction carried out with 2,5-hexanedione, 0.2 M of diketone (Alfa Aesar) was added with 1.4 M DMF solution in n-heptane. The reactor was purged with N_2, heated to 250 °C and held at 250 °C for 1 h prior to addition of ethylene (62 bar).

5.3 Results and discussions

To demonstrate the catalytic activity of solid Lewis acid catalysts for the Diels-Alder dehydration reaction pathway, siliceous zeolite BEA with substituted metal atoms (Zr-, Sn-, and Ti-BEA) at framework positions were prepared according to the methods reported in literature and applied in the reaction. Other conventional metal oxide catalysts including ZrO_2, SnO_2, TiO_2 were also tested in the reaction. The corresponding XRD patterns for the Lewis acid zeolites used in this study are shown in Figure 5.1. Typical reflections for zeolite BEA were observed for all samples, and no impurity phase (i.e., metal oxides) was detected, indicating high-quality crystals were obtained. The acid site concentrations of the Lewis acid zeolites were determined by the Si/M ratio obtained from elemental analysis measurement (ICP-OES), and further confirmed by diethylether TPD-TGA measurement (Table 5.1). It has been known that diethylether forms 1:1 complex pair with Lewis acid site (Sn
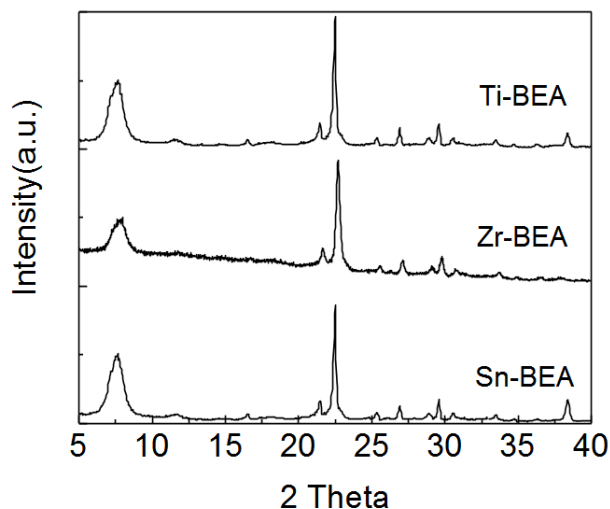
Figure 5.1 XRD patterns for Sn-, Zr-, and Ti-BEA. Typical reflections for zeolite BEA were observed for all samples, and no impurity phase (i.e., metal oxides) was detected, indicating high-quality crystals were obtained.

center) in Sn-BEA catalyst, and desorbs from the Sn site at the temperatures from 350K to 450K. Measuring the weight change between the temperatures can provide the amount of Lewis acid sites in the samples.[54] Diethylether TPD-TGA-MS results obtained from Sn-BEA, Zr-BEA and Ti-BEA catalysts are shown in Figure 5.2. Mass to charge ratio 31 was recorded due to that it is the most abundant species for diethylether using eletron ionization. As shown in Table 5.1, the TPD-TGA measurements for Sn- and Zr-BEA show good agreement with the elemental analysis, while the measurement for Ti-BEA shows a lower acid site density than the Ti concentration in the sample determined by the elemental analysis (40 μmol/g vs. 129 μmol/g). This may be due to the weak interaction between diethylether and Ti site in the Ti-BEA sample, resulting in desorption of the probe molecule from the sample in vacuo prior to heating. For Al-BEA, isopropylamine TPD-TGA was employed to obtain the Brønsted acid site concentration, 620 μmol/g.[133] The amount of Brønsted acid site in the Al-BEA is lower than the Al concentration indicating the presence of extra framework Al in the sample. Contribution from extra framework Al species was neglected due to low activity from Al_2O_3 according to our previous report, summarized in Chapter 4.[14] For the reaction rate calculations, the acid site concentrations determined by TPD-TGA analysis were used. Due to the weak adsorption of Ti-BEA to diethylether, the Ti concentration determined by element analysis was used in the reaction rate calculations.

Table 5.1 Acid site density of the zeolites

Catalyst	Si/T	Acid site density (μmol/g)	
	ICP	ICP	Chemical TPD[b]
Zr-BEA	168	98	95
Sn-BEA	126	130	120
Ti-BEA	128	129	40
Al-BEA	12.5[a]	1230	620[c]

[a]Zeolyst
[b]Diethylether TPD except for otherwise noted
[c]Isopropylamine TPD for Brønsted acid sites
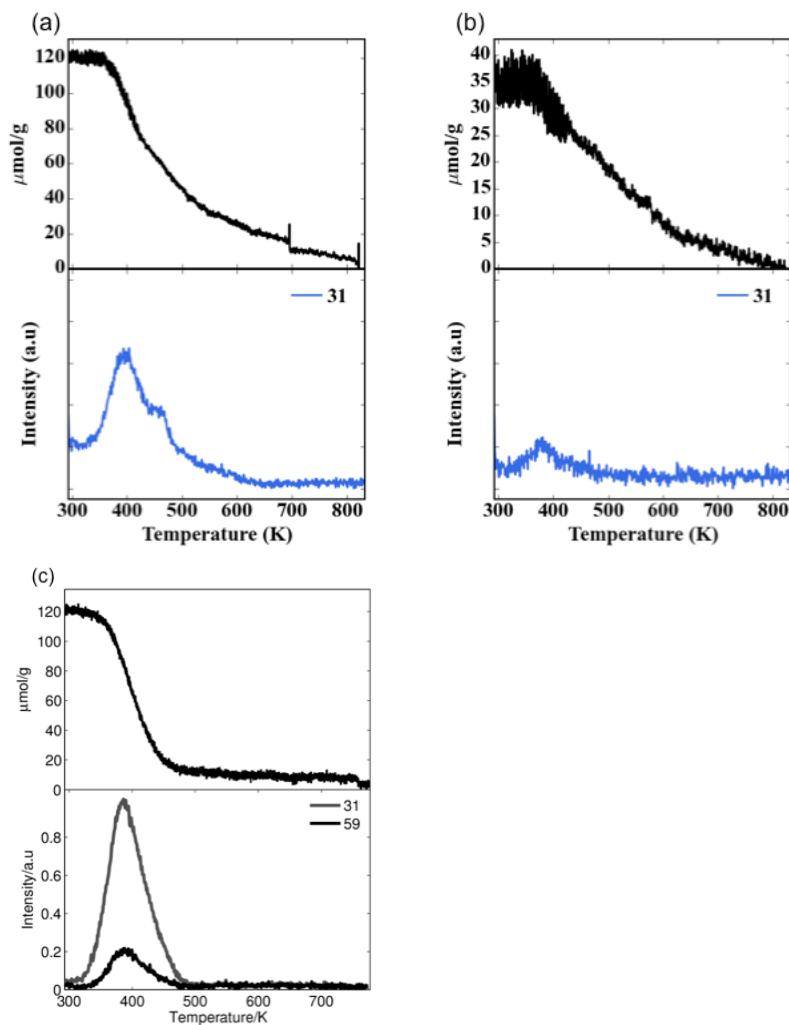
Figure 5.2 Diethylether TPD data for (a) Zr-, (b) Ti-, and (c) Sn-BEA. In each figure, top plot shows the TGA data, and the bottom depicts the signal from mass spectrometer (MS) recording during desorption. Under electron ionization, m/e=31 is the most abundant species (m/e=59 is the second largest) of diethylether recorded from MS, so it was used as indication of desorption of diethylether.

Figure 5.3 reveals the reaction profiles for yield and selectivity to *p*-xylene with respect to DMF conversion over different catalysts at the same acid site amount (1 mM) in the reaction system (1.4 M DMF in heptane and 62 bar of ethylene) at 250 °C. Interestingly, all tested Lewis acid zeolites are able to catalyze the reactions to produce *p*-xylene. This is apparently attributed to the Lewis acidity from the isolated metal atoms located in the zeolite frameworks, as metal oxides (ZrO_2, SnO_2, and TiO_2) and pure siliceous BEA do not show considerable catalytic activity, as shown in Figure 5.4.[15] Among all the tested catalysts, Zr-BEA shows superior performance with 80% selectivity to *p*-xylene

at 80% conversion of DMF (Figure 5.3(b)) in 24 hrs. Sn-, Ti-, and Al-BEA, however, deactivated noticeably faster, and only reach about 60% of DMF conversion after 24 hr reaction with lower selectivity to *p*-xylene. Furthermore, Zr-BEA yielded ~33 % more *p*-xylene than Al-BEA at 60% conversion (Figure 5.3(c)). It is worth noting that the activity of Sn-MFI is considerably lower (8 mM/hr; Table 5.2) at the same conditions, as it converts less than 20 % of DMF after 24 hr reaction, which highlights the uniqueness of zeolite BEA structure for this reaction. The result is consistent with our previous report[14] which suggested the small micropore structure of ZSM-5 is not favorable for the reaction and implies either the Diels-Alder reaction could not be catalyzed or the formed cycloadduct intermediate could not easily diffuse within the micropore structures of MFI resulting in a significant diffusion limitation.

Figure 5.3 (a) Kinetics of conversion of DMF and (b) selectivity and (c) yield to *p*-xylene as a function of DMF conversion for the reaction of DMF and ethylene at 1 mM acid loading of Sn-BEA, Zr-BEA, and Ti-BEA as well as Al-BEA.
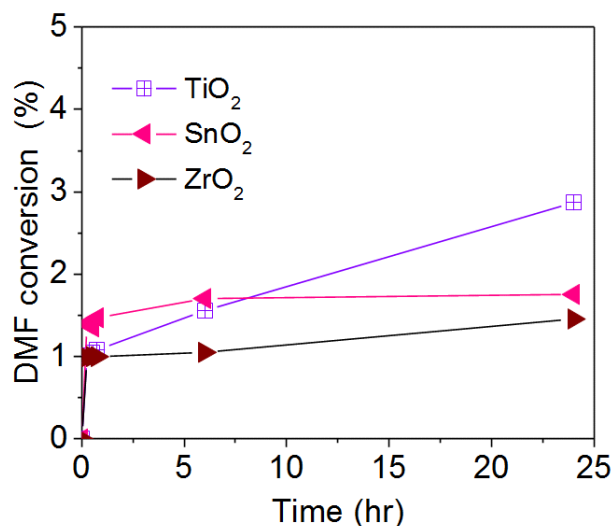
Figure 5.4 DMF conversion versus time for SnO_2, TiO_2, and ZrO_2. Reaction conditions are the same with the Lewis acid zeolites except for the amount of catalyst used (0.8 g for metal oxides).

Table 5.2 Summary of reaction results for the catalysts[a]

Catalyst	Rate of p-xylene production (mM/hr)	DMF conversion after 24 hr	p-Xylene yield after 24 hr
Al-BEA	122 ± 11	55 ± 3.7	30 ± 0.5
Sn-BEA	113 ± 6.8	63 ± 0.1	43 ± 1.8
Zr-BEA	121 ± 4.9	83 ± 1.6	61 ± 1.5
Ti-BEA	65 ± 11.2	60 ± 3.5	41 ± 4.5
Sn-MFI	8	17	17
SnO_2	0.6	2	0.3
ZrO_2	0.7	2	0.5
TiO_2	1.1	3	1.4

[a]Reaction conditions: 1 mM acid (0.8 g for metal oxides), 1.4 M DMF in n-heptane, 62 bar ethylene, 250 °C

The byproduct distributions for the reactions over the Lewis acid zeolite catalysts and Brønsted acid zeolite catalyst are shown in Figure 5.5. As shown in the plot, Sn-BEA preferentially catalyzes the side reactions and produces more hydrolysis product, 2,5-hexanedione, and oligomers at lower conversion, which explains the low p-xylene selectivity for Sn-BEA. Zr-BEA, however, is able to minimize the hydrolysis of DMF, showing low 2,5-hexanedione yield at all conversion (Figure. 5.5(a)). In addition, Zr-BEA also minimizes the formation of oligomers (Figure 5.5(b)) but promotes

88

the reactions between cycloadduct and ethylene, giving the highest yield for alkylated products (Figure 5.5(c)). Al-BEA, on the other hand, produces small amount of oligomer and more 2,5-hexanedione and alkylated products. At low conversions, strong Brønsted acidity of Al-BEA can effectively catalyze the hydrolysis reaction of DMF, which explains the even lower *p*-xylene selectivity at high catalyst loading shown later. All the results suggest that using Zr-BEA is beneficial at low conversion of DMF due to its low activity for catalyzing side reaction of hydrolysis of DMF. The reaction results reveal that the characteristics of the acid type can manipulate the product distributions by affecting the reaction rates between the competing reaction pathways, while the selectivity towards *p*-xylene for all catalysts are not significantly different at high conversion of DMF.
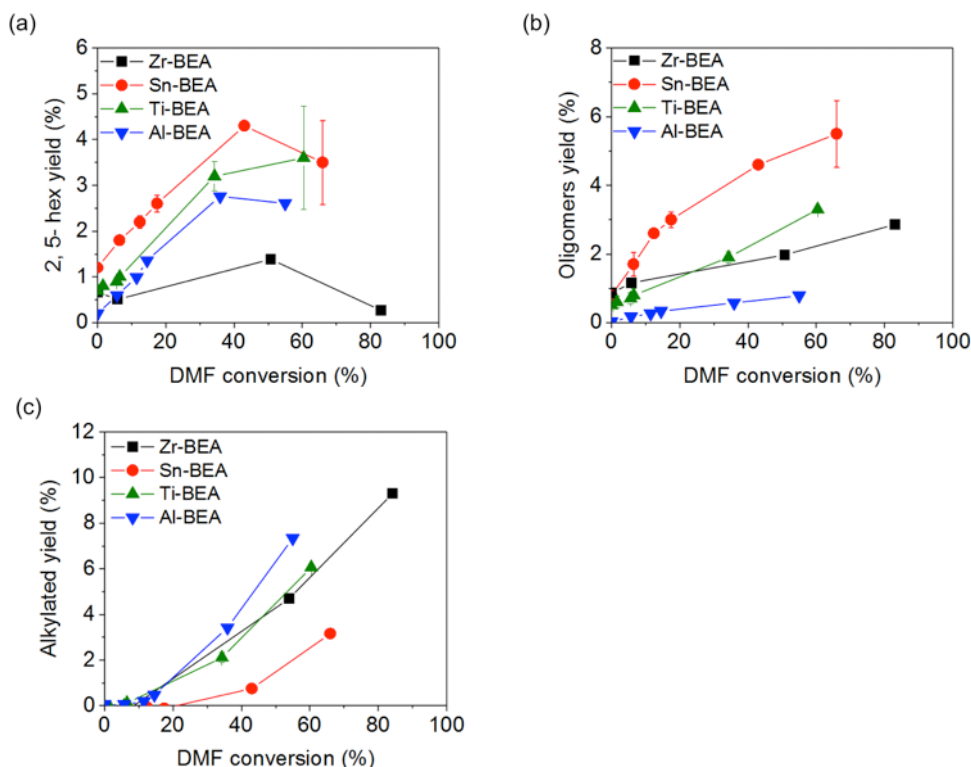
Figure 5.5 Yield of (a) 2, 5 hexanedione, (b) oligomers and (c) alkylated products as a function of DMF conversion for the reaction of DMF in heptane with ethylene (62 bar) at 250 °C with various catalysts Sn-BEA, Zr-BEA, and Ti-BEA as well as Al-BEA with 1 mM acid concentration.

89

In order to understand the effects of active site concentration on the reaction system, a high loading of Zr-BEA catalyst (acid concentration of 3.1 mM) was studied and compared to Brønsted acid zeolite catalyst, Al-BEA. It was found that the kinetics of DMF conversion and overall *p*-xylene yield were very similar (Figure 5.6) between Zr-BEA and Al-BEA, but the selectivity to *p*-xylene for Zr-BEA is significantly higher at low conversion (80% vs. 60%). The discrepancy is much larger compared to low acid loading case which is due to the low activity of Zr-BEA for catalyzing the hydrolysis reaction of DMF. Zr-BEA reaches highest selectivity of *p*-xylene (~90 %) at the full conversion of DMF at acid concentration of 3.5 mM, which is similar to the previous reported *p*-xylene selectivity achieved over Al-BEA. It has to be noted that the Al-BEA exhibits extra framework Al which is likely inactive for the reaction since Al_2O_3 didn't show noticeable activity in the reaction test.[14]
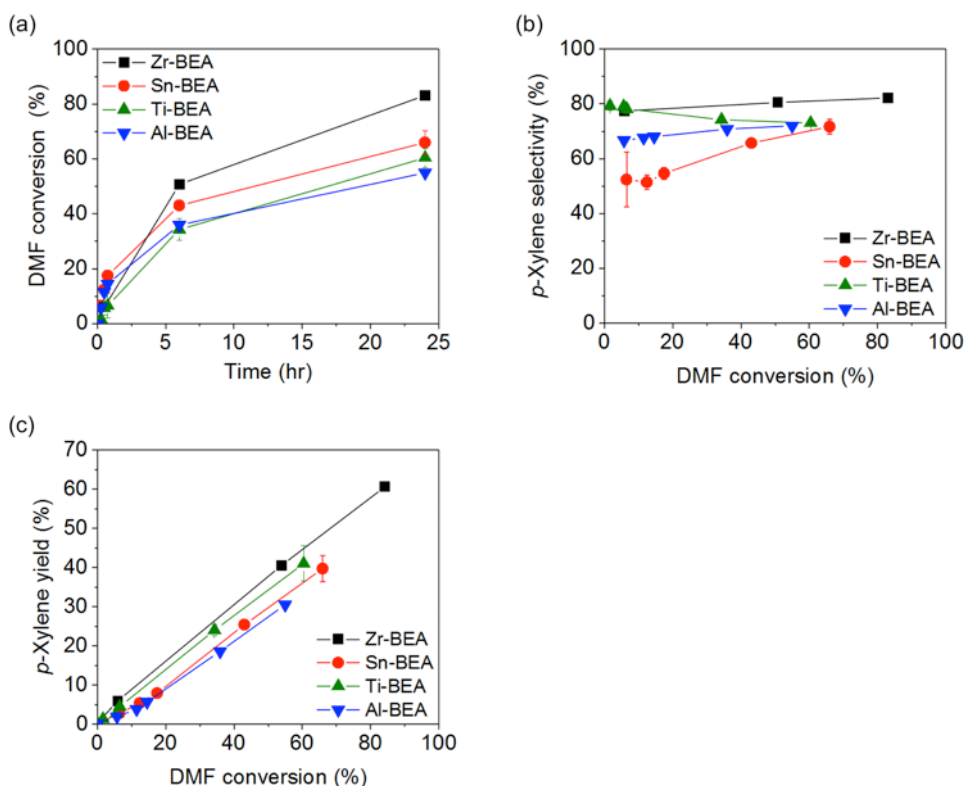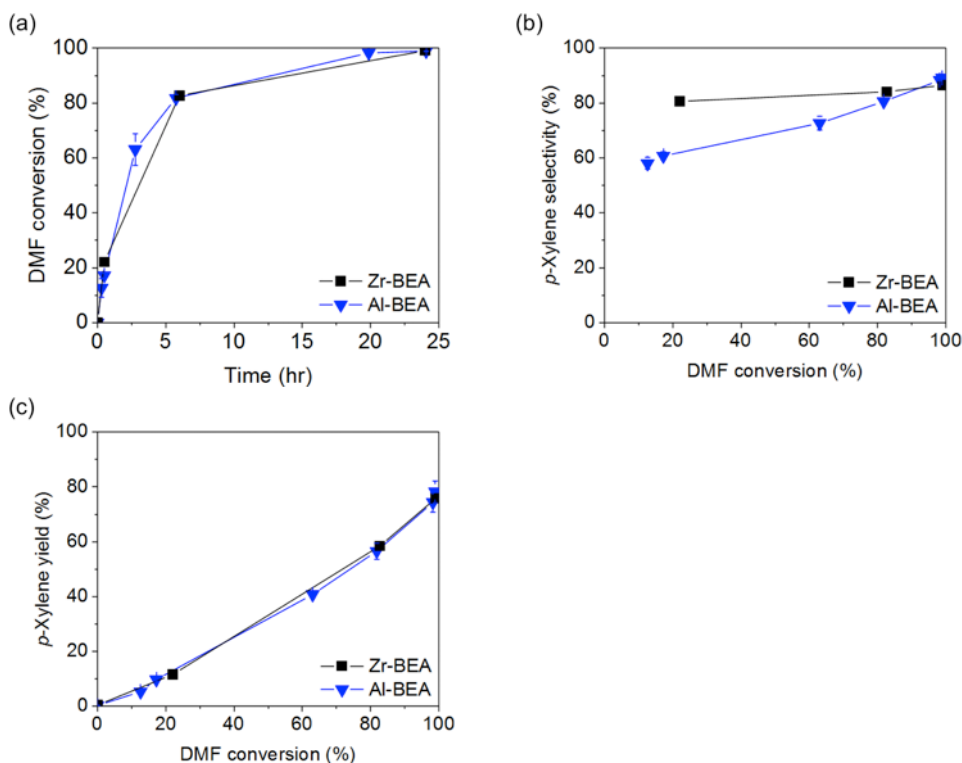

Figure 5.6 (a) Kinetics of conversion of DMF, (b) selectivity, and (c) yield to *p*-xylene as a function of DMF conversion for the reaction of DMF at high acid loading of Zr-BEA (3.5 mM) and Al-BEA (3.1 mM).

Figure 5.7 shows the plot of rate of production of *p*-xylene versus acid site concentration for different catalysts. Reaction rates were deliberately presented on a volumetric basis of mM/hr (rather than TOF), due to previous work which indicated experimental conditions whereby the overall reaction was limited by an uncatalyzed reaction.[14, 15, 131] At low acid site concentration, the rate of *p*-xylene production is proportional to the acid concentration and reaches a maximum when the acid site concentration is higher than ~2.5 mM for both Brønsted acid, Al-BEA, and Lewis acid zeolites, Sn-BEA and Zr-BEA. This is consistent with our recent report on the kinetic study for the same system using zeolite Y.[131] The kinetic behavior and rate dependence on acid site concentration was interpreted as a transition in the rate controlling reaction. The overall reaction from DMF and ethylene to *p*-xylene is a sequence of Diels-Alder cycloaddition of ethylene and DMF followed by subsequent dehydration of the cycloadduct. At low acid site concentration, the overall rate is controlled by dehydration reaction due to insufficient quantity of catalytic sites; at high acid site loadings, the reaction is limited by the cycloaddition reaction, which results in the plateau (i.e. maximum reaction rate) of *p*-xylene production.
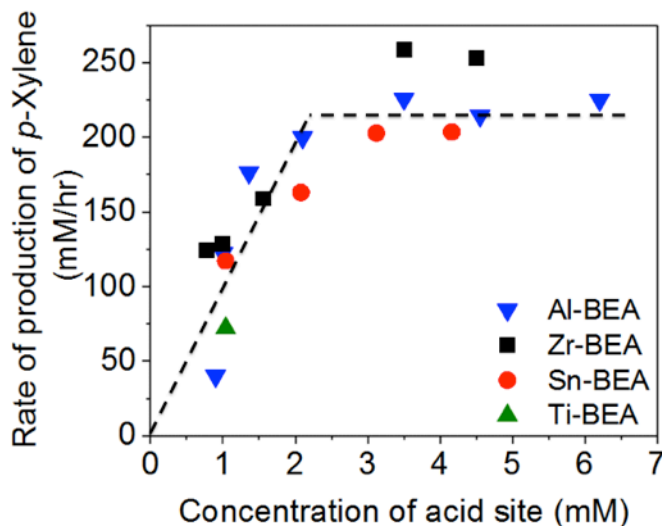
Figure 5.7 *p*-Xylene production rate with the active site amount for Zr-BEA, Sn-BEA, Ti-BEA and Al-BEA for the reaction of DMF in n-heptane with ethylene (62 bar) at 250 °C. The rate is calculated at < 20% conversion of DMF. Dash line is a guide to the eyes.

The activity of the catalysts was compared using the turnover frequencies (TOF) calculated at dehydration-limited region (linear dependent region) using the production rate of *p*-xylene normalized with the amount of acid sites of the catalysts (only Brønsted acid sites were considered for Al-BEA). Interestingly, Zr-BEA shows higher TOF (121 ± 4.9 hr^{-1}) than Sn-BEA (113 ± 6.8 hr^{-1}) and Ti-BEA (65 ± 11 hr^{-1}), and is similar to Al-BEA (122 ± 11 hr^{-1}). Apparent activation energy ($E_{a, app}$) of the reaction in the dehydration-limited region over Zr-BEA (0.78 mM) was determined by constructing an Arrhenius plot, shown in Figure 5.8. The measured $E_{a, app}$ is 45.5 kJ/mol, which is close to the valued that Patet *et al.* reported for zeolite Y (45.2 kJ/mol).[131] The results suggest that Zr-BEA is an efficient catalyst for this sequential reaction to produce *p*-xylene. The result was unexpected since it has been known that Lewis acid zeolites are not efficient dehydration catalysts for several alcohols compared with Brønsted acid zeolites.[134] Our control experiment for dehydration of cyclohexanol to cyclohexene using Al-BEA and Zr-BEA also indicates that Al-BEA is superior in dehydration reactions (Figure 5.9). Further study on the catalytic activity of Zr-BEA for the dehydration from to *p*-xylene is necessary in order further improving the catalytic system.
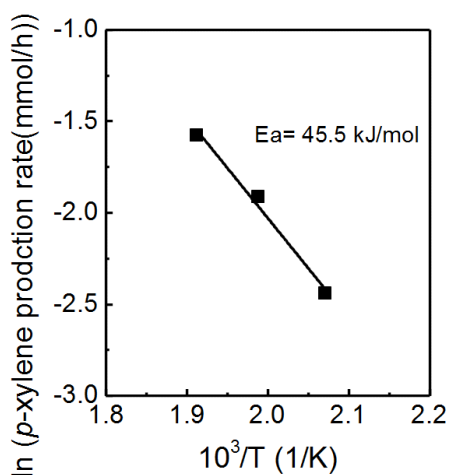
Figure 5.8 Arrhenius plot for Zr-BEA at 0.78 mM acid concentration, 1.3 M DMF, 62 bar ethylene. The reaction rates were calculated at conversion of DMF < 20 %.
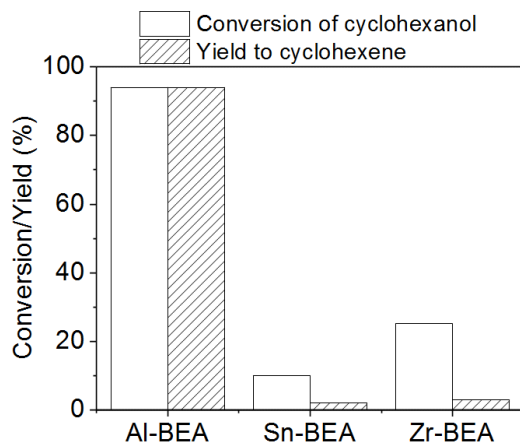
Figure 5.9 Production rate of cyclohexene from cyclohexanol over Al- and Zr-BEA. Conditions: 0.1 M cyclohexanol in 1,4-dioxane, 0.02 g catalyst, 200 °C for 30 min.

Despite significant catalytic differences under dehydration-controlling reaction conditions, only subtle differences were observed between Lewis acid catalysts within the 'plateau region" (catalyst independent region, >2.5 mM acid sites in Figure 5.7) where the Diels-Alder reaction controls the overall rate. Comparing the formation rates of p-xylene, Zr-BEA exhibited about 10-20% higher production rate than Sn-BEA and Al-BEA, which might indicate a slight enhancement in catalysis of the Diels-Alder reaction. However, the enhancement of the overall reaction with Lewis acids is minor; variation of the Lewis acid site concentration for either Sn-BEA or Zr-BEA (3.5-5.0 mM acid sites in Figure 5.7) did not result in measurable differences in overall rate.

To confirm the limited catalytic activity of Zr-BEA for the Diels-Alder reaction, the concentration of cycloadduct produced from the Diels-Alder reaction during the reaction was monitored at low catalyst loadings. The formation of the DMF/ethylene cycloadduct was confirmed by reactor liquid sampling and compositional characterization via GC/MS (Figure 5.10). As shown in Figure 5.11, the Lewis acid zeolites are moderately more active to catalyze the Diels-Alder reaction compared to Al-BEA, and they produce slightly higher cycloadduct intermediate concentration during the tandem reaction than Al-BEA. In particular, Zr-BEA produced the most cycloadduct intermediate throughout the reaction while exhibiting the same initial production rate of p-xylene as Al-BEA

93
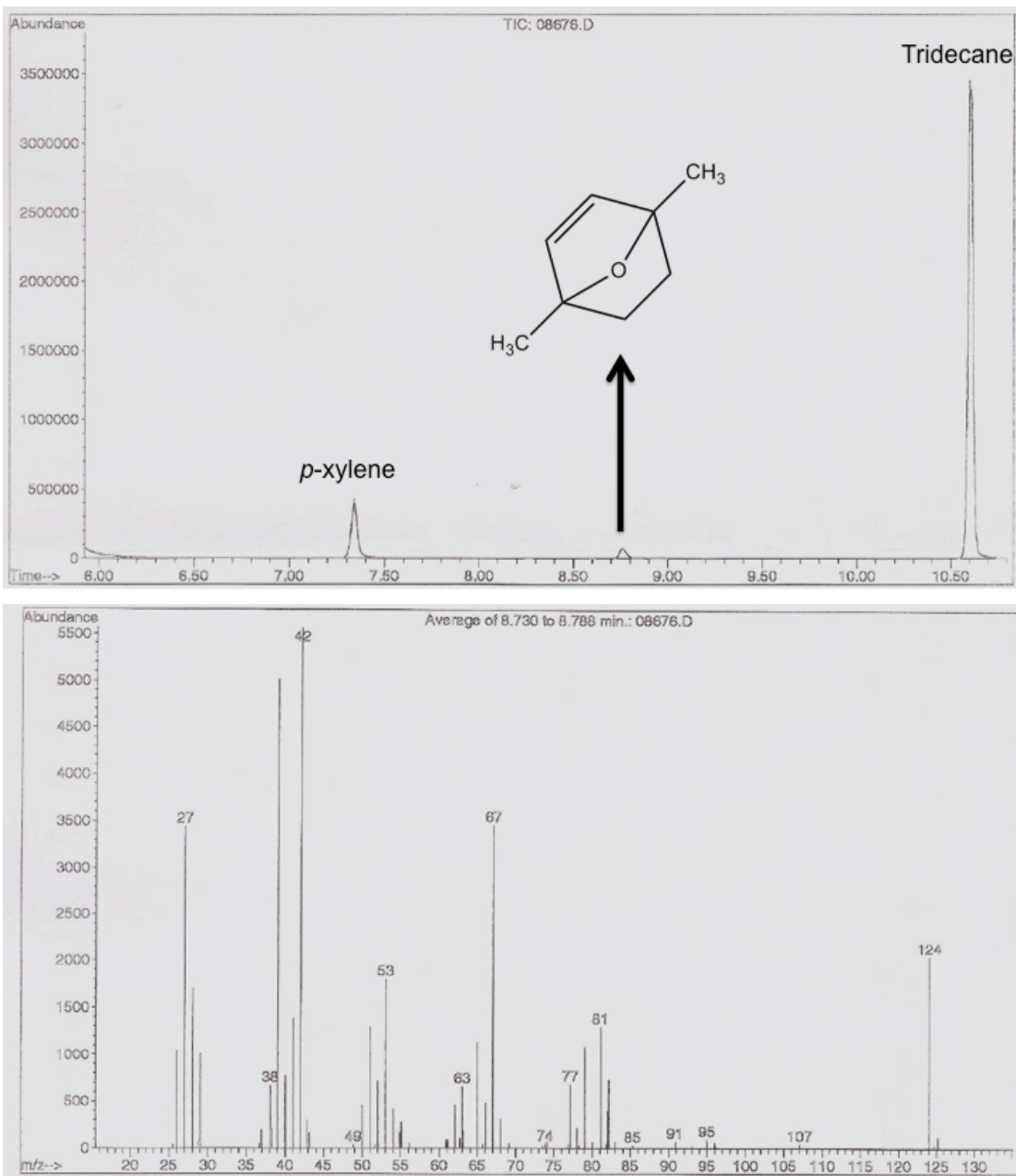
Figure 5.9 GC chromatogram and electron ionization (EI) spectrum of cycloadduct. The reaction mixture was taken at 30 min reaction time for Zr-BEA at 1 mM acid loading under usual reaction conditions. The EI spectrum is consistent with previous report.[16]

94
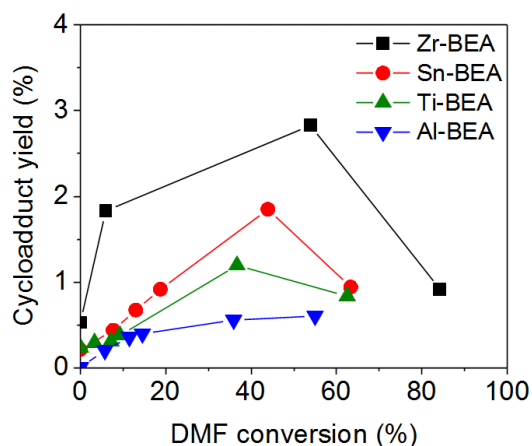
Figure 5.10 Yield of cycloadduct versus DMF conversion (1. 3 M DMF in heptane, 250 °C, 62 bar ethylene). The concentration of cycloadduct was estimated by using the response factor of *p*-xylene. The acid concentration is 1 mM for all.

(Figure 5.7), possibly revealing Zr center is moderately effective for the cycloaddition reaction and less efficient for dehydration reaction.

In the *p*-xylene selectivity plot (Figure 5.3), it was observed that both Lewis and Brønsted acid zeolite catalysts exhibit a counter-intuitive behavior of increasing selectivity to *p*-xylene with DMF conversion. For the Zr-BEA catalyst, the selectivity to *p*-xylene at the DMF conversion of 20% is around 60%, while it increases to 80% at higher conversion. The phenomena has been observed for the Brønsted acid zeolite, Al-BEA, which was attributed to the equilibrium-driven formation of DMF from its hydrolysis byproduct, 2,5-hexanedione, and the formation of the thermodynamically stable final product, *p*-xylene, from cycloaddition-dehydration reaction pathway during the proceeding of the reaction.[14] It has been suggested by Do et al. that 2,5-hexanedione formed from the hydrolysis of DMF can cause catalyst deactivation by forming insoluble surface condensates via acid catalyzed aldol-type reactions.[16] In order to further understand the slow deactivation of Zr-BEA in the reaction, 2,5-hexanedione (0.2 M) was intentionally added in the reaction mixture as a reactant with Zr-BEA and Al-BEA catalysts (at 1 mM acid concentration). The reaction mixture were well mixed and heated at 250 °C under nitrogen for 1 hr prior to the addition of ethylene. The changes in the concentration of 2, 5-hexanedione and *p*-xylene with the reaction time are shown in Figure 5.11. It
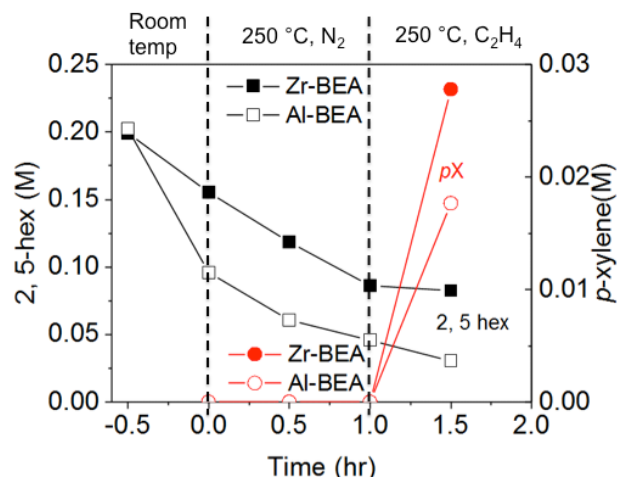
Figure 5.11 The concentration evolution of 2, 5 hexanedione (2, 5-hex) and *p*-xylene with time for the deactivation-simulated reaction with 2, 5 hexanedione added with DMF as reactant for Al-BEA and Zr-BEA. The reaction mixture was heated at 250 °C under N_2 for 1 h before ethylene (62 bar) was introduced into the reactor. Acid concentration is 1 mM in the system.

was found that with increasing the temperature, the concentration of 2,5-hexanedione quickly decreases over both Zr-BEA and Al-BEA catalysts. After 1 hr at 250 °C, the concentration of 2,5-hexanedione is 0.05 M for Al-BEA catalyst and 0.1 M for Zr-BEA catalyst, indicating a faster reaction rate of 2,5-hexanedione over the Brønsted acid zeolite catalyst. After the introduction of ethylene, *p*-xylene was produced in both cases. Zr-BEA shows higher *p*-xylene formation rate than Al-BEA (56 mM/hr vs. 35 mM/hr). However, the production rates of *p*-xylene are significantly lower than the one achieved without adding 2,5-hexanedione at the beginning of the reaction (120 mM/hr). In addition, it was observed that during the reaction the concentration of DMF does not increase with the decrease of 2,5-hexanedione, which indicates that 2,5-hexanedione didn't undergo a dehydration reaction to form DMF under the reaction conditions (Figure 5.12). The results clearly suggest that the addition of 2,5-hexanedione indeed cause the catalyst deactivation, in particular for Brønsted acid zeolite catalyst, Al-BEA. Zr- BEA, however, deactivated slower under the same conditions. It could be due to weaker acid sites on Zr-BEA compared to Al-BEA which is not efficient to catalyze the condensation reactions of 2,5-hexanedione to form carbonaceous species on the catalysts. Hence, the longer catalyst life (slower deactivation) of Zr-BEA may be attributed to (1) slower production rate of
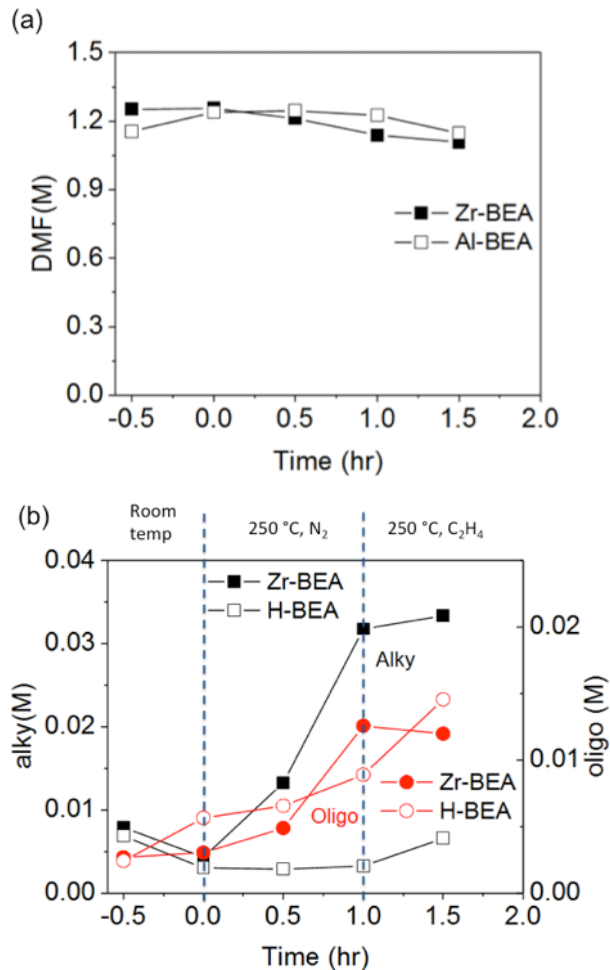
Figure 5.12 (a) DMF, (b) alkylated products and oligomers concentration evolution with intentional addition of 2, 5-hexanedione into initial reactant solution. The concentration of DMF for Al-BEA and Zr-BEA during the time holding at 250 °C is invariant or slightly decreasing, which suggesting the decrease of diketone is not due to dehydration reaction to form DMF.

2,5-hexanedione (Figure 5.5) and (2) weaker acid sites that are not efficient for catalyzing condensation reactions of 2,5-hexanedione (Figure 5.11).

The cycloaddition/dehydrative aromatization chemistry can be extended to 2-methylfuran (MF) and furan to produce toluene and benzene.[14, 120, 133] Due to lack of protecting methyl groups on the furan α-carbon, the yields of toluene and benzene were generally lower than the reaction for producing p-xylene from DMF. As shown in Figure 7, the conversion of MF and yield of toluene achieved over Zr-BEA catalyst were slightly higher than Al-BEA after a 24 hour reaction. However,

the selectivity to toluene was similar, which indicates that Zr-BEA can prevent fast catalyst deactivation but does
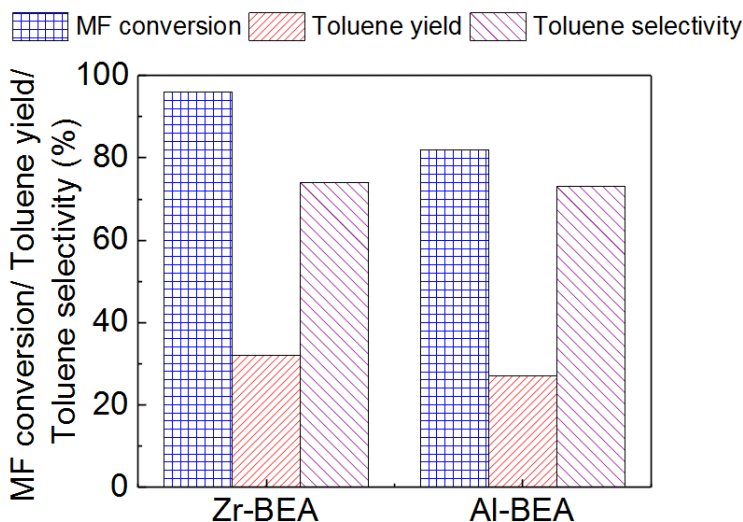
Figure 5.13 MF conversion, toluene yield, and toluene selectivity for the reaction of MF and ethylene with Zr-BEA and Al-BEA after 24 hr reaction. The reaction involves 1.4 M of MF in n-heptane with 62 bar of ethylene at 250 °C. The acid concentration for both catalysts is 0.8 mM.

not significantly enhance the production rate of toluene (70 vs. 68 mM/hr toluene production rate for Zr-BEA and Al-BEA, respectively). In the reaction with furan, Zr-BEA only produced ~5% of benzene after 24 hr reaction (~70 % conversion), revealing that Lewis acid zeolite (Zr-BEA) is not effective in improving the yield of benzene. Overall, the performance of Zr-BEA was slightly better in furan and MF reactions in terms of catalyst life, but they exhibited no significant difference with regard to selectivity of benzene and toluene when compared with Al-BEA.

In summary, solid Lewis acid zeolites including Zr-, Sn-, and Ti-BEA were evaluated in *p*-xylene production from DMF and ethylene. Lewis acids are shown to be able to catalyze the aromatizative dehydration reaction. It is found that, Lewis acids shows longer life time than Al-BEA, and Zr-BEA shows best performance by displaying high turnover frequencies and slow deactivation, which could be attributed to its low selectivity to hydrolysis product, 2,5-hexandione and weaker acid site nature

to prevent surface reaction of diketone. It is also demonstrated the production rate of *p*-xylene is dependent of the amount of Lewis acid catalysts at low loading and independent of that at high loading due to the nature of the tandem reaction, which is similar to the observations with Brønsted acid catalysts. Finally, it is revealed that Zr-BEA moderately promotes the Diels-Alder cycloaddition reaction by producing more oxanorbornene while being a less efficient dehydration catalyst, and it results in mild enhancement of *p*-xylene production by ~10-20 % compared to Al-BEA. Current findings can guide to design efficient and long-lasting catalysts for the Diels-Alder cycloaddition/dehydration reactions

CHAPTER 6

CONCLUSIONS

In the first part, the thesis concerned about the issue of synthesis of an interesting Lewis acid catalyst, Sn-Beta, demonstrated high activity in glucose isomerization reaction in water and attempted to alleviate the key problems in the field: lengthy crystallization time and the utilization of hydrofluoric acid. A seeded growth method was successfully invented and it was found that, with crystalline, well-defined, and well-dispersed zeolite beta seeds, the crystallization time to form highly crystalline Sn-Beta can be substantially shortened from more than 200 hr to 3 hr at elevated temperature. By controlling the water content in the synthesis gel, 1 hr crystallization can yield high quality crystals at 200 °C. Temporal crystallization study demonstrates that the addition of the seed greatly reduced the energy barrier of the induction period of crystallization process, and the induction time is greatly decreased. The synthesized materials exhibit the same catalytic activity in isomerization reaction of glucose to fructose in water compared to the sample obtained from the conventional method. It was demonstrated Sn was incorporated into the zeolite framework without detectable extraframework Sn species. Final crystal size can be finely tuned using this highly reproducible approach. The method is expected to be able to extend to the synthesis of other metal substituted zeolite Beta catalysts. The findings here can facilitate the market-viability, exploration of novel applications, and further understanding of local Sn structure of Sn-Beta.

Furthermore, a fluoride-free route in a caustic medium (dry gel conversion method, DGC) was successfully demonstrated for the first time for direct synthesis of Al-free Sn-Beta. The parameter studies have highlighted the key roles of seeding and alkali ions, without which no pure Sn-Beta crystals can be obtained, likely due to their structure leading and compensation of charge from organic structure directing agent (OSDA), respectively. It has shown that ion-exchange with ammonium ion is critical to preserve the formed crystalline structure upon removal of occluded OSDA, which is explained by the structure instability when alkali ions locate within the structure at

high temperature. Finally, although the characterizations of Sn environment indicate the sample possess mostly framework Sn without evident presence of extraframework species, the catalytic activities in sugar isomerization reactions are lower than Sn-Beta made from fluoride medium. The discrepancy in activity of the two materials might be a combined effect from the difference in local Sn environment and hydrophobicity of the surface. The novel method provides an alternative and more environmentally benign approach to synthesize Sn-Beta zeolite.

In the second part, development of catalysts for the renewable pathway to produce *p*-xylene, a primary precursor for polyethylene terephthalate, from 2,5-dimethylfuran (DMF) and ethylene was reported. It is shown that zeolite Beta exhibits superior catalytic performances to catalyze the tandem Diels-Alder cycloaddition of DMF and ethylene and dehydration of the cycloadduct to yield *p*-xylene. It shows great resistance to deactivation compared to zeolite Y and ZSM-5, and it able to reach 90 % selectivity to *p*-xylene at 99 % conversion of DMF. Hydrolysis product of DMF, 2,5-hexanedione, dehydrates to DMF at high DMF conversion owing to equilibrium, and it allows the initial carbon loss to recover and results in high selectivity. Besides, it is found that the production rate of *p*-xylene is dependent on the amount of the catalysts and shows a linear dependence on the Brønsted acid concentration in the system at low catalyst loadings, while the rate is zero-order dependent at high catalyst loadings, exhibiting a maxium rate universal for all catalysts. The phenomenon is explained by a transition in kinetic control reaction from dehydration reaction limited (low loading) to Diels-Alder cycloaddition reaction limited (high loading). The results indicate a need for an exceptional catalyst by featuring the bifuncation active sites that can efficiently catalyze cycloaddition and dehydration reactions.

Finally, Lewis acid catalysts were examined in the tandem cycloaddition/dehydration reactions of DMF and ethylene to produce *p*-xylene. The data suggest that the Lewis acids (Sn-, Zr-, and Ti-Beta) are able to catalyze the reaction to form *p*-xylene. Zr- and Sn-Beta are particularly effective, giving similar rate of *p*-xylene production to zeolite Beta (aluminosilicate, Brønsted acid). The transition of kinetic control reaction also holds for the Lewis acid catalysts. It is noteworthy that, in general, Lewis

101

acid catalysts shows better recalcitrance to deactivation, and Zr-Beta is the best among tested catalysts. The slow deactivation of Zr-Beta may be resulted from its low activity to hydrolysis reaction of DMF to 2,5-hexanedione and weak acidity which is insufficient to catalyze surface condensation reaction. In addition, Zr-Beta can reach high yield (76 %) and high selectivity (90 %) to *p*-xylene at 99 % conversion of DMF. Zr-Beta also exhibits 10-20 % higher production rate of *p*-xylene due to its effectiveness for catalyzing Diels-Alder reaction and moderate activity for dehydration reaction. The discovery could lead to rational design of the efficient catalysts for the tandem cycloaddition/dehydration reaction for renewable *p*-xylene production and highlights the potential benefit of applications of Lewis acid catalysts.

CHAPTER 7

SUGGESTED FUTURE DIRECTIONS

While an efficient method of synthesis was invented, the crystallization process of Sn-Beta is still poorly understood. Understanding the crystallization in fluoride medium is crucial to rationally design synthesis strategy to target zeolite materials. In particular, the study on the crystallization in fluoride medium (solid like precursor) is scarce compared to the hydroxide system. This might be partly due to the nature of the synthesis gel that hinders the observation of the process, as the "clear solution" form of the synthesis precursor has been studied more extensively, where scattering techniques are allowed to follow the nucleation process *in situ*.[21, 31] To study the crystallization behavior of Sn-Beta from fluoride medium, the research would focus on analysis of the precursor gel and the evolution of gel structure change with function of time. Raman spectroscopy is particularly sensitive technique to the ring structures of silica, and it will be an important tool in the study.[21, 135, 136] Another technique could be used to study the crystallization would be high energy X-ray diffraction (HEXRD). The technique has been shown to be able to resolve medium-range order in amorphous material (the zeolite precursors), that is, the distribution of the ring structures formed by silicate and aluminate, thanks to high X-ray energies in advanced synchrotron radiation facilities. Using the method, Wakihara et al. was able to reveal the medium range order of secondary amorphous phase prior to zeolite crystallization.[137] For example, combined with Monte Carlo simulartion, it was revealed that 6-membered ring (6R) and 4-membered ring (4R) were dominated species in the synthesis precurosrs of zeolite A, while the formation of double 4-membered ring (D4R) is the last step of crystallization. The change of the morphology and distribution of Sn can be monitored using electron microscopy techniques to provide macro scale view and to infer how the precursor interact with existing crystals and how/when Sn incorporates into the framework. The local atom/molecule environment (Si, Sn, F, and structure directing agent) can be studied by solid-state NMR technique. It is particularly

interesting to know how Sn reacts in the synthesis gel, but it is particularly challenging due to the low natural abundance of NMR responsive ^{119}Sn, usually resulting in poor spectrum quality even with few days continuous measurement. Synthesizing the material with enriched Sn could circumvent the problem. However, ^{119}Sn enriched precursors are not readily available and pricey, and the enriched precursor might not be in the same chemical form as usual Sn source (tin metal or tin dichloride rather than tin tetrachloride). Recently, dynamic nuclear polarization (DNP) NMR technique has been used in characterization of Sn-Beta with natural abundance of Sn, and the measurement can be done in the order of hours.[138, 139] With this technique, it could be possible to efficiently probe the local environment of Sn(IV) during the course of crystallization, providing unprecedented insight to incorporation of Sn into *BEA framework. It is suggested that Si-Beta (pure siliceous sample) and Sn-Beta should be studied side by side and contrast each other. It is expected the set of experiments can help us comprehend (1) the mechanism of crystal growth of zeolite Beta in fluoride medium and (2) the role of Sn incorporation in the synthesis. It is also of interest to study the detail crystallization mechanism of Sn-Beta from dry gel conversion method, which occurs under caustic medium, using the techniques mentioned above. Inagaki et al. has done an impressive work on study the formation of zeolite Beta (aluminosilicate) by elucidating the medium range structure during the crystal formation by combining high energy X-ray diffraction and Raman spectroscopy.[135] The study is then expected to provide the knowledge of the difference between the crystal growth from caustic and fluoride media.

Another direction is to extend the tandem Diels-Alder cycloaddition/dehydration reaction using different bio-renewable substrates to form functionalized aromatics with Lewis acid catalysts. Paccheco et al. has demonstrated similar chemistry can be applied to 5-hydroxymethylfurfural oxidized variants and ethylene to form para functionalized aromatics, which can be precursors to terephthalic acid.[57, 140] It is shown that the functional groups on the furan ring affect the stability and activity of the dienes in the Diels-Alder reactions. A recent effort ongoing in our lab is to locate a diene that features easy preparation from biomass, stability at high temperature, and electron donating

groups that could facilitate the cycloaddition reaction to further improve the rate and yield to the product that can be used to form terephthalic acid.

BIBLIOGRAPHY

1. R. A. Sheldon, *Green Chem.*, 2014, **16**, 950-963.
2. M. J. Climent, A. Corma and S. Iborra, *Green Chem.*, 2014, **16**, 516-547.
3. J. S. Luterbacher, D. Martin Alonso and J. A. Dumesic, *Green Chem.*, 2014, **16**, 4816-4838.
4. G. W. Huber, S. Iborra and A. Corma, *Chem. Rev.*, 2006, **106**, 4044-4098.
5. P. Dornath, H. J. Cho, A. Paulsen, P. Dauenhauer and W. Fan, *Green Chem.*, 2015, **17**, 769-775.
6. P. Wantanachaisaeng and K. O'Neil*,* Capturing oppurtunities for para-xylene production, UOP LLC, 2007.
7. United Nations Environment Programme. Global chemistry outlook: toward sound management of chemicals. 2013).
8. S. H. Bhosale, M. B. Rao and V. V. Deshpande, *Microbiological Reviews*, 1996, **60**, 280-300.
9. M. Moliner, Y. Román-Leshkov and M. E. Davis, *Proc. Nat. Acad. Sci.*, 2010, **107**, 6164-6168.
10. Y. Román-Leshkov, J. N. Chheda and J. A. Dumesic, *Science*, 2006, **312**, 1933-1937.
11. Y. Román-Leshkov, C. J. Barrett, Z. Y. Liu and J. A. Dumesic, *Nature*, 2007, **447**, 982-985.
12. J. Jae, W. Zheng, R. F. Lobo and D. G. Vlachos, *ChemSusChem*, 2013, **6**, 1158-1162.
13. J. I. Di Cosimo, V. K. Díez, M. Xu, E. Iglesia and C. R. Apesteguía, *J. Catal.*, 1998, **178**, 499-510.
14. C.-C. Chang, S. K. Green, C. L. Williams, P. J. Dauenhauer and W. Fan, *Green Chem.*, 2014, **16**, 585-588.
15. C. L. Williams, C.-C. Chang, P. Do, N. Nikbin, S. Caratzoulas, D. G. Vlachos, R. F. Lobo, W. Fan and P. J. Dauenhauer, *ACS Catal.*, 2012, **2**, 935-939.
16. P. T. M. Do, J. R. McAtee, D. A. Watson and R. F. Lobo, *ACS Catal.*, 2013, **3**, 41-46.
17. D. Wang, C. M. Osmundsen, E. Taarning and J. A. Dumesic, *ChemCatChem*, 2013, **5**, 1-8.
18. N. Nikbin, P. T. Do, S. Caratzoulas, R. F. Lobo, P. J. Dauenhauer and D. G. Vlachos, *J. Catal.*, 2013, **297**, 35-43.
19. Z. Lin, M. Ierapetritou and V. Nikolakis, *AIChE J.*, 2013, **59**, 2079-2087.
20. D. W. Breck, *Journal*, 1973.
21. S. M. Auerbach, K. A. Carrado and P. K. Dutta, *Handbook of Zeolite Science and Technology*, CRC Press, 2003.
22. S. Valencia and A. Corma*,* Stannosilicate molecular sieves, U.S. Patent 5,968,473, 1999.
23. J. M. Newsam, M. M. J. Treacy, W. T. Koetsier and C. B. D. Gruyter, *Structural Characterization of Zeolite Beta*, 1988.
24. http://www.iza-structure.org/databases/).
25. A. Shriver D.F. , P. W., Overton T.L., Rourke J.P., Weller M.T., Armstrong F.A., *Shriver & Atkins Inorganic Chemistry*, Oxford University Press, Oxford, 4th edn., 2006.
26. A. Corma, L. T. Nemeth, M. Renz and S. Valencia, *Nature*, 2001, **412**, 423-425.
27. A. Corma, M. E. Domine and S. Valencia, *J. Catal.*, 2003, **215**, 294-304.
28. A. Corma, M. E. Domine, L. Nemeth and S. Valencia, *J. Am. Chem. Soc.*, 2002, **124**, 3194-3195.
29. J. N. Chheda, G. W. Huber and J. A. Dumesic, *Angew. Chem., Int. Ed.*, 2007, **46**, 7164-7183.
30. A. Mukherjee, M.-J. e. Dumont and V. Raghavan, *Biomass Bioenergy*, 2015, **72**, 143-183.
31. C. S. Cundy and P. A. Cox, *Microporous Mesoporous Mater.*, 2005, **82**, 1-78.
32. M. Renz, T. Blasco, A. Corma, V. Fornés, R. Jensen and L. Nemeth, *Chem. Eur. J.*, 2002, **8**, 4708-4717.
33. C. M. Lew, N. Rajabbeigi and M. Tsapatsis, *Microporous Mesoporous Mater.*, 2012, **153**, 55-58.
34. Z. Kang, X. Zhang, H. Liu, J. Qiu and K. L. Yeung, *Chem. Eng. J.*, 2013, **218**, 425-432.

35. C.-C. Chang, Z. Wang, P. Dornath, H. J. Cho and W. Fan, *RSC Adv.*, 2012, **2**, 10475-10477.
36. Fluoride: Does-Response Analysis for Non-Cancer Effects, http://water.epa.gov/action/advisories/drinking/fluoride_index.cfm, (accessed February, 2015, 2015).
37. P. Li, G. Liu, H. Wu, Y. Liu, J.-g. Jiang and P. Wu, *J. Phys. Chem. C*, 2011, **115**, 3663-3670.
38. C. Hammond, S. Conrad and I. Hermans, *Angew. Chem., Int. Ed.*, 2012, **51**, 11736-11739.
39. J. Dijkmans, D. Gabriels, M. Dusselier, F. de Clippel, P. Vanelderen, K. Houthoofd, A. Malfliet, Y. Pontikes and B. F. Sels, *Green Chem.*, 2013, **15**, 2777-2785.
40. X. Ouyang, S.-J. Hwang, D. Xie, T. M. Rea, S. I. Zones and A. Katz, *ACS Catal.*, 2015.
41. X. Ouyang, Y.-J. Wanglee, S.-J. Hwang, D. Xie, T. Rea, S. I. Zones and A. Katz, *Dalton Transactions*, 2014.
42. I. Ogino, E. A. Eilertsen, S.-J. Hwang, T. Rea, D. Xie, X. Ouyang, S. I. Zones and A. Katz, *Chem. Mater.*, 2013, **25**, 1502-1509.
43. W. Partenheimer, *Catal. Today*, 1995, **23**, 69-158.
44. T.-C. Tsai, S.-B. Liu and I. Wang, *Appl. Catal., A*, 1999, **181**, 355-398.
45. Y. Y. Fong, A. Z. Abdullah, A. L. Ahmad and S. Bhatia, *Chem. Eng. J.*, 2008, **139**, 172-193.
46. L. D. Schmidt and P. J. Dauenhauer, *Nature*, 2007, **447**, 914-915.
47. Matthew W. Peters, Joshua D. Taylor, Madeline Jenni, Leo E. Manzer and D. E. Henton.*, Integrated Process to Selectively Convert Renewable Isobutanol to *p*-Xylene, US Patent 20110087000 A1, 2011.
48. M. Shiramizu and F. D. Toste, *Chem. Eur. J.*, 2011, **17**, 12452-12457.
49. M. V. Gómez, Á. Cantín, A. Corma and A. de la Hoz, *J. Mol. Catal. A: Chem.*, 2005, **240**, 16-21.
50. Y. Hayashi, M. Nakamura, S. Nakao, T. Inoue and M. Shoji, *Angew. Chem., Int. Ed.*, 2002, **41**, 4079-4082.
51. R. M. Dessau, *J. Chem. Soc., Chem. Commun.*, 1986, 1167-1168.
52. P. Vogel, J. Cossy, J. n. Plumet and O. n. Arjona, *Tetrahedron*, 1999, **55**, 13521-13642.
53. N. Nikbin, S. Feng, S. Caratzoulas and D. G. Vlachos, *J. Phys. Chem. C*, 2014, **118**, 24415-24424.
54. S. Roy, K. Bakhmutsky, E. Mahmoud, R. F. Lobo and R. J. Gorte, *ACS Catal.*, 2013, **3**, 573-580.
55. S. Roy, G. Mpourmpakis, D.-Y. Hong, D. G. Vlachos, A. Bhan and R. J. Gorte, *ACS Catal.*, 2012, **2**, 1846-1853.
56. D. D. Claeys, C. V. Stevens, B. I. Roman, P. Van De Caveye, M. Waroquier and V. Van Speybroeck, *Org. Biomol. Chem.*, 2010, **8**, 3644-3654.
57. J. J. Pacheco and M. E. Davis, *Proc. Nat. Acad. Sci.*, 2014, **111**, 8363-8367.
58. H. Y. Chen, J. Wydra, X. Y. Zhang, P. S. Lee, Z. P. Wang, W. Fan and M. Tsapatsis, *J. Am. Chem. Soc.*, 2011, **133**, 12390-12393.
59. M. Moliner, Y. Roman-Leshkov and M. E. Davis, *Proc. Natl. Acad. Sci. U. S. A.*, 2010, **107**, 6164-6168.
60. V. Choudhary, A. B. Pinar, S. I. Sandler, D. G. Vlachos and R. F. Lobo, *ACS Catal.*, 2011, **1**, 1724-1728.
61. E. Taarning, S. Saravanamurugan, M. S. Holm, J. M. Xiong, R. M. West and C. H. Christensen, *ChemSusChem*, 2009, **2**, 625-627.
62. M. A. Camblor, A. Corma and S. Valencia, *J. Mater. Chem.*, 1998, **8**, 2137-2145.
63. M. M. J. Treacy and J. M. Newsam, *Nature*, 1988, **332**, 249-251.
64. M. A. Camblor, A. Corma and S. Valencia, *Chem. Commun.*, 1996, 2365-2366.
65. K. Egeblad, M. Kustova, S. K. Klitgaard, K. Zhu and C. H. Christensen, *Microporous Mesoporous Mater.*, 2007, **101**, 214-223.
66. S. Tolborg, A. Katerinopoulou, D. D. Falcone, I. Sadaba, C. M. Osmundsen, R. J. Davis, E. Taarning, P. Fristrup and M. S. Holm, *J. Mater. Chem. A*, 2014.

67.   G. Pasquale and E. Senderov, Manufacture of ZSM-12 and beta zeolites using quaternary ammonium hydroxides and halides as structure directing agents, US Patent 20030091504A1, 2003.

68.   V. Nikolakis, E. Kokkoli, M. Tirrell, M. Tsapatsis and D. G. Vlachos, *Chem. Mater.*, 2000, **12**, 845-853.

69.   P.-P. E. A. de Moor, T. P. M. Beelen and R. A. van Santen, *J. Phys. Chem. B*, 1999, **103**, 1639-1650.

70.   L. Ren, Q. Wu, C. Yang, L. Zhu, C. Li, P. Zhang, H. Zhang, X. Meng and F.-S. Xiao, *J. Am. Chem. Soc.*, 2012, **134**, 15173-15176.

71.   Q. Wu, X. Liu, L. Zhu, L. Ding, P. Gao, X. Wang, S. Pan, C. Bian, X. Meng, J. Xu, F. Deng, S. Maurer, U. Müller and F.-S. Xiao, *J. Am. Chem. Soc.*, 2015, **137**, 1052-1055.

72.   Z. Kang, X. Zhang, H. Liu, J. Qiu, W. Han and K. L. Yeung, *Mater. Chem. Phys.*, 2013, **141**, 519-529.

73.   H. Y. Luo, L. Bui, W. R. Gunther, E. Min and Y. Román-Leshkov, *ACS Catal.*, 2012, **2**, 2695-2699.

74.   B. Tang, W. Dai, G. Wu, N. Guan, L. Li and M. Hunger, *ACS Catal.*, 2014, **4**, 2801-2810.

75.   R. Buzzoni, S. Bordiga, G. Ricchiardi, C. Lamberti, A. Zecchina and G. Bellussi, *Langmuir*, 1996, **12**, 930-940.

76.   C. Paze, S. Bordiga, C. Lamberti, M. Salvalaggio, A. Zecchina and G. Bellussi, *J. Phys. Chem. B*, 1997, **101**, 4740-4751.

77.   M. R. Basila, T. R. Kantner and K. H. Rhee, *J. Phys. Chem.*, 1964, **68**, 3197-3207.

78.   F. Bonino, A. Damin, S. Bordiga, C. Lamberti and A. Zecchina, *Langmuir*, 2003, **19**, 2155-2161.

79.   C. Ngamcharussrivichai, P. Wu and T. Tatsumi, *J. Catal.*, 2005, **235**, 139-149.

80.   P. Li, G. Q. Liu, H. H. Wu, Y. M. Liu, J. G. Jiang and P. Wu, *J. Phys. Chem. C*, 2011, **115**, 3663-3670.

81.   M. Boronat, P. Concepción, A. Corma, M. Renz and S. Valencia, *J. Catal.*, 2005, **234**, 111-118.

82.   C. M. Osmundsen, M. S. Holm, S. Dahl and E. Taarning, *Proc. R. Soc. A*, 2012, **468**, 2000-2016.

83.   Y. Román-Leshkov, M. Moliner, J. A. Labinger and M. E. Davis, *Angew. Chem., Int. Ed.*, 2010, **49**, 8954-8957.

84.   G. Majano, A. Darwiche, S. Mintova and V. Valtchev, *Ind. Eng. Chem. Res.*, 2009, **48**, 7084-7091.

85.   N. D. Hould, S. Senapati, H. Koller and R. F. Lobo, *Top. Catal.*, 2012, **55**, 1332-1343.

86.   J. Čejka, G. Centi, J. Perez-Pariente and W. J. Roth, *Catal. Today*, 2012, **179**, 2-15.

87.   M. Stöcker, *Angew. Chem., Int. Ed.*, 2008, **47**, 9200-9211.

88.   M. A. Snyder and M. Tsapatsis, *Angew. Chem., Int. Ed.*, 2007, **46**, 7560-7573.

89.   S. G. Wettstein, D. M. Alonso, E. I. Gürbüz and J. A. Dumesic, *Curr. Opin. Chem. Eng.*, 2012, **1**, 218-224.

90.   Y. Zhu, G. Chuah and S. Jaenicke, *Chem. Commun.*, 2003, 2734-2735.

91.   T. Blasco, M. A. Camblor, A. Corma, P. Esteve, A. Martinez, C. Prieto and S. Valencia, *Chem. Commun.*, 1996, 2367-2368.

92.   P. Concepción, Y. Pérez, J. C. Hernández-Garrido, M. Fajardo, J. J. Calvino and A. Corma, *Phys. Chem. Chem. Phys.*, 2013, **15**, 12048-12055.

93.   C. Paris, M. Moliner and A. Corma, *Green Chem.*, 2013, **15**, 2101-2109.

94.   C. M. Lew, N. Rajabbeigi and M. Tsapatsis, *Ind. Eng. Chem. Res.*, 2012, **51**, 5364-5366.

95.   E. Nikolla, Y. Román-Leshkov, M. Moliner and M. E. Davis, *ACS Catal.*, 2011, **1**, 408-410.

96.   T. J. Schwartz, S. M. Goodman, C. M. Osmundsen, E. Taarning, M. D. Mozuch, J. Gaskell, D. Cullen, P. J. Kersten and J. A. Dumesic, *ACS Catal.*, 2013, 2689-2693.

97.   W. R. Gunther, Q. Duong and Y. Román-Leshkov, *J. Mol. Catal. A: Chem.*, 2013, **379**, 294-302.
98.   M. Boronat, P. Concepción, A. Corma and M. Renz, *Catal. Today*, 2007, **121**, 39-44.
99.   M. S. Holm, S. Saravanamurugan and E. Taarning, *Science*, 2010, **328**, 602-605.
100.   A. Corma, S. Iborra and A. Velty, *Chem. Rev.*, 2007, **107**, 2411-2502.
101.   R. Gounder and M. E. Davis, *AIChE J.*, 2013, **59**, 3349-3358.
102.   A. Corma and M. E. Davis, *ChemPhysChem*, 2004, **5**, 304-313.
103.   F. Vaudry, F. Di Renzo, P. Espiau, F. Fajula and P. Schulz, *Zeolites*, 1997, **19**, 253-258.
104.   V. Shen and A. T. Bell, *Microporous Mater.*, 1996, **7**, 187-199.
105.   W. Xu, J. Dong, J. Li, J. Li and F. Wu, *J. Chem. Soc., Chem. Commun.*, 1990, 755-756.
106.   P. R. Hari Prasad Rao, K. Ueyama and M. Matsukata, *Appl. Catal., A*, 1998, **166**, 97-103.
107.   X. Ke, L. Xu, C. Zeng, L. Zhang and N. Xu, *Microporous Mesoporous Mater.*, 2007, **106**, 68-75.
108.   M. Ogura, S.-i. Nakata, E. Kikuchi and M. Matsukata, *J. Catal.*, 2001, **199**, 41-47.
109.   R. Bermejo-Deval, R. Gounder and M. E. Davis, *ACS Catal.*, 2012, **2**, 2705-2713.
110.   R. Gounder and M. E. Davis, *J. Catal.*, 2013, **308**, 176-188.
111.   C. Buttersack, W. Wach and K. Buchholz, *J. Phys. Chem.*, 1993, **97**, 11861-11864.
112.   T. Blasco, M. A. Camblor, A. Corma, P. Esteve, J. M. Guil, A. Martinez, J. A. Perdigon-Melon and S. Valencia, *J. Phys. Chem. B*, 1998, **102**, 75-88.
113.   G. Yang, E. A. Pidko and E. J. M. Hensen, *J. Phys. Chem. C*, 2013, **117**, 3976-3986.
114.   A. I. Biaglow, D. J. Parrillo and R. J. Gorte, *J. Catal.*, 1993, **144**, 193-201.
115.   C. A. Emeis, *J. Catal.*, 1993, **141**, 347-354.
116.   S. Bischoff and F. Kasper, *J. Prakt. Chem.*, 1986, **328**, 449-453.
117.   R. M. Dessau, *Zeolites*, 1990, **10**, 205-206.
118.   A. I. Torres, P. Daoutidis and M. Tsapatsis, *Energy Environ. Sci.*, 2010, **3**, 1560-1572.
119.   W. Fan, M. A. Snyder, S. Kumar, P. S. Lee, W. C. Yoo, A. V. McCormick, R. L. Penn, A. Stein and M. Tsapatsis, *Nat. Mater.*, 2008, **7**, 984-991.
120.   D. Wang, C. M. Osmundsen, E. Taarning and J. A. Dumesic, *ChemCatChem*, 2013, **5**, 2044-2050.
121.   R. A. F. Tomás, J. C. M. Bordado and J. F. P. Gomes, *Chem. Rev.*, 2013, **113**, 7421-7469.
122.   Y. Tachibana, S. Kimura and K.-i. Kasuya, *Sci. Rep.*, 2015, **5**, 8249.
123.   M. N. Masuno, P. B. Smith, D. A. Hucul, K. Brune, R. L. Smith, J. Bissell, D. A. Hirsch-Weil and E. J. Stark, Methods of producing *p*-xylene from 2,5-hexanedione and ethylene in the presence of catalysts and solvents, US Patent 8889938B2, 2014.
124.   B. Saha and M. M. Abu-Omar, *ChemSusChem*, 2015, **8**, 1133-1142.
125.   Y.-T. Cheng, Z. Wang, C. J. Gilbert, W. Fan and G. W. Huber, *Angew. Chem., Int. Ed.*, 2012, **51**, 11097-11100.
126.   T. W. Lyons, D. Guironnet, M. Findlater and M. Brookhart, *J. Am. Chem. Soc.*, 2012, **134**, 15708-15711.
127.   M. W. Peters, J. D. Taylor, M. Jenni, L. E. Manzer and D. E. Henton, Integrated process to selectively convert renewable isobutanol to *p*-xylene, US Patent 20110087000, 2011.
128.   T. A. Brandvold, Carbohydrate route to para-xylene and terephthalic acid, US Patent 20100331568, 2010.
129.   A. Morschbacker, *Polym. Rev.*, 2009, **49**, 79-84.
130.   A. P. Kagyrmanova, V. A. Chumachenko, V. N. Korotkikh, V. N. Kashkin and A. S. Noskov, *Chem. Eng. J.*, 2011, **176-177**, 188-194.
131.   R. E. Patet, N. Nikbin, C. L. Williams, S. K. Green, C.-C. Chang, W. Fan, S. Caratzoulas, P. J. Dauenhauer and D. G. Vlachos, *ACS Catal.*, 2015, **5**, 2367-2375.
132.   Y.-P. Li, M. Head-Gordon and A. T. Bell, *J. Phys. Chem. C*, 2014, **118**, 22090-22095.

133. S. K. Green, R. E. Patet, N. Nikbin, C. L. Williams, C.-C. Chang, J. Yu, R. J. Gorte, S. Caratzoulas, W. Fan, D. G. Vlachos and P. J. Dauenhauer, *Appl. Catal. B.*, 2016, **180**, 487-496.
134. J. Luo, J. Yu, R. J. Gorte, E. Mahmoud, D. G. Vlachos and M. A. Smith, *Catal. Sci. Tech.*, 2014, **4**, 3074-3081.
135. S. Inagaki, K. Nakatsuyama, Y. Saka, E. Kikuchi, S. Kohara and M. Matsukata, *J. Phys. Chem. C*, 2007, **111**, 10285-10293.
136. Y. Yu, G. Xiong, C. Li and F.-S. Xiao, *Microporous Mesoporous Mater.*, 2001, **46**, 23-34.
137. T. Wakihara, S. Kohara, G. Sankar, S. Saito, M. Sanchez-Sanchez, A. R. Overweg, W. Fan, M. Ogura and T. Okubo, *Phys. Chem. Chem. Phys.*, 2006, **8**, 224-227.
138. W. R. Gunther, V. K. Michaelis, M. A. Caporini, R. G. Griffin and Y. Román-Leshkov, *J. Am. Chem. Soc.*, 2014, **136**, 6219-6222.
139. P. Wolf, M. Valla, A. J. Rossini, A. Comas-Vives, F. Núñez-Zarur, B. Malaman, A. Lesage, L. Emsley, C. Copéret and I. Hermans, *Angew. Chem., Int. Ed.*, 2014, **53**, 10179-10183.
140. M. Davis, *Top Catal*, 2015, 1-5.